INFORMATION TO USERS

This manuscript has been reproduced from the microfilm master. UMI films the text directly from the original or copy submitted. Thus, some thesis and dissertation copies are in typewriter face, while others may be from any type of computer printer.

The quality of this reproduction is dependent upon the quality of the copy submitted. Broken or indistinct print, colored or poor quality illustrations and photographs, print bleedthrough, substandard margins, and improper alignment can adversely affect reproduction.

In the unlikely event that the author did not send UMI a complete manuscript and there are missing pages, these will be noted. Also, if unauthorized copyright material had to be removed, a note will indicate the deletion.

Oversize materials (e.g., maps, drawings, charts) are reproduced by sectioning the original, beginning at the upper left-hand corner and continuing from left to right in equal sections with small overlaps. Each original is also photographed in one exposure and is included in reduced form at the back of the book.

Photographs included in the original manuscript have been reproduced xerographically in this copy. Higher quality 6" x 9" black and white photographic prints are available for any photographs or illustrations appearing in this copy for an additional charge. Contact UMI directly to order.

U·M·I

University Microfilms International
A Bell & Howell Information Company
300 North Zeeb Road, Ann Arbor, MI 48106-1346 USA
313/761-4700 800/521-0600

Order Number 9405535

Nuclear quadrupole resonance studies of the SORC sequence and nuclear magnetic resonance studies of polymers

Jayakody, Jayakody R. Pemadasa, Ph.D.

City University of New York, 1993

U·M·I
300 N. Zeeb Rd.
Ann Arbor, MI 48106

Nuclear Quadrupole Resonance studies of the "SORC" sequence and Nuclear Magnetic Resonance Studies of Polymers.

by

J. R. P. Jayakody

A dissertation submitted to the Graduate Faculty in Physics in partial fulfillment of the requirements for the degree of Doctor of Philosophy, The City University of New York.

1993

This manuscript has been read and accepted for the Graduate Faculty in Physics in satisfaction of the dissertation requirement for the degree of Doctor of Philosophy.

May 4, 1993 Robert A. Marino

Date Chair of Examining Committee: Professor Robert A.Marino

May 25, 1993 Joseph B. Krieger

Date Executive Officer: Professor Joseph Krieger

Dr Surja Bulusu
Surya N. Bulusu

Professor Steve Greenbaum

Professor Godfry Gumbs
Godfrey Gumbs

Professor Fredrick Smith
Frederick W. Smith

Supervisory Committee

The City University of New York

Abstract

Nuclear Quadrupole Resonance studies of the "SORC" sequence and Nuclear Magnetic Resonance Studies of Polymers.

by

J. R. P. Jayakody

Advisor: Professor Robert A. Marino

The behavior of induction signals during steady-state pulse irradiation in ^{14}N NQR was investigated experimentally. Because Strong Off-resonance Comb (SORC) signals recur as long as the pulsing continues, very efficient signal-averaging can result. The dependence of these steady-state SORC signals on pulse parameters and on frequency offset are presented, together with a discussion of the applicability of the method.

Also as part of the NQR work, Cocaine base has been detected using conventional NQR techniques. The experimental results show that SORC detection can be of sufficient sensitivity to form the basis of narcotics screening devices for both mail and airline baggage.

A new NMR technique, to obtained the correlation time of the random thermal motion of a polymer at temperatures near the glass transition has been introduced. The

method relies on the fact that the NMR chemical shift anisotropy (CSA) has a temperature dependence as a result of thermal motion. For slow-motion of a polymer chain near the glass transition, the CSA parameter begins to decrease. This motional narrowing can be interpreted to yield the correlation time of the thermal motion. In this work Nitrocellulose isotopically highly enriched with ^{15}N was studied at four different temperatures between 27° and 120° Celsius and the correlation times for polymer backbone motions were obtained.

Nafion films containing, water (D_2O and $H_2{}^{17}O$) and methanol (CH_3OD, $CH_3{}^{17}OH$), have been studied using Deuteron and Oxygen-17 NMR spectroscopy. Glassy behavior of the water domains at low temperature is evidenced by the specific nature of the ^2H NMR lineshapes. Activation energies extracted from ^2H spin-lattice relaxation data on the high temperature side of the T_1 minimum exhibit a steady increase with increasing water content. In spite of a high degree of molecular mobility, angular-dependent spectra of both unstretched and stretched samples reflect considerable anisotropy of the host polymer. Activation volumes corresponding to a specific dynamical process were obtained from measurements of spin-lattice relaxation vs. pressure. From the NMR measurements of Nafion films containing methanol, it was found that the molecular motion is much more rapid than the molecular motion of water in Nafion membranes.

Acknowledgements

I am deeply grateful to Professor Robert A. Marino, not only for the broad background and excellent guidance he has given me as my thesis advisor, but also for his friendship and kindness. It has been my great fortune to have as an advisor someone who is knowledgeable and well respected in his field.

I would like to express my deep and special appreciation to Professor Steve Greenbaum for providing me access to NMR instrumentation and for many valuable and helpful discussions.

Mr. Rensheng Chen, who collaborated with me for nearly two years, deserves a special thanks for his friendship and many useful discussions.

Mr. R.Krumm deserves my gratitude for his help in building the CW spectrometer.

I would also like to thank Dr. S.S.Kim, Dr. S.Li, Dr. Y.Li, Ms. J.Li, Ms. S. Brown Mr.X.T. Cao and Dr. P.Stallworth for many useful discussions and their friendship.

All the people of the Hunter College Physics department are greatly appreciate for their friendship and help they offered me the last four years.

I would like to thank the thesis committee members, Dr. Surya Bulusu, Professor Steve Greenbaum, Professor Godfry Gumbs and Professor Fredrick Smith for their friendly participation and careful reading of this manuscript.

Of course, my wife Darshini has been a saint of patience and understanding through out my long graduate career. Her warm companionship, support and love are as much a part of this work as anything can be.

Dedication

I would like to dedicate this thesis to my parents.

Table of contents

List of Tables

List of Figures

Chapter 1

Introduction

Nuclear Quadrupole Resonance (NQR) is a means of detecting the interaction of the nuclear quadrupole moment with an electric field gradient (EFG) in solids. The electric field gradient is, in turn, determined by the nature of the chemical bonds and other neighboring atoms. The quadrupole moment arises as a result of a non-spherical nuclear charge distribution. Because the nuclear quadrupole moment is associated with the nuclear angular momentum, or spin, discrete energy levels are established. Resonance occurs when transitions from one spin state to another are excited by radio-frequency electro-magnetic oscillations. In this way NQR is quite similar in principle to Nuclear Magnetic Resonance (NMR). Since energy levels depend on the coupling to the field gradient, measurement of the resonance frequencies allows the magnitude of the electric field gradient to be determined. NQR is thus a tool which provides a sensitive probe of the electrical environment of quadrupolar nuclei and thus of chemical structure and bonding.

NQR, particularly, has seen significant developments over the past ten years. Various experimental techniques, for instance the strong off-resonance comb (SORC) sequence, have been developed primarily to enhance explosives detection capabilities of NQR. These techniques originally proposed for NQR use by R.Marino, et al [1,2],and suggested for large volume detection use by Garroway et al [3], now make NQR detection of a variety of materials possible and promise a substantial increase in narcotic detection capabilities.

Part of the work I described in this thesis is an experimental investigation of the

Strong Off-resonance Comb (SORC) Pulse sequence [1] in Nitrogen-14 NQR and detection and study of NQR lines in cocaine base (CB).

Under favorable conditions the Strong Off-resonance Comb (SORC) sequence can enable extremely sensitive detection of NQR signals by virtue of high duty-cycle signal averaging. In this work we attempt to make clear just what these favorable conditions are. Also the behavior of induction signals during steady-state pulse irradiation in ^{14}N NQR are investigated experimentally. The radio-frequency (RF) field H_1 is applied as a long train of equally spaced identical pulses, ie., a long comb, rather than a continuous wave (CW). A non-trivial advantage of the pulse analogues of CW experiments is that they enable the observation and coherent sum of signals between successive pairs of pulses and they then can result in significantly increased sensitivity [4-10].

A search for NQR signals was conducted in a crystallized sample of CB. Continuous Wave (CW) and pulse techniques were used at room temperature and 77K. Then signals was detected by both CW and pulse method. Relaxation times T_1, T_2, and T_2^* were measured at room temperature for ν_- and ν_+ lines. The relatively long value of T_2 at room temperature made this substance very easy to detect by SORC pulse methods.

Nuclear Magnetic Resonance (NMR) spectroscopy is a well established and powerful technique which can be used to probe molecular structure and dynamics. One of the major advantage of NMR is sensitivity to various types of polymer motions. NMR interactions can be modulated or averaged by molecular motion, greatly affecting the NMR spectrum and associated relaxation times T_1, T_2. Since some of the NMR characteristics are angular dependent, NMR is widely applied to probe the anisotropy of materials, especially in solid samples such as poly-crystals, fibers or films. In this thesis,

my attention was mainly focused on molecular motion and the anisotropic properties of polymer samples, reflected by NMR line shape and relaxation times.

NMR techniques can be used to obtain the correlation time τ of the random thermal motions of polymers at temperature near the glass-to-rubber transition. The correlation time is important since it is the parameter that describes the time scale of the motion. Measurement of τ in Nitrocellulose (NC) were undertaken as part of a project to understand the mechanical properties of this material at the microscopic level.

The method begins with Sook Lee's analytical theory [13,14,15] of anisotropic paramagnetic centers undergoing slow orientational diffusion. The NMR chemical shift anisotropy (CSA) has the required orientational dependence with respect to the externally applied magnetic field, and the theory can readily be expressed in terms of its natural variables from Lee's examples of dipole-dipole and quadrupole interactions. For this work, the choice of CSA interaction was dictated by the fact that it could be measured with considerably higher precision in nitrocellulose and other polymers than for either dipole-dipole or quadrupole parameters. CSA information is contained in the intensity of the spinning sidebands of a NMR Magic angle spinning experiment. It was extracted by the numerical method of Herzfeld and Berger [49]. Finally the correlation times of the polymer chain motion were obtained at four different temperature using a modification of Sook Lee's result.

Deuterium NMR experiments and applications to polymers have been comprehensively reviewed by Smith [16], Spiess [17], and Jelinski [18]. Most of their work involves studies of deuterated polymers with the deuterons existing in C-D bonds on the polymer chain. Also many NMR investigations have been done on water in

oriented polymeric materials such as collagen fibers [19,20,21], cellulose [22,23] and polyimide [24].

In this part of this thesis, deuteron NMR has been carried out with variable water content to investigate the nature of its behavior in nitrocellulose (NC). Two forms of NC were used, NC fibers (nitrated surgical cotton), and NC films of 75 and 200 μm thick. In addition to measuring spectral line-shape parameters such as the linewidth or other powder pattern features, we also measured the spin-lattice relaxation time (T_1) in our samples as a function of temperature, moisture, and film thickness using inversion-recovery [25] method.

Perfluorinated ion exchange membranes, a commercial example of which is Nafion (Dupont), have been subject to a wide variety of intensive investigation because of their use as separators in present and possible future fuel cells [26]. The most important property of Nafion membranes in this capacity is their high proton transport numbers, which requires the presence of significant quantities of water (20wt%) in the membrane [27]. Water molecular diffusion and charge transport across the membrane are, to some extent, correlated. The physical nature of water in Nafion has been characterized by several techniques and found to be significantly different than in the bulk state [28,29,30].

The present work consists of Deuteron and ^{17}O NMR measurement to study molecular dynamics thus utilizing these quadrupolar nuclei as probes. We obtained line shapes and spin-lattice relaxation time T_1 measurements as a function of water contents and temperatures in Nafion-117 films containing D_2O and $H_2{}^{17}O$ (20% enrichment). One of the main results of this study was the observation of anisotropic molecular motion in

the film [31] plane, with dramatic enhancement of the anisotropy in modesty stretched films. Activation energies were also extracted from low temperature measurement for different water content.

We also have employed hydrostatic pressure as an additional thermodynamical variable in our NMR measurements. One particular advantage of this approach is that activation volume corresponding to a specific dynamical process can be extracted directly from the data. Knowledge of activation volumes as a function of water contents is expected to provide some insight into the relation between molecular rotation/translation and charge transport.

The prospect of employing methanol directly as a fuel in low temperature fuel cells has obvious appeal. For this reason we employ NMR to investigate issues related to methanol molecular mobility in Nafion-117 containing CH_3OD and $CH_3{}^{17}OH$(10% ^{17}O-enriched).

Chapter 2

Basic theory of NMR and NQR

2.1 NMR Background

A nucleus with a spin, **I**, has a magnetic moment, μ , collinear with **I** given by $\mu=\gamma\hbar\mathbf{I}$, where γ is called the gyromagnetic ratio and $\hbar$ is Plank's constant. The Hamiltonian of a magnetic moment in an external magnetic field $\mathbf{H}_o$ is

$$\mathcal{H} = - \mu \cdot \mathbf{H}_o .$$

If the uniform field H_o is applied along Z axis, then the resulting energy eigenvalues are $E_m = - \mu_z H_o = -\gamma\hbar H_o m$

where m is the magnetic quantum number which can have the following values,

$$m = I, (I-1), (I-2), - - - -I.$$

It is clear then,that the difference between two adjacent energy levels is

$$\Delta E = \gamma\hbar H_o$$

This splitting of the nuclear energy level is called the Zeeman effect. The Zeeman energy levels for a spin 1/2 and spin 1 nucleus are displayed in Figure 2.1.

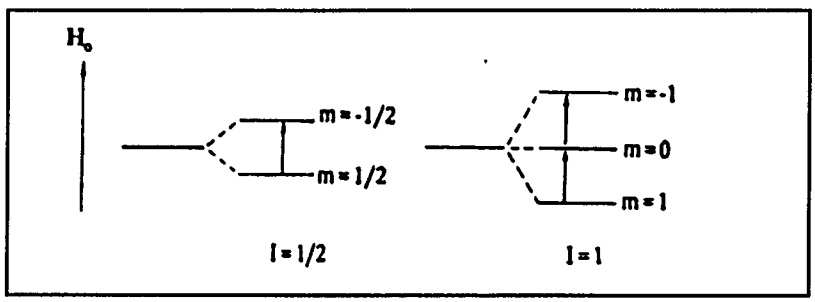

Figure 2.1:Zeeman energy levels for spin-1/2 and spin-1.

When a radio-frequency (RF) electromagnetic field of angular frequency ω_o is applied to the system, energy will be absorbed when

$$\Delta E = \hbar\omega_o$$

where ω_o is the Larmor frequency. This is the resonance condition that forms the basis of all nuclear magnetic resonance phenomena.

In order to induce transitions between two nuclear spin levels, an oscillating magnetic field $\mathbf{H}_1$ is applied perpendicular to $\mathbf{H}_o$. This alternating field with frequency ω can be taken to be in the x direction and can be written as $H_1 \cos\omega t$. The Hamiltonian of the interaction of the rf field with an isolated spin is then given by

$$\mathcal{H}_1 = -\mu.\mathbf{H} = -\gamma\hbar H_1 \cos\omega t.$$

The effects of this interaction can be determined by the use of standard time-dependent perturbation theory. The probability that a transition is induced by the RF field between the levels m and m' is proportional to the square of the matrix element $<m'|\mathcal{H}_1|m>$.

$$|<m'|\mathcal{H}_1|m>|^2 = \gamma^2\hbar^2H_1^2\,|<m'|I_x|m>|^2 \cos^2\omega t$$

where $|m>$ and $|m'>$ are eigenstates of the unperturbed Hamiltonian. The quantity $|<m'|I_x|m>|^2$ is given by

$$|<m'|I_x|m>|^2 = (1/4)\,|[I(I+1)-m(m+1)]^{1/2}\delta_{m',m+1} + [I(I+1)-m(m-1)]^{1/2}\delta_{m',m-1}|^2.$$

Hence, the RF field induced transitions between adjacent energy levels ($\Delta m = \pm 1$) only (Fig. 2.1).

If the nuclear spins are in thermal equilibrium then the population of each energy level will be proportional to the Boltzman factor, $\exp.(-E_m/kT)$, where k is Boltzman's constant and T is the temperature of the system. Alternatively, one can define a spin temperature T which gives the correct ratio for the spin populations. The effect of

applied radiation will be to equalize the spin population, thus rasing the spin temperature. This results from a net absorption of energy by the spin system. NMR can be detected by observing this energy absorption or by observing the spin system radiate this energy after the applied radiation stops.

2.2 Detection of the Resonance Phenomenon

As mentioned in the previous section resonance is detected by subjecting the spin system to electromagnetic radiation of a specific frequency. There are two basic ways to apply the radiation, continuous wave (CW) excitation and pulsed excitation. Each technique offers both advantages and disadvantages depending on the line width and other spectral parameter. This section describes the principles and operation of the both types of detection methods.

To understand how resonance is detected, the effect of the applied radiation on the spins needs to be understood. The total magnetization of the sample is the sum of all the individual nuclear magnetizations, μ_k,

$$\vec{M} = \Sigma \vec{\mu}_k$$

When a magnetization **M** is placed in a steady magnetic field **H**, in the absence of thermal relaxation, it undergoes precession about the static field direction as shown in Figure 2.2 according to the equation.

$$\frac{dM}{dt} = \gamma M \times H_o$$

In an NMR experiment the sample is placed inside an inductor L with its axis along the x axis. The radiation is created by applying an AC voltage

$$V_c = V_o \sin\omega t.$$

This will create an AC magnetic field

$$H_x(t) = H_{xo} \cos\omega t.$$

Then, the total field applied to the sample is

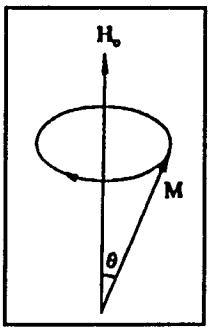

Figure 2.2: Magnetization **M** in a static magnetic field.

$$H_T = H_o\hat{z} + H_{xo}\cos\omega t\hat{x}$$

The alternating magnetic field $H_x(t)$ could be broken down into two components, each of amplitude H_1, one rotating clockwise and the other counter clockwise, as follows:

$$H_R = H_1(\cos\omega t\,\hat{x} + \sin\omega t\,\hat{y})$$

$$H_L = H_1(\cos\omega t\,\hat{x} - \sin\omega t\,\hat{y})$$

where $H_1 = H_{xo}/2$.

We shall assume we have only the field H_R, but this causes of no loss in generality because the use of a negative ω will convert it to H_L. Now the equation of motion of a spin, including the effects both of $H_1(t)$ and of the static field H_o is,

$$\frac{dM}{dt} = \gamma M \times [H_o + H_1(t)]$$

Now we introduce a frame of reference X',Y',Z', rotating at frequency ω. Then, the equation of motion for **M** in the rotating frame is [33],

$$\frac{dM}{dt} = \gamma M \times [(H_o + \frac{\omega}{\gamma})\hat{Z} + H_1\hat{X}] = M \times \gamma H_{eff}$$

The last equality defines the magnitude H_{eff}, the "effective field". We can see that **M** will precess about $\mathbf{H}_{eff}$. At resonance, ie. when $\omega = -\gamma H_o$ the magnetization **M** will precess about x′ with frequency γH_1.

The precession of **M** is driven by $\mathbf{H}_1$, thus energy is being absorbed by the spin system. The amount of energy absorbed can be related to the magnitude of the magnetization which develops in the x-y plane of the laboratory reference frame. The response of the x component of the magnetization to the applied field $\mathbf{H}_x(t)$ is [33]

$$M_x = H_{xo}\,[\chi'(\omega)\cos\omega t + i\chi''(\omega)\sin\omega t]$$

where $\chi'(\omega)$ and $\chi''(\omega)$ are defined as the real and imaginary parts of the complex magnetic susceptibility.

2.2.1 Continuous Wave Spectrometers

In this technique the radiation is applied continuously and the resonance condition is sampled by sweeping either the RF frequency or the magnetic field and monitoring the detector which gives a voltage output which is proportional to either $\chi'(\omega)$ or $\chi''(\omega)$. When a material with a complex susceptibility $\chi(\omega)$ is placed inside a coil then the inductance L of that coil will change from its empty value L_o to

$$L = L_o\,[1 + 4\pi\chi(\omega)].$$

The impedance Z_c of the coil whose resistance without the sample is R_o is

$$Z_c = iL\omega + R_o = iL_o\omega[1 + 4\pi\chi'(\omega)] + L_o\omega 4\pi\chi''(\omega) + R_o$$

Thus the fractional change in resistance of the coil is

$$\Delta R/R_o = (L_o\omega/R_o)\, 4\pi\chi''(\omega) = 4\pi\chi''(\omega)Q_o$$

where Q_o is the quality factor of the coil and is proportional to the ratio of the amount of energy in the coil divided by the amount of energy absorbed by the coil per period of oscillation. An NMR detector of this type supplies a constant RF current I_c to the coil. When the sample passes through resonance the increased resistance results in a drop in the voltage $V_c = I_cZ$ across the coil. The NQR CW circuit built for this thesis operates on this principle.

2.2.2 Pulse Spectrometer

From the results derived in section 2.2, it can be seen that if **M** is originally at equilibrium, aligned along the z axis, and radiation of frequency $\omega_o=\gamma H_o$ is turned on at t=0 then **M** will rotate about the x' axis with a frequency γH_1. After a time t_w the angle between **M** and the Z axis will be $\theta=\gamma H_1 t_w$. If the RF field is left on for a period $t_{\pi/2}$ such that $\theta=\pi/2$ and then turned off, then **M** will be aligned along the Y' axis and will thus induce a voltage in the coil as the spins dephase. Because the spins are now processing freely without a driving radiation, the signal detected in this way is called a free induction decay (FID). The characteristic decay time of the FID is named T^*_2.

The above described pulse is called a $\pi/2$ pulse. After application of $\pi/2$ pulse the individual spins will not remain in phase with each other due to the distribution of resonance frequencies because of the field inhomogeneity and interactions of the spins with their surroundings. Some spins will precess faster and some slower than the resonance frequency. On the other hand, **M** also tends to regrow along the z' direction because thermal equilibrium is being re-established. As a result of this dephasing, the

components of **M** in the x'-y' plane eventually go to zero causing the detected signal to decay to zero. Since it is the distribution of resonance frequencies which determines the shape of the FID, all of the information of the spin system is contained in FID. By taking the fourier transform of the FID the shape of the line is obtained. Different pulse sequences used in this theses will be discus later.

2.3 NQR Background

Nuclei with spin **I** > 1/2 have an electric quadrupole moment in addition to a nuclear magnetic moment. It arises from an asymmetry of their electric charge distribution. The existence of an electric quadrupole moment is an indication of the departure of the nucleus from spherical symmetry. When a nucleus of charge density ρ(r) is located in an electric potential V(r) arising from all the other charges surrounding the nucleus, the electrostatic energy of interaction is given by

$$E = \int \rho(r) V(r) d^3r$$

Where ρ(r) is the nuclear charge density and V(r) is electrostatic potential arising from all the other charges surrounding the nucleus. Expanding the potential V(r) into a power series about the center of nuclear charge,

$$V(x,y,z) = V_o + \sum_i \left(\frac{\partial V}{\partial x_i}\right)_{r=0} x_i + \frac{1}{2}\sum_{ij}\left(\frac{\partial^2 V}{\partial x_i \partial x_j}\right)_{r=0} x_i x_j + \cdots$$

then we have

$$E = V_o\int \rho(r)d^3r + \sum_i V_i\int x_i\rho(r)d^3r + \frac{1}{2}\sum_{ij} V_{ij}\int x_i x_j \rho(r)d^3r .$$

The first term is the point-charge interaction of the nucleus with the potential V_o. The effect of this term is only to shift all Zeeman levels by an equal amount and thus it can be ignored for our purposes. The second integral is the electric dipole moment of the nucleus. It vanishes by a symmetry argument based on the assumption that nuclear state have definite parity. The third term is the electric quadrupole term, V_{ij} is a component of the electric field gradient (EFG) tensor at the nucleus.It is convenient to consider the quantities Q_{ij} defined by the equation

$$Q_{ij} = \int (3x_i x_j - \delta_{ij} r^2)\rho(\vec{r})d^3r$$

In terms of the Q_{ij}, we have the classical quadrupole energy E_Q

$$E_Q = \frac{1}{6}\sum_{ij} V_{ij}Q_{ij}$$

The quantum mechanical analog of E_Q can be calculated as [34]

$$\mathcal{H}_Q = \frac{eQ}{6I(2I-1)}\sum_{ij} V_{ij}\left[\frac{3}{2}(I_iI_j + I_jI_i) - \delta_{ij}I(I+1)\right]$$

Where eQ is the quadrupole moment of the nucleus.It is possible to choose a principal axis of the EFG tensor so that V_{ij} is diagonal. We choose the principal axis (xyz) such that

$$|V_{xx}| \leq |V_{yy}| \leq |V_{zz}|$$

In the principal axis system of the EFG, H_Q is reduced to a simpler form

$$\mathcal{H}_Q = \frac{e^2qQ}{4I(2I-1)}\left[3I_z^2 - I(I+1) + \eta(I_x^2 - I_y^2)\right]$$

Where eq = V_{zz}, the largest component of the EFG, e^2qQ is the quadrupole coupling constant and η is called asymmetry parameter, defined as

$$\eta = \frac{V_{xx} - V_{yy}}{V_{zz}}.$$

When the EFG is spherically symmetric, or of cubic symmetry, eq=0, so that $\mathcal{H}_Q$=0; When the EFG is cylindrically symmetric, η=0. When $\eta \neq 0$, the matrix elements of $\mathcal{H}_Q$ will be,

$$<m|\mathcal{H}_Q|m'> = A\{[3m^2 - I(I+1)]\delta_{mm'} + (\eta/2)[(I \mp m)(I \mp m)(I \pm m + 1)(I \pm m + 2)]^{1/2}\,\delta_{m\pm 2,m'}\}$$

where $A = (e^2\,qQ)/4I(2I-1)$.

The degree of mixing of the nuclear eigenstates clearly increases as η increases and is zero when η=0.

When η=0 the energy levels will be

$$E_m = A[3m^2 - I(I+1)]$$

which for spin I=1 gives

$$E_{\pm 1} = A, \text{ and } \quad E_o = -2A$$

Here there is $\pm$m degeneracy. When $\eta \neq 0$ this degeneracy is lifted, and one can see that for the spin I=1 case, there are in general three energy levels. Quadrupole energy levels for a spin 1 nucleus are shown in Figure 2.3.

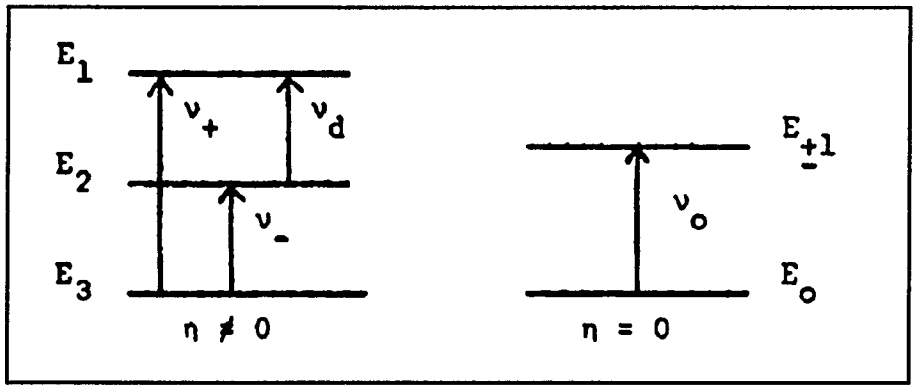

Figure 2.3: Quadrupole energy levels for spin-1.

The Bohr resonance condition yields three transition frequencies for $\eta \neq 0$. They are

$$\nu\pm = 3e^2qQ(1\pm\eta/3)/4h,$$

$$\nu_d = \eta e^2 qQ/2h.$$

The single frequency for $\eta=0$ is

$$\nu = 3e^2 qQ/4h.$$

Of course $\nu_d = \nu_+ - \nu_-$

For unit spin, therefore, the asymmetry parameter and the individual diagonal components of the field gradient can be determined from the frequency of the spectrum, by combining with Laplace's equation. Thus

$$\eta = \frac{\nu_+ + \nu_-}{\nu_d}$$

$$V_{zz} = eq$$

$$V_{yy} = -eq(\eta+1)/2$$

$$V_{xx} = eq(\eta-1)/2.$$

2.3.1 Transitions

Now that the quadrupolar energy levels have been established, it is appropriate to consider means of exciting transitions between the nuclear spin states. In principle, transitions might be excited by immersing the sample containing the nuclear system in a small perturbing field gradient which couples to the nuclear electric quadrupole. This, however, has never been done for the simple reason that field gradients which can be produced in the laboratory fail by many orders of magnitude to have sufficient intensity to produce transitions.

Consequently transitions between the quadrupole energy levels are induced by means of a time varying magnetic field which couples to the nuclear magnetic dipole. The situation is then exactly the same as that encountered in NMR.

The intensity of the resonance line depends directly upon the number of particles participating per unit time in transitions and this depends on differences in population between the levels. Thus it is generally desirable to cool the sample to liquid nitrogen temperature (77K) in order to increase the population excess of the lower level. Under the resonance conditions nuclei are pumped from the lower state to the higher, and if this were the only operative factor the populations would soon be equalized, a condition known as saturation. A number of additional phenomena, however, act to restore thermal equilibrium with the lattice and these are known as relaxation processes. Further discussion about the relaxation will be given later.

2.4 The Zeeman effect in NQR

The application of a constant magnetic field, H_o, in a direction with polar coordinates θ,ϕ in the field-gradient axis system, introduces an additional term into the Hamiltonian operator given by

$$\mathcal{H}_M = -\hbar\Omega(I_z \cos\theta + I_x \sin\theta\cos\phi + I_y \sin\theta\sin\phi),$$

where $\Omega=\gamma H_o$.

For $\hbar\Omega << e^2qQ$, consider $\mathcal{H}_M$ as a small perturbation of the NQR levels. For states with $|m| > 1/2$ the presence of the magnetic field removes the degeneracy between the $\pm m$ levels and first order perturbation theory yields

$$E\pm m = A[3m^2 - I(I+1)] \mp m\hbar\Omega\cos\theta.$$

The treatment for the $m=\pm 1/2$ states is somewhat different because the Hamiltonian has off diagonal matrix element between these sates. The energy levels are

$$E\pm = A[3/4 - I(I+1)] \mp f/2\ \hbar\Omega\cos\theta$$

where $f = [1+(I+1/2)^2 \tan^2\theta]^{1/2}$.

The energy levels for spin-5/2 nuclei in the presence of a small magnetic field are shown in Figure 2.4.

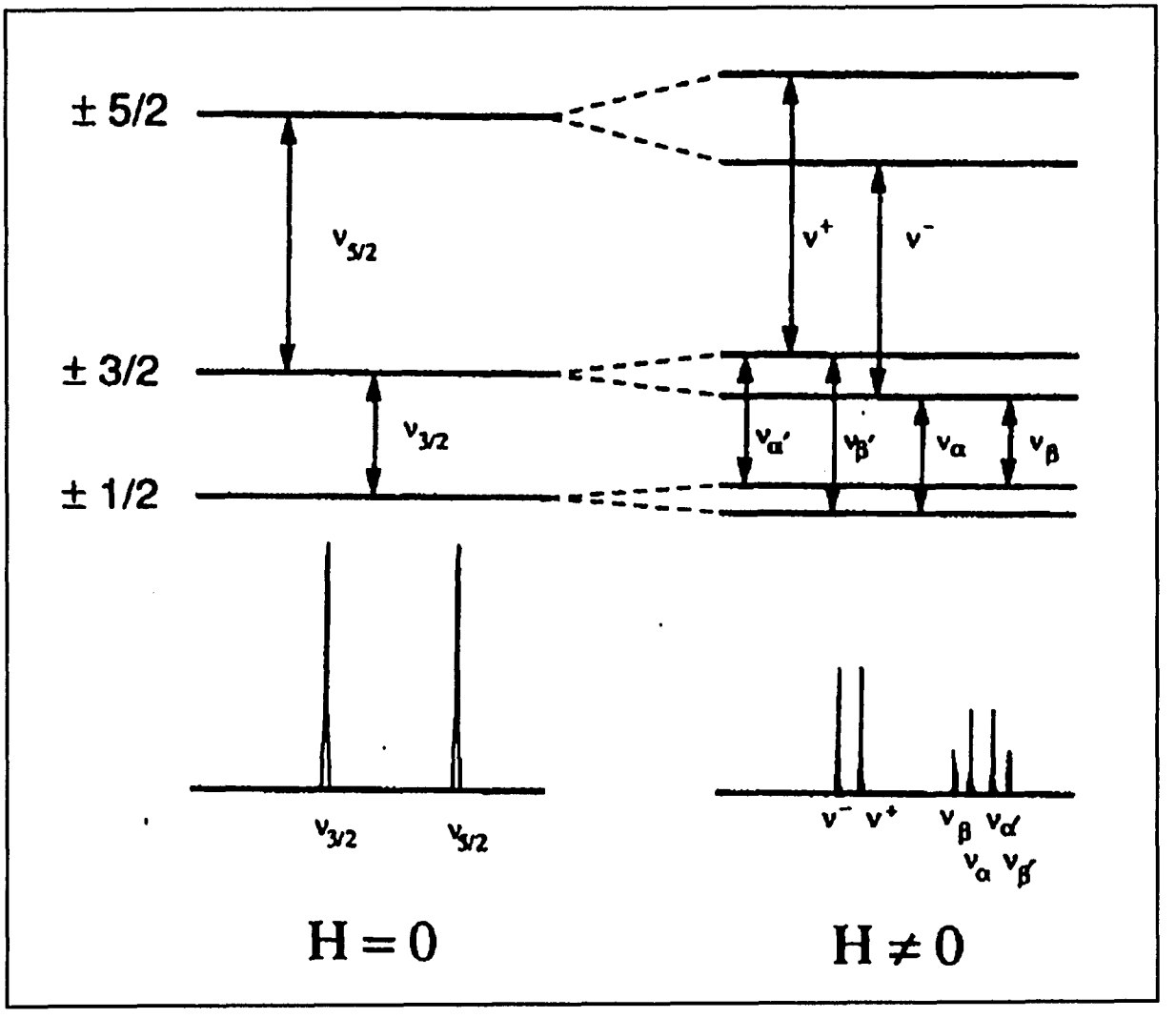

Figure 2.4 : Energy levels of spin-5/2 nuclei when $\eta=0$.

2.5 The Quadrupole effect in NMR

When H_o is large such that $\hbar\Omega >> e^2qQ$, we can consider $\mathcal{H}_Q$ to be a perturbation of the Zeeman levels. In the case of $\eta=0$,

$$\mathcal{H} = \mathcal{H}_M + \mathcal{H}_Q,$$

$$\mathcal{H}_Q = \frac{e^2qQ}{4I(2I-1)}\left[3I_Z^2\cos^2\theta + 3I_X^2\sin^2\theta + 3(I_ZI_X + I_XI_Z)\sin\theta\cos\theta - I(I+1)\right]$$

Treating $\mathcal{H}_Q$ as a perturbation energy of the Zeeman energy, the energy shift of Zeeman energy levels up to the first order perturbation will be

$$E_m = \frac{e^2qQ}{8I(2I-1)}(3\cos^2\theta - 1)\left[3m^2 - I(I+1)\right] \quad .$$

The effect of the quadrupole coupling is shown in Figure 2.5 for the case of spin I=1.

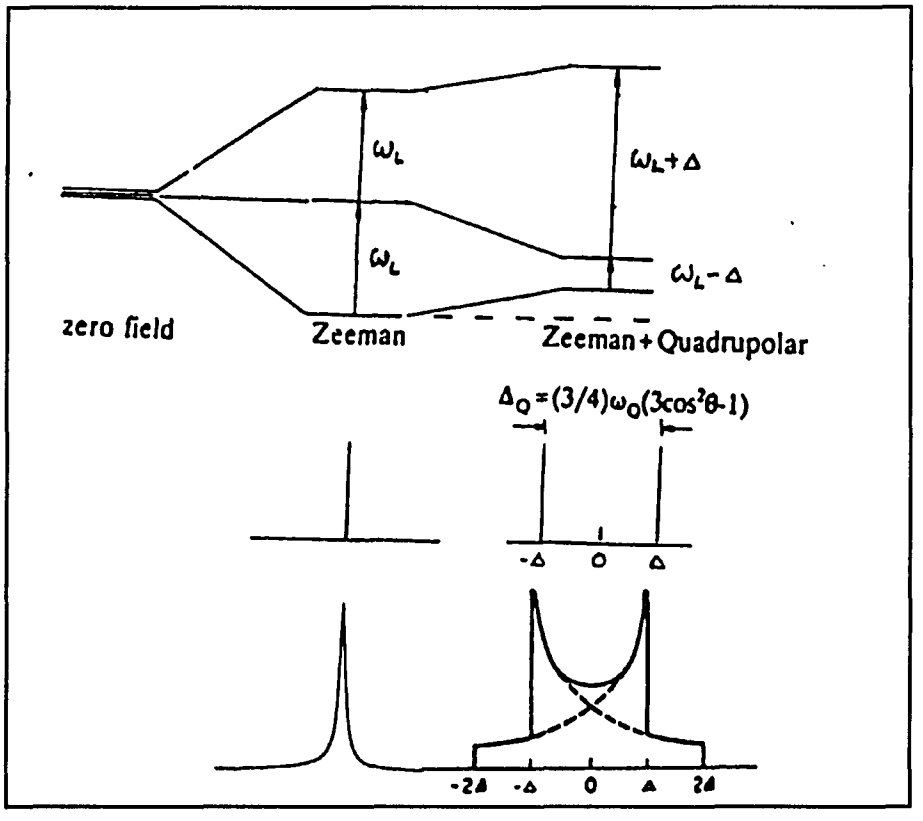

Figure 2.5: a) The energy levels b) Spectrum of single crystal c) Powder pattern for spin-1 nucleus with quadrupole interaction.

In Figure 2.5, $\Delta = (3/8)(e^2qQ/\hbar)(3\cos^2\theta-1)$, $\omega_Q = e^2qQ/\hbar$

The situation of spin-3/2 and spin-5/2 with $\eta=0$, are shown in Figure 5. The central transition is unshifted. The other transitions are called 'satellite' transitions. In a glass or powdered crystal, all possible orientations will be equally likely and the resulting line shape will be a "powder pattern" shown in the last part of Figure 2.6.

There are several interactions in solids for example quadrupole, dipole-dipole and chemical shift anisotropy, and it is interesting to point out that all have the same orientation dependence $(3\cos^2\theta-1)$ which causes an inhomogeneous broadening on the spectra. More details of orientation effect on spectra will be discuss later.

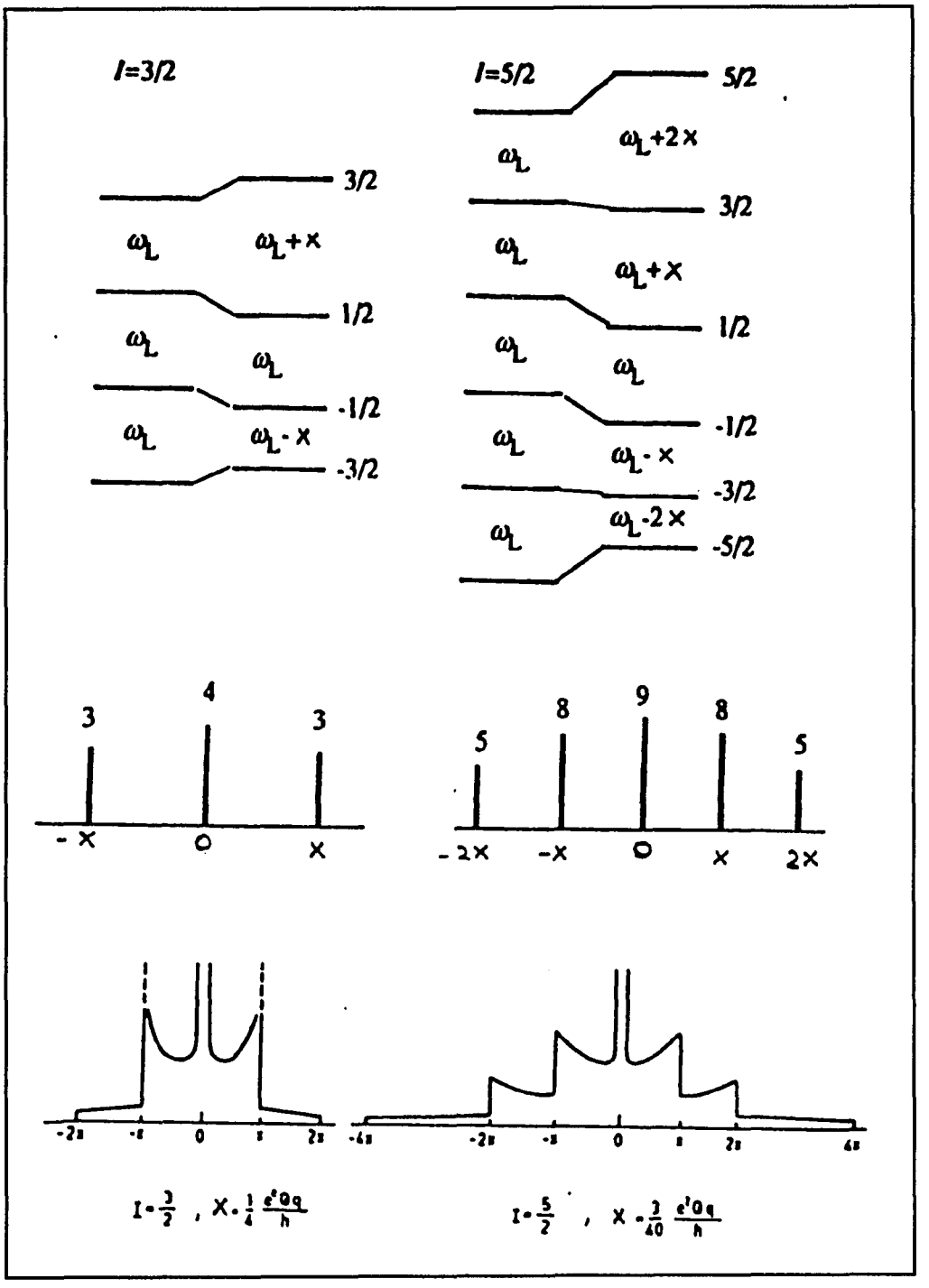

Figure 2.6: a) The energy levels b) Spectrum of single crystal c) Powder pattern.

2.6 Chemical shift anisotropy: MAS/NMR Spectroscopy

The magnetic coupling of the electrons to the nucleus arises from the magnetic field originating from the motion of the electrical charges. This gives rise to the so called Chemical shift. The nuclei experience fields of local origin that are different for different molecular surroundings. If nuclei see a magnetic field ΔH in addition to the applied field $\mathbf{H_o}$, we may say the resonance frequency ω obeys the equation

$$\omega = \gamma(\mathbf{H_o} + \Delta H).$$

Because $\Delta H \propto \mathbf{H_o}$, we may therefore define a quantity σ by the equation

$$\Delta H = -\sigma \mathbf{H_o}.$$

The Hamiltonian for this interaction can be written as

$$H_C = \gamma \hbar I \bullet \bar{\sigma} \bullet H$$

where σ is the chemical shift tensor. The shift in the NMR resonance frequency is,

$$\nu = \nu_o (1 - \sigma_{zz})$$

where σ_{zz} is the component of the shift tensor along the direction of $\mathbf{H}$. σ_{zz} can be expressed in terms of the diagonal components in its principal axis system as

$$\sigma_{zz} = \sum_{1}^{3} \sigma_i \cos^2\phi_i$$

where ϕ_i angle between the magnetic field and principal axis.

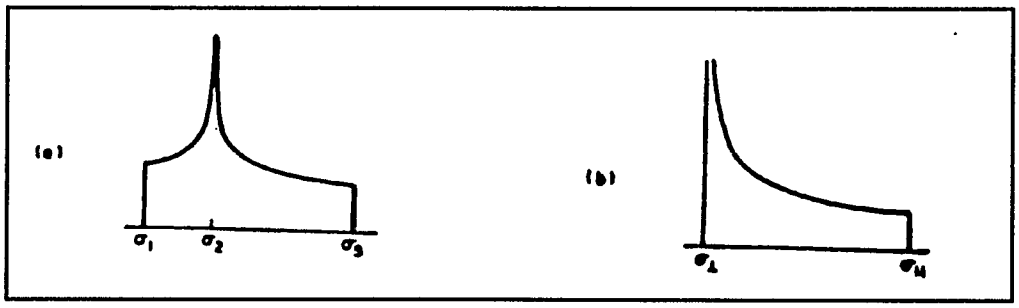

Figure 2.7: NMR line shapes for polycrystalline samples with a)axially asymmetric b)axially symmetric chemical shielding tensors. The principal values σ_1, σ_2, σ_3, can be read off directly.

For axial symmetry, $\sigma_1 = \sigma_2 = \sigma_\perp$ and $\sigma_3 = \sigma_\parallel$.

In ordinary isotropic fluid, $\sigma_{zz} = (1/3)\,(\sigma_1 + \sigma_2 + \sigma_3) = \sigma$.

MAS/NMR techniques [35] were first developed to average out broadening of NMR spectra due to anisotropy interactions. The Hamiltonian which describes the NMR spectrum of a solid may be written as the sum of four terms:

$$H = H_Z + H_Q + H_D + H_C$$

Which are respectively the Zeeman, Electric Quadrupolar, Magnetic Dipolar, and Chemical shift terms. When the solid is rotated with uniform frequency ν_r about an axis inclined at angle β to $\mathbf{H}_o$ as shown in Figure 2.8, all the anisotropic terms in the Hamiltonian become time dependent with periodicity ν_r. Thus the Zeeman term is not affected by the motion, but all the other three are affected. These three terms are often small compared to the Zeeman term and are treated as perturbations. It is convenient to divide the Hamiltonian into two parts

$$H = \bar{H} + H(t),$$

where H is the time average of the Hamiltonian, while H(t) is the time-dependent part.

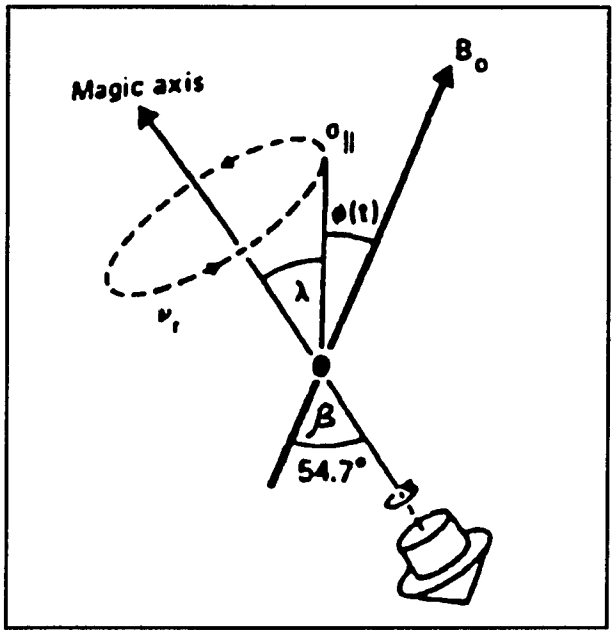

Figure 2.8: Diagram illustrating the geometry of the MAS experiment when a solid is rotated with frequency ν_r about an axis inclined at angle β to $\mathbf{H}_o$.

The angle ϕ_i becomes time dependent and can be expressed in terms of other angles of the system:

$$\cos \phi_i = \cos \beta \cos \lambda_i + \sin \beta \sin \lambda_i \cos(\nu_r t)$$

where λ_i is the angle between the rotational axis and principal axis. Using the above mathematical identity one can easily show the time average of $\cos^2 \phi_i(t)$ to be given by

$$<\cos^2 \phi_i(t)> = (1/6)(3\cos^2 \beta - 1)(3\cos^2 \lambda_i - 1) + 1/3.$$

Taking the time average we find that for each nucleus:

$$\bar{\sigma}_{zz} = \sum_{1}^{3} \sigma_i \langle \cos^2\phi_i \rangle = \sigma + (1/2)(3\cos^2\beta - 1)\sum_{i} \sigma_i \cos^2\lambda_i .$$

When β is 54.7° the so called "magic angle" $\cos^2 \beta = 1/3$, and the second term of above equation become zero. Then the average part of Hamiltonian of the Chemical shift are found to be

$$\bar{H} = \hbar \gamma \sigma I H_o .$$

This is precisely the form of NMR Hamiltonian in an isotropic fluid. Now we consider the time dependent part of the Hamiltonian $H_c(t)$. Again using the above mathematical identity we can obtain

$$H(t) = \hbar \gamma I \sigma_{zz}(t) H_o = \frac{\hbar}{2} \gamma I H_o \sum_{1}^{3} \sigma_i [\sin 2\beta \sin 2\lambda_i \cos 2\pi \nu_r t + \sin^2\beta \sin^2\lambda_i \cos 4\pi \nu_r t] .$$

This part thus consists of two terms periodic in ν_r and $2\nu_r$. When the spinning frequency is less than the Chemical shift anisotropy, this generates satellite spectra set on either side of the central resonance spectrum at integer multiples of ν_r. The intensities of the spinning sidebands are related to the chemical shift anisotropy and provide an opportunity to recover the chemical shift parameters. However as the rate of rotation increases the satellites move further out and become weaker.In this way, the anisotropy broadening interactions due to Quadrupolar, Dipolar, and Chemical shift in the original Hamiltonian are effectively removed by rotating about the magic axis. The intensity of any visible satellites reflect the original anisotropy. Methods have been developed to recover this information.

2.7 Relaxation

The observation of resonance requires the absorption of electromagnetic energy associated with a transition of nuclear spins from lower to upper energy level, and if this were the only operative factor the populations would soon be equalized. A number of additional phenomena, however, act to restore thermal equilibrium with the lattice and these are known as relaxation processes.

From the thermodynamic point of view the spins may be consider as an isolated system. Incident RF pulse transfer "heat" to the spins and raises their "spin temperature". The relaxation mechanisms transfer "heat" to the lattice bath and thus restore thermal equilibrium.The rate of this energy transfer is measured by the spin-lattice relaxation time T_1. Usually growth of magnetization along z direction M_z can be described by an exponential function,

$$M_z(t)=M_o\,[1\text{-}\exp.(t/\tau)]$$

where M_o is the equilibrium net magnetization.

Spin-spin relaxation, also called transverse relaxation T_2, is a process in which the magnetization in the X'-Y' plane, perpendicular to the static laboratory field decays. Figure 2.9 exhibits the process of the relaxation corresponding to the variation of magnetization **M** in a rotating frame.

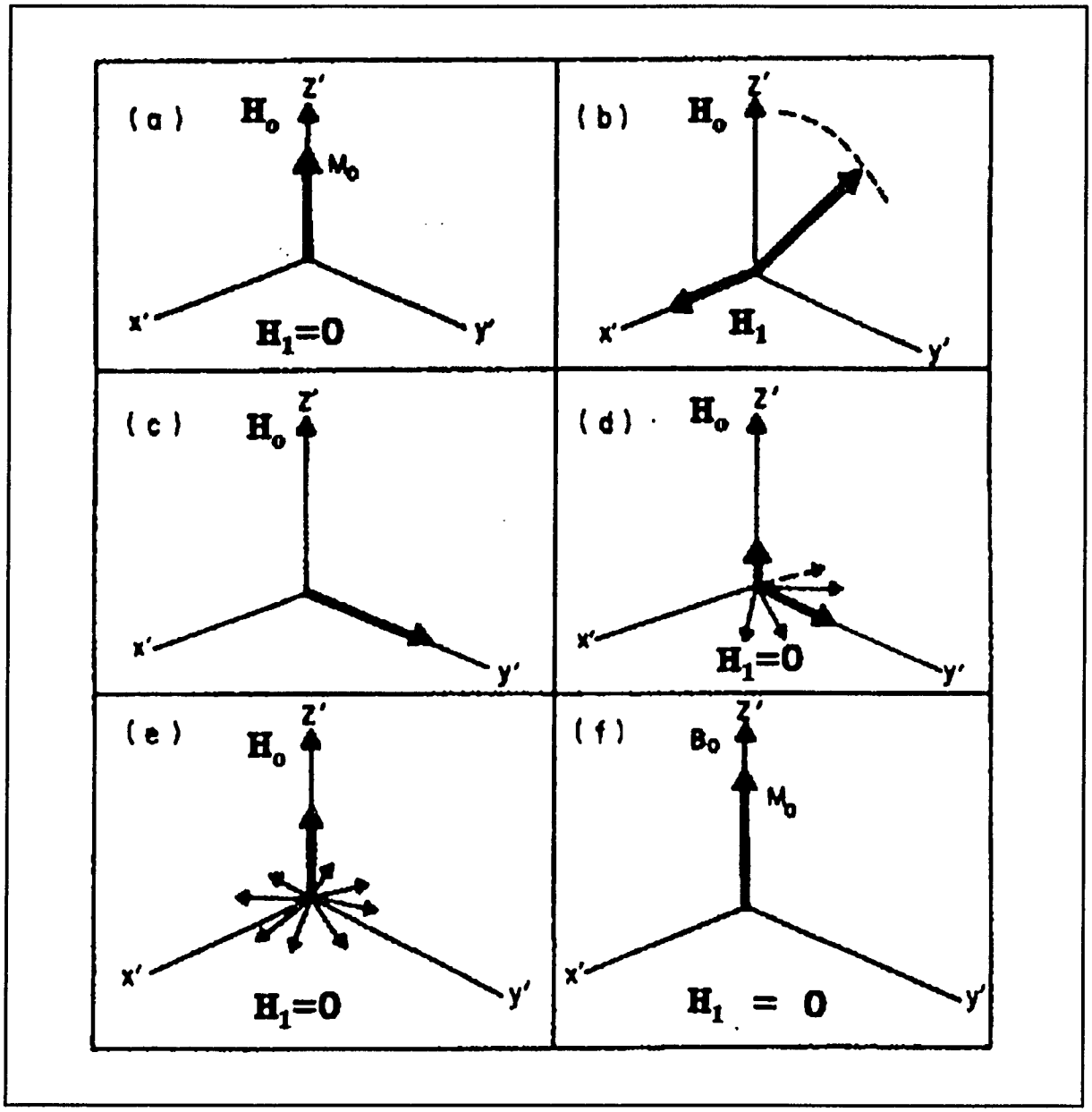

Figure 2.9: Relaxation described by rotating-frame Diagrams. a) The net M_o is aligned with H_o. b) and c) An RF pulse H_1 is applied perpendicular to H_o. The duration of H_1 is sufficient to tip the net magnetization by $\pi/2$. d) and e) The spins begin to relax in the x'-y' plane by spin-spin (T_2)relaxation processes and in the z' direction by spin-lattice (T_1) relaxation processes. f) The equilibrium magnetization M_o is reestablished along H_o.

In order to undergo a transition, the nucleus needs to see fields fluctuating at its Larmor frequency. There are two randomly fluctuating fields effective in NMR relaxation. One is time varying magnetic fields which can interact with the nuclear magnetic dipole moments (dipole-dipole relaxation) and the other is fluctuating electric field gradient (EFG) which can interact with the quadrupole moment (quadrupolar relaxation) of the nucleus. Each one gives rise to a spin-lattice relaxation mechanism. The important point to get out of all this is that since spin-lattice relaxation processes usually depend on the existence of molecular motion to generate randomly fluctuating magnetic fields or EFG's, we can get valuable information about these motions from the measurement of relaxation rates T_1 and T_2. The EFG variation will be manifested by a spread in resonance frequencies of NQR (characterized by T_2^*) with analogy to static magnetic field inhomogeneities in NMR.

In the case of random molecular motions, the correlation time is defined as the time in which a molecule remains in any given position before a collision causes it to change its position or orientation, and the correlation function is given in the form of [36]

$$G(t) = G(0) \exp(t/\tau_c).$$

This function defines the position of molecule at time t relative to its position at an arbitrary initial time G(0). The equation says that the new position, G(t), is related to the initial position in an exponential manner. The correlation time τ_c is very small for a molecule with a fast average motion. The frequency spectrum corresponding to the correlation function G(t), obtained by Fourier analysis, can be defined as [36]

$$J(\omega) = \int_{-\infty}^{\infty} G(t) e^{-i\omega t} d\tau = G(o)\left[\frac{\tau_c}{1+\omega^2\tau_c^2}\right]$$

where J(ω) is called the spectral density function.

The relationship between T_1, T_2 and J(ω) can be derived through time dependent perturbation theory as was done originaly by Blombergen, Purcell, and Pound (BPP)[37]. Here we list the result in the case for a model of random molecular rotation from reference[38]. For spin I=1, the relaxation rate $1/T_{1Q}$ contributed by quadrupole interactions with afluctuating EFG is

$$\frac{1}{T_{1Q}} = \frac{3}{40}\left(1+\frac{\eta^2}{3}\right)\left(\frac{e^2qQ}{\hbar}\right)^2\left[\frac{\tau_c}{1+\omega^2\tau_c^2} + \frac{4\tau_c}{1+4\omega^2\tau_c^2}\right]$$

In the extreme narrowing case, $\omega\tau_c << 1$,

$$\frac{1}{T_{1Q}} = \frac{3}{8}\left(1+\frac{\eta^2}{3}\right)\left(\frac{e^2qQ}{\hbar}\right)^2\tau_c$$

The relaxation rate contributed by the dipole interaction for like spins $1/T_{1D}$ is[]

$$\frac{1}{T_{1D}} = \frac{2}{5}\frac{\gamma_D^4\hbar^2}{r^6}I(I+1)\left[\frac{\tau_c}{1+\omega^2\tau_c^2} + \frac{4\tau_c}{1+4\omega^2\tau_c^2}\right]$$

Then the total relaxation rate for deuteron pair in D_2O can be written as

$$\frac{1}{T_1}(^2H) = \frac{1}{T_{1Q}} + \frac{1}{T_{1D}}$$

where the quadrupole term is much stronger than the dipole term for deuteron NMR.

Similar equations hava been derived for spin-spin relaxation rates for spin I=1 due

to quadrupole and dipole relaxation. They can be written as,

$$\frac{1}{T_{2Q}} = \frac{3}{80}\left(1+\frac{\eta^2}{3}\right)\left(\frac{e^2qQ}{\hbar}\right)^2\left[3\tau_c + \frac{5\tau_c}{1+\omega^2\tau_c^2} + \frac{2\tau_c}{1+4\omega^2\tau_c^2}\right]$$

$$\frac{1}{T_{2D}} = \frac{\gamma_D^4\hbar^2}{r^6}I(I+1)\left[\frac{3\tau_c}{5} + \frac{5\tau_c}{1+\omega^2\tau_c^2} + \frac{16}{15}\frac{\tau_c}{1+4\omega^2\tau_c^2}\right]$$

Again, total spin-spin relaxation rate is given by the sum of the two rates,

$$\frac{1}{T_2}(^2H) = \frac{1}{T_{2Q}} + \frac{1}{T_{2D}}$$

In this work the dipolar contribution to the total relaxation rate and also to the line width of the spectrum are very much smaller than those due to the quadrupolar effect.

The relaxation time T_1 vs. correlation time τ at a fixed frequency is plotted in Figure 2.10.

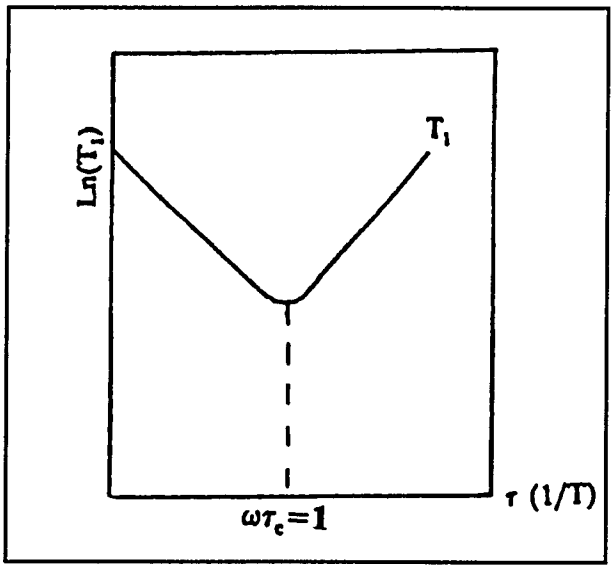

Figure 2.10: Spin-lattice relaxation time T_1 as a function of correlation time τ or reciprocal of temperature (1/T).

The curve shows a minimum value of T_1 at $\omega\tau_c \approx 1$, this means that the frequency of molecular motion is comparable with Larmor frequency at that temperature. So that the relaxation is most efficient and leads to the minimum of T_1. In the higher temperature region, the frequency of molecular motion is too fast to relax efficiently at the Larmor frequency and results in a longer T_1. On the right side of the T_1 minimum (low temperature region), as the temperature decrease, the molecules motion become slower than the Larmor frequency, and the contribution to the relaxation also become smaller and results in a longer value of T_1.

2.8 Orientation effect

As we seen before in Figure 2.5, NMR interactions cause line splitting. In the quadrupole case the magnitude of the splitting depends on ω_Q and on the orientation factor $(3\cos^2\theta\text{-}1)$. In the liquid state, the angular factor will be averaged to zero by isotropic motion of the molecules, therefore, no splitting effect is observed. In a solid the line splitting is a characteristic of the degree of solidstate molecular orientation. One extreme case is that the molecule is isotropically oriented, for example a rigid solid powder sample, where the orientation effect contributed by all nuclei results in a special line shape called Pake's pattern. For a sample (spin-1/2 dipole-dipole or spin-1 quadrupole) that is partially oriented, the splitting can be seen but the separation may be reduced due to averaging by molecular motions. If this motion is anisotropic then there will be a residual orientation present. So the orientation-dependent information could be used to determine the orientation of the specific functional group in a solid sample as well as the degree of motion of molecules. Figure 2.11 shows the deuteron spectra for

different situations. Where S_{OD} describe the degree of molecular orientation ($0 \leq S_{OD} \leq$).

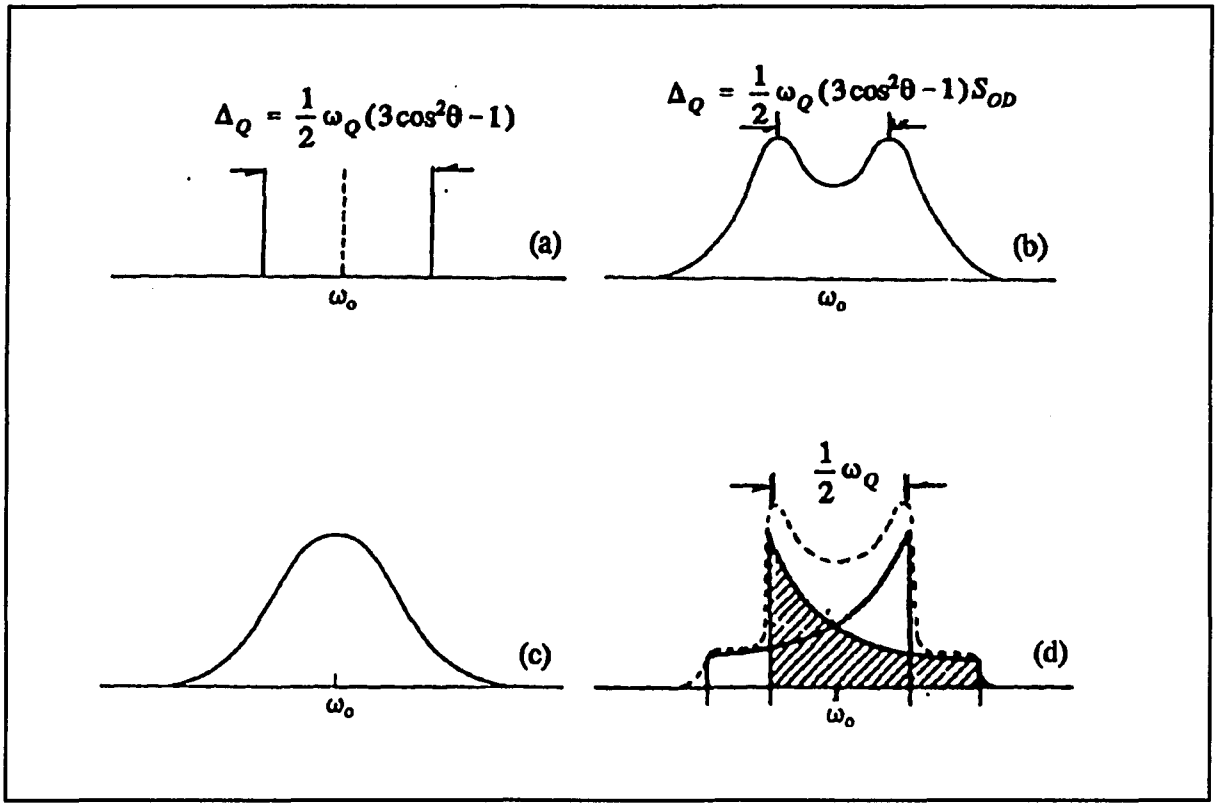

Figure 2.11: Effect of quadrupole interaction: (a) an isolated deuteron, (b) many deuterons interacted each other with partially oriented, (c) motional narrowing, (d) Pake's pattern corresponds to a powder or an isotropically oriented static sample.

2.9 Pulse sequences

In our NMR work the following pulse sequences used: a single pulse, an inversion recovery sequence, and a quadrupole echo (solid echo) sequence. A single pulse is used to obtain the FID, and Fourier transformation then yields the NMR absorption spectrum. The inversion recovery sequence is shown in Figure 2.12 and is used to measure T_1 [25,39]. It consists of a π_x pulse followed by $(\pi/2)_x$ separated by time τ. The equilibrium magnetization M_0 is inverted by the first pulse then relaxes back towards z-axis during

the interval time τ and finally tips to x'-y' plane by the second pulse. Specifically, the magnetization as a function of the pulse spacing time τ is given by

$$M(\tau) = M_0(1-2e^{-\tau/T1}).$$

By varying the value of τ, we can get a set of $M(\tau)$ data which can be fit in the above equation to find T_1. T_1 can also be measured approximately using the single τ_0 value, where $\tau_0 = T_1/\ln 2$ corresponding a null signal.

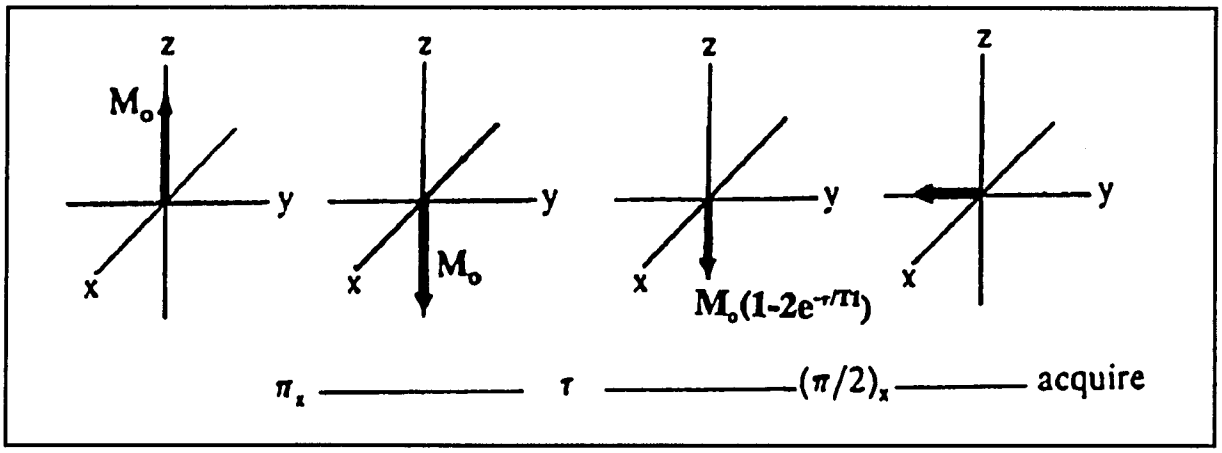

Figure 2.12: The inversion recovery sequence method for T_1 measurement.

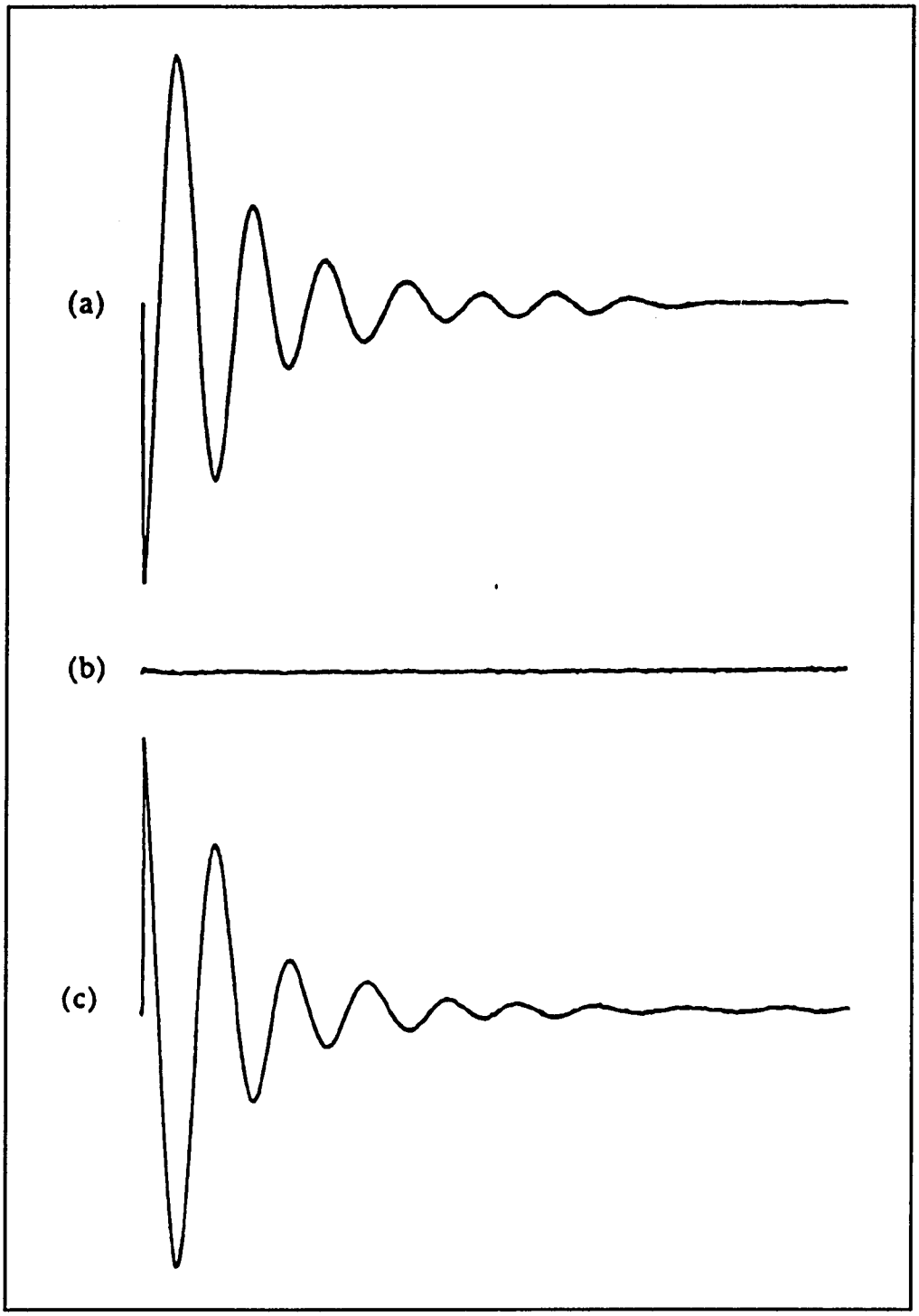

Figure 2.13 : FID signal after applying inversion recovery sequence. a) $\tau < \tau_o$, b) $\tau = \tau_o$, and c) $\tau > \tau_o$, where $\tau_o = T_1/\ln 2$ corresponding a null signal.

The quadrupole echo sequence is useful when the induction signal decays very rapidly for instance because of quadrupole broadening at low temperature. In this case, the time for decay is too short so that the lineshape investigations in solid is limited by the "deadtime" of the spectrometer. This sequence enables us to get a refocused signal. It consists of $(\pi/2)_x$, $(\pi/2)_y$ pulses separated by τ and the acquisition of the signal starts at $t=2\tau$.

Chapter 3

Experimental Investigations of the Strong Off-Resonance Comb (SORC) Pulse Sequence[1]

3.1 Introduction

The behavior of induction signals during steady state pulse irradiations in ^{14}N NQR was investigated experimentally. It has been known [40] that the signal response to a long sequence of RF pulses will dramatically increase for pulse spacing less than T_2. This increase is exponential, and can result in signals comparable to optimally prepared FID signal. Because these SORC signals recur as long as the pulsing continues, very efficient signal averaging can result. The dependence of these steady-state signals on pulse parameters and on frequency offset are presented, together with a discussion of the applicability of the method.

The steady state response of an ensemble of nuclear spins, I=1/2, in high field H_0 to a strong radio frequency field H_1 applied off-resonance by an amount Δf has long been known [40,34]. When the conditions for the establishment of a spin temperature in the rotating frame are met [34], the x-component of the magnetization, which is experimentally observable, is given by

$$M_x = M_0 \frac{H_1 \, 2\pi \, \Delta f/\gamma}{H_1^2 + H_{loc}^2 + (2\pi \Delta f/\gamma)^2} \qquad (3.1)$$

where M_0 is the equilibrium longitudinal magnetization, γ is the magnetogyric ratio of

---

This work is published as reference #2 with R.A.Marino and S.S.Kim

the nucleus, and H_{loc} is a measure of the local field at the nuclear site under study due to its neighbors. Results analogous to Eq. 3.1 have also been derived and observed [41,42] for a quadrupolar system with nuclear spin I = 3/2 when subjected to the analogous strong, long, near-resonant irradiation H_1.

In this work we are concerned with the pulsed analogue of these experiments for a quadrupolar system. The field H_1 is applied as a long train of equally spaced identical pulses, i.e., a long comb, rather than as a continuous wave (cw). This experimental work is concerned with quadrupolar systems with spin I=1.

3.2 Experimental Details

A Matec 1kW pulsed spectrometer was used to detect the NQR induction signals. A block diagram of the spectrometer is shown in Figure 3.1. The frequency synthesizer produces continuous wave signal of near one volt r.m.s. at the nuclear resonance frequency. This sine-wave signal is fed into the gated amplifier and also into the receiver for phase sensitive detection. The gated amplifier has pulse power of 1kW and 50Ω output impedance, it amplifies the cw signal into the desired pulse sequence to about a few hundred volts. The impedance matching network steps up the pulse voltage from the gated amplifier to few thousand volts to the sample coil and isolates the sample and receiver from the amplifier during the time NQR signals are being detected. A single coil is used for both exciting and picking up signals from the nuclei. The signal averager coherently adds up NQR signals and increases the signal-to-noice ratio by the square root of the number of counts.

Figure 3.2a shows the parameters of the SORC sequence. A long train of radio-

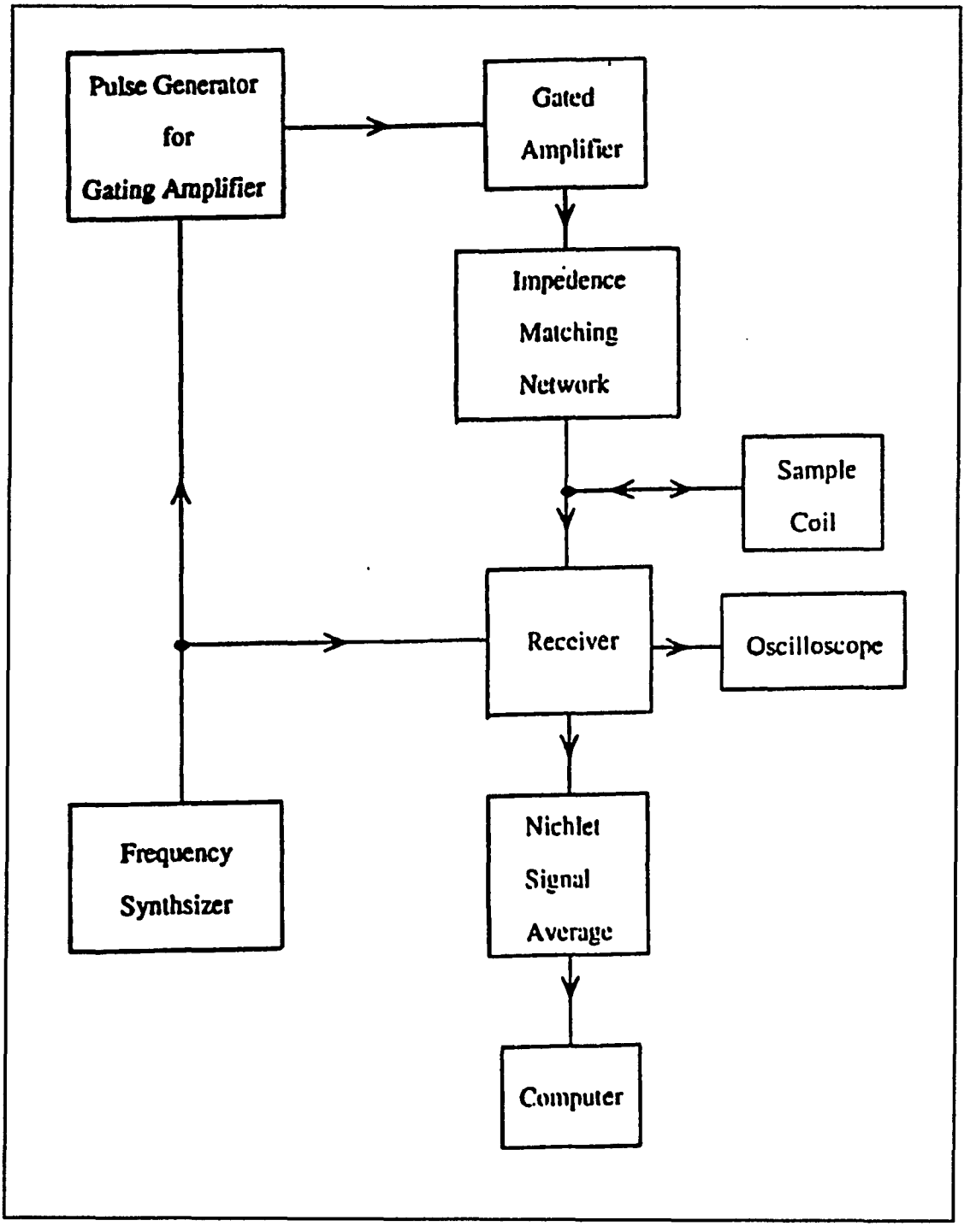

Figure 3.1 :Block diagram of the Matec pulse spectrometer.

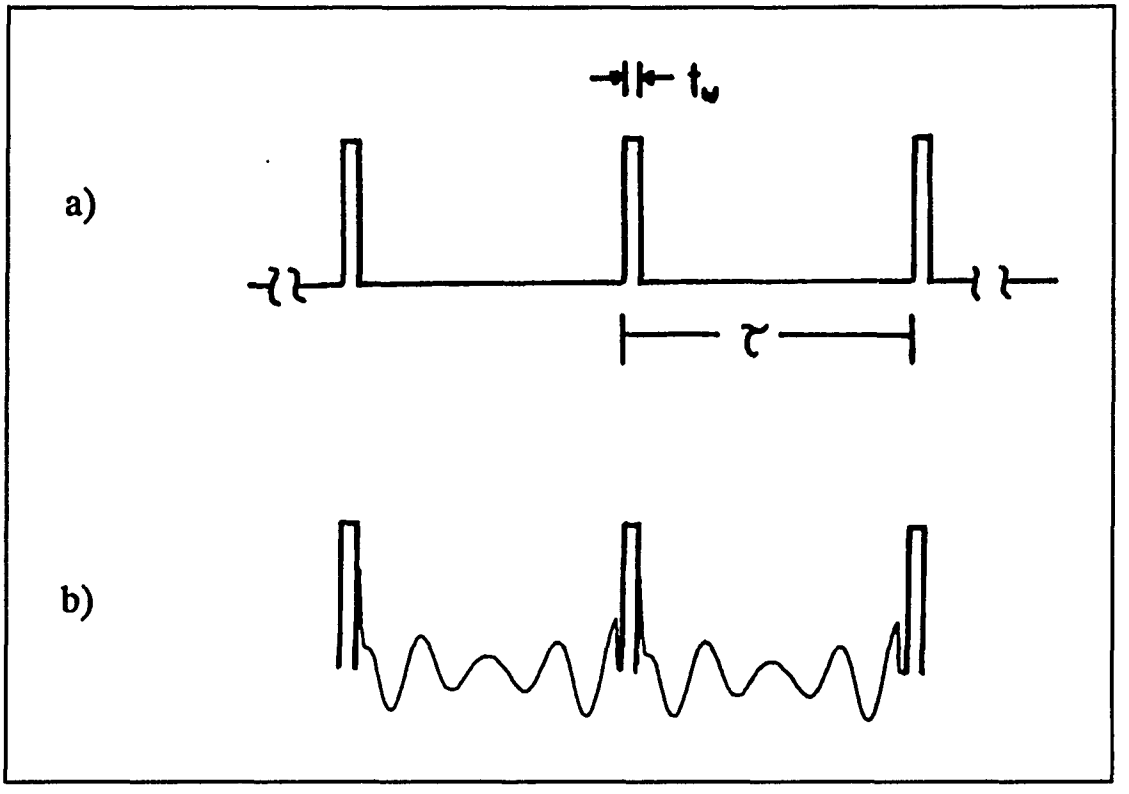

Figure 3.2 : "SORC" sequence parameter. a) A long train of RF pulses, each of width t_w and spacing τ, is applied Δf away from exact resonance. b) Nuclear induction signals are received between pulses.

frequency pulses, each of duration t_w and spacing τ is applied to a pure nuclear electric quadrupole system Δf away from exact resonance in zero external magnetic field. If H_1 is the magnitude of the rf field during irradiation pulses, one can define the time-average of this quantity over the whole experiment as $\langle H_1 \rangle = H_1 t_w/\tau$. This work is concerned with the signal observed in the time interval between pulses after the SORC sequence has been applied for a time sufficient to establish a steady state, of the order of a few $T_{1\rho}$. A typical result is shown in Figure 3.2b.

Data were taken on two different NQR transitions, both at liquid nitrogen temperature. One was the ν_- line of Sodium Nitrite at 3757 kHz [11]. The other, chosen because of its relatively long spin-spin relaxation time, was the ν_+ line of 4-picoline at 3688 kHz [12]. The value of the relaxation times (T_1, T_2, T_2^*), respectively for the two transitions, were measured to be approximately (34 s, 10 ms, 3 ms) and (6 s, 25 ms, 6 ms). The spin-lattice relaxation time T_1 was measured using the method of progressive saturation [43]. The spin-spin relaxation time T_2 was measured from the two-pulse spin-echo decay, and the line-shape parameter T_2^* was estimated from the displayed FID signal. Data were coherently summed using a Nicolet 1170 signal averager.

3.3 Results and Discussion

A commonly used method [43] to estimate T_1 monitors the decrease of the size of the FID signal following each pulse in a long series of rf pulses with spacing $\tau \geq T_1$. Typical data obtained in this way are shown in Fig. 3.3a, which displays both the size of the fully relaxed FID signal and its decrease at higher pulse repetition rates, i.e., smaller values of τ. In this paper we are concerned with what happens when the pulse

Figure 3a →

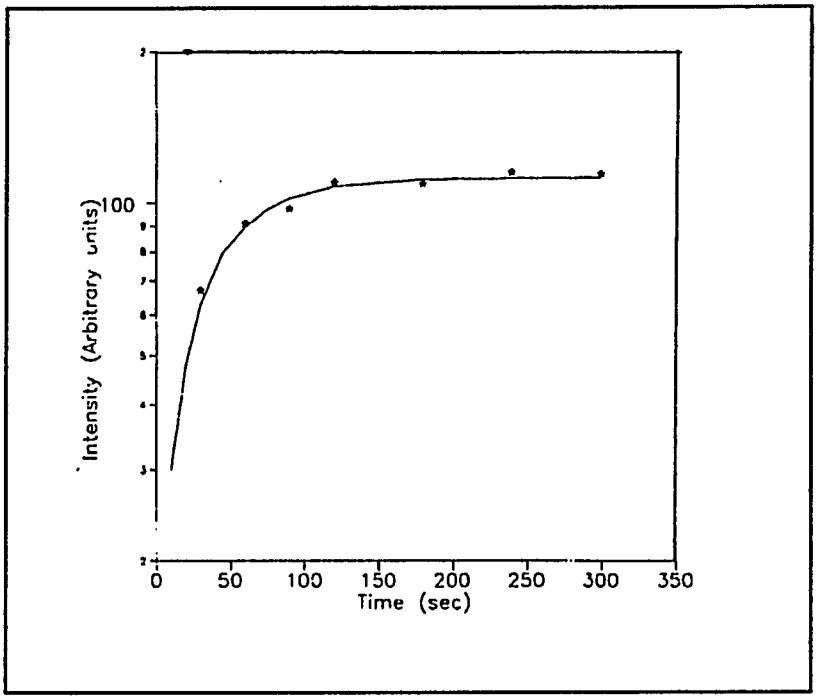

Figure 3b →

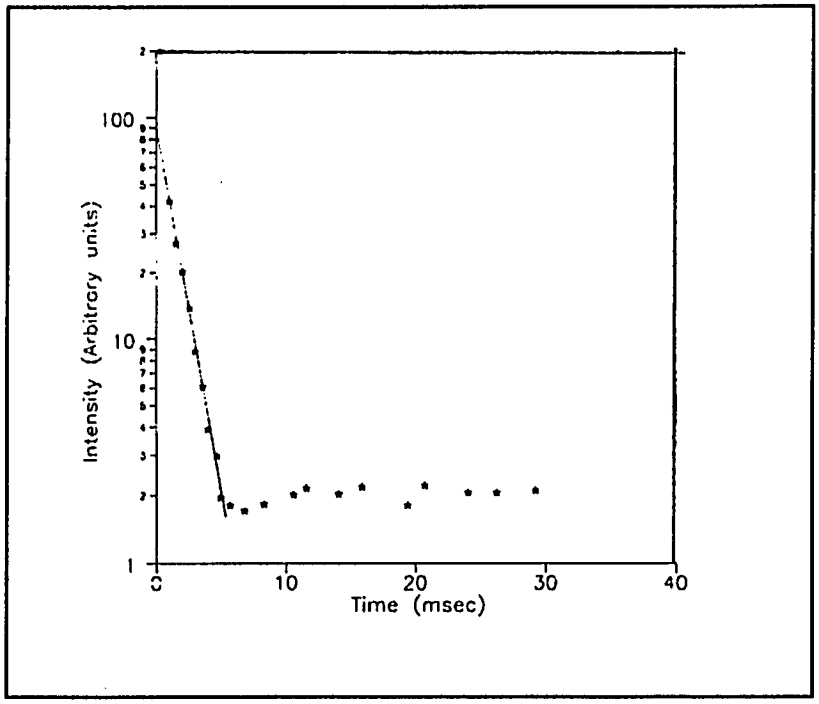

Figure 3.3 : Amplitude of FID signal vs. pulse spacing τ for $NaNO_2$ ν_- line at 77K. a) Data shown are for the long τ region and show expected T_1 behavior. b) Data for short τ region show exponentially increasing SORC signal for τ approaching zero.
Note : Signal intensities for short and long τ are comparable in magnitude.

spacing τ is further reduced, to values of the order of T_2 or lower. Fig. 3.3b shows the size of the FID signal obtained for the same sample that yielded the data plotted in Fig.3.3a, but for much shorter values of τ. The calibration of the vertical scales for both parts of Fig. 3.3 is identical. Also, in both cases the transmitter frequency was set slightly off resonance. Fig. 3.3b depicts the remarkable result that as the pulse spacing is further reduced, the nuclear induction signal begins to increase in magnitude exponentially and reaches values comparable to the fully relaxed FID in the limit of $\tau \mapsto 0$. Furthermore, the signal is rapidly repeated every τ seconds, enabling very efficient signal averaging. The exponential decay time in Fig. 3.3b is about 1 msec, a value about an order of magnitude lower than the measured value of T_2 in this material.

The signal available in the "observation window" between successive rf pulses actually consists of the sum of two separate signals, a decaying signal after the pulse and a rising signal before the pulse. These might be considered two halves of an echo signal bisected by the rf pulse. When T_2^* is sufficiently smaller than τ, the two signals are each present at the ends of the observation window and do not overlap. For smaller τ, the two signals begin to overlap in the middle of the window and can therefore destructively interfere with one another as τ is further decreased. Fig. 3.4 depicts this interference phenomenon for the NQR transitions we have studied. Note that the vertical scale is logarithmic and that under some conditions destructive interference can cause a signal decrease of as much as an order of magnitude. The effect is much more pronounced in 4-picoline where the linewidth is narrower and the relaxation time T_2 is longer than in Sodium Nitrite. The distance $\Delta\tau$ between interference minima or maxima in Fig. 3.4 is given by the condition

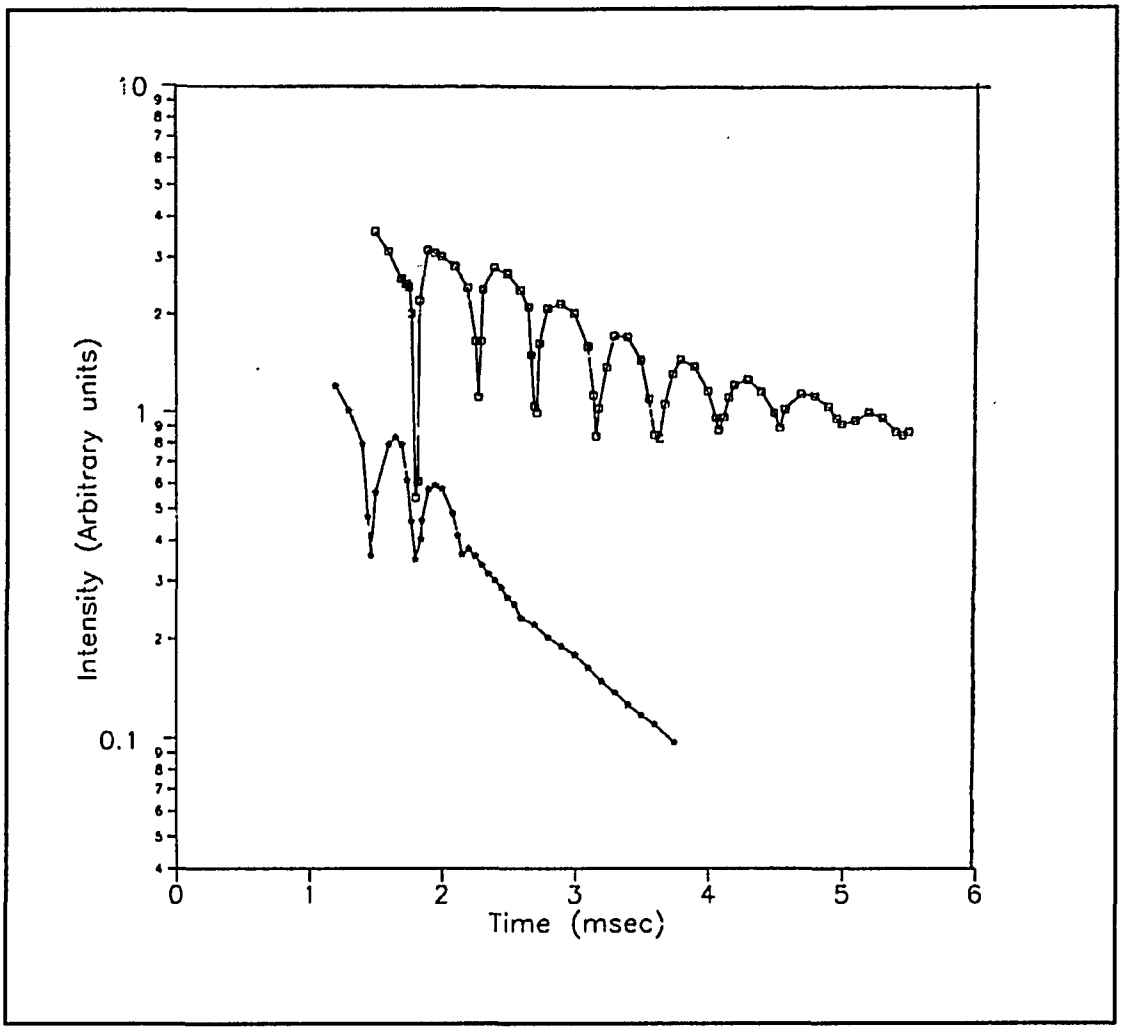

Figure 3.4 : Amplitude of SORC signal vs. pulse spacing. Note modulation effect due to interference of signals when $\tau\Delta f = n + 1/2$, a half-integer.

$$\Delta\tau\,\Delta f = 1 \tag{3.2}$$

where Δf, the transmitter offset from exact resonance, is also the frequency of the induction signal after phase-sensitive detection.

We measured the intensity of the SORC signal as a function of the pulse height H_1, the pulse spacing τ, and the pulse width t_w, for a given resonance offset Δf. The results are plotted in Fig. 3.5a for Sodium Nitrite, and Fig 3.5b for 4-picoline. The data clearly show that the signal intensities fall on a family of curves analogous to Eq.3.1:

$$M_x = M_0(\tau)\frac{\langle H_1\rangle}{\langle H_1\rangle^2 + h^2} \tag{3.3}$$

where h is an adjustable parameter.

Consideration of the data in Fig. 3.5a and 3.5b leads us to conclude that the time-averaged rf field $\langle H_1\rangle$ is indeed the proper variable to consider, and the data are well explained by an equation like Eq. (3.1). Furthermore, when the variation of the signal amplitude vs. Δf is studied, the results are also consistent with the functional dependence given by Eq. (3.1). Figs. 3.5a and 3.5b also show that the maximum value of the induction signal for a particular value of τ depends on τ. This observation is summarized in Fig. 3.6. This figure contains the departure from the first-order theory summarized by Eq. 3.3; it is the part of the data that depends intimately on the **pulsed** nature of the SORC experiment. An explanation of Fig. 3.5 will be the aim of a theory that takes into account subsequent Fourier components of the SORC irradiation. In particular, the physical meaning of the parameter h would have to be explained. In the cw theory, h reflects both the frequency offset and the local field, as is clear from a comparison of

Figure 5a →

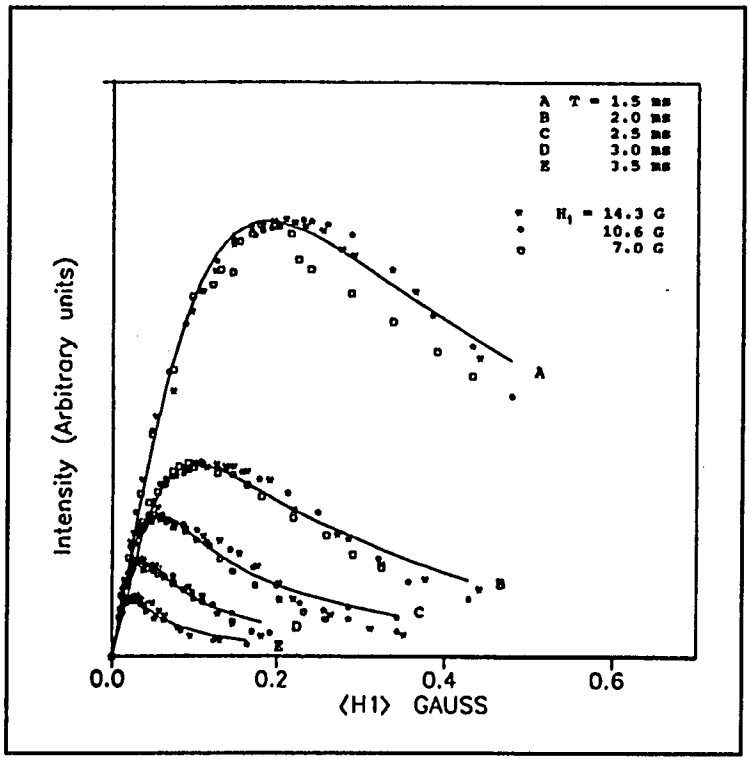

Figure 5b →

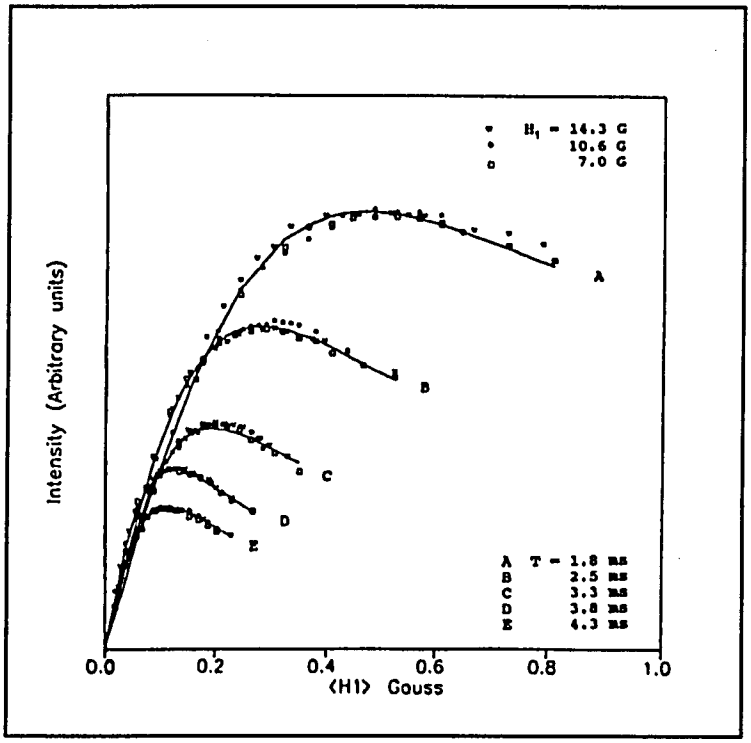

Figure 3.5 : Intensity of nuclear induction signal in **SORC** excitation vs. the time average of the RF field strength, $\langle H_1 \rangle = H_1 t_w/\tau$. a) Data for Sodium Nitrite. b) Data for 4-picoline. The solid curves are a fit to the function, $\langle H_1 \rangle / [\langle H_1 \rangle^2 + B^2]$.

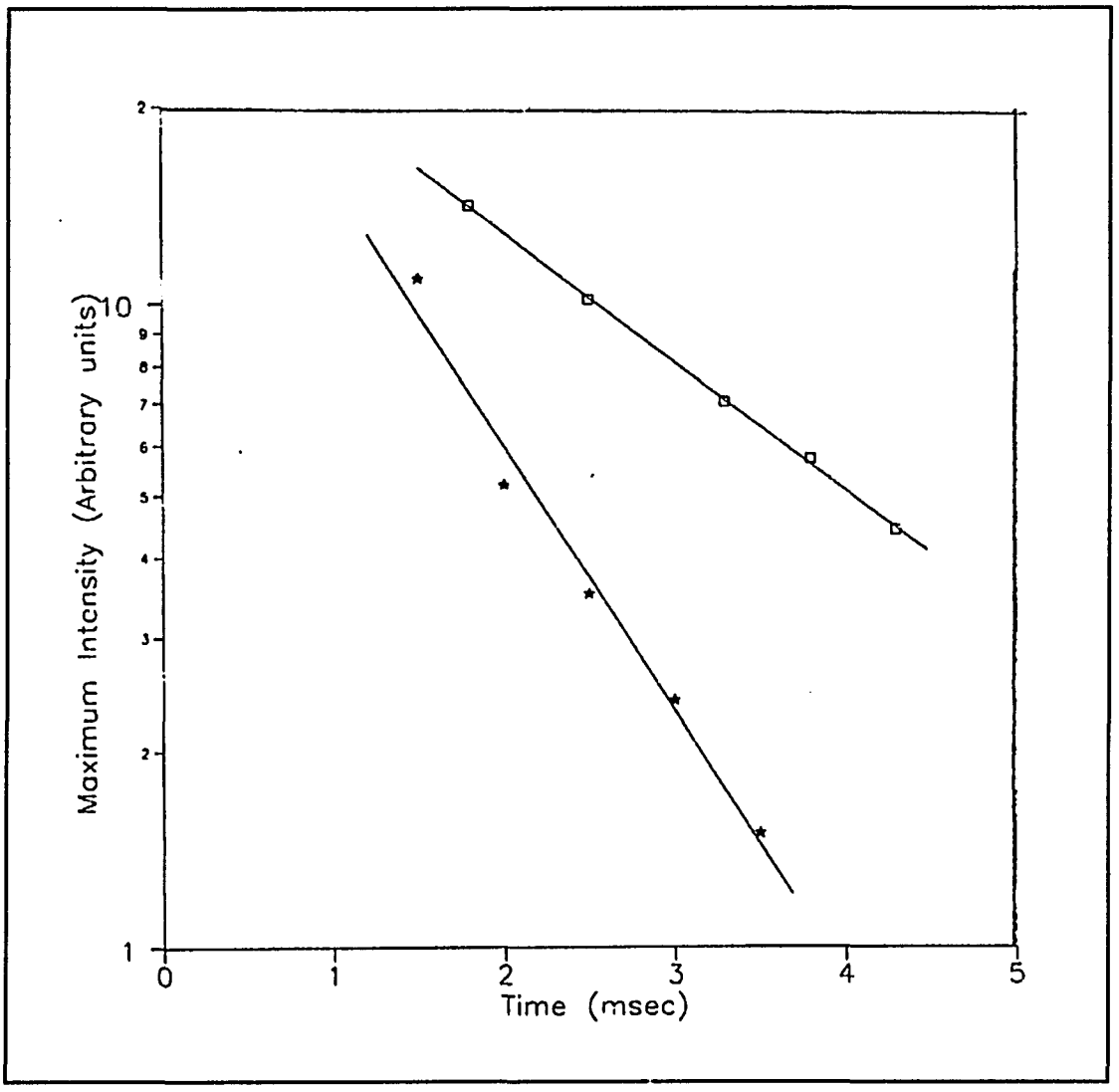

Figure 3.6: Maximum induction signals fall exponentially with the pulse spacing, τ. The decay constants are 1.1 and 2.2 msec, respectively, for Sodium nitrite and 4-picoline. These times about an order of magnitude lower than the corresponding values of T_2.

Eq. 3.1 and Eq. 3.3. However, the experimental values of h obtained in these pulsed SORC experiments are uniformly too low. Explaining this discrepancy remains one of the aims of a more complete theory.

Fig. 3.6 is presented to underline the observation that the size of the optimized SORC signal falls exponentially with the pulse spacing τ. Then, any experimental devices that reduce the pulse recovery time, thus enabling smaller values of τ to be used, can result in considerably larger signals. It is useful to present the data in Fig. 3.6 in a way that directly answers the question, What must be the flip-angle of each pulse to obtain the biggest SORC signal? The empirical answer is depicted in Fig. 3.7. The optimum value of the flip angle is itself a strong function of τ. Note that the extrapolation to zero τ gives a value of the flip angle comparable to the optimum value for observing a fully relaxed FID, which was 0.8×10^{-3} Gauss-seconds for our experimental conditions.

Finally, we would like to address the question of how the parameters M_0 and h, defined in Equation 3.4, depend on τ. Least square fits to the data, shown in Figures 3.5a and 3.5b, allow us to extract these parameters and to present their variation with τ. This is done in Figures 3.8 and 3.9. The data points plotted in these two figures clearly show exponential dependence on τ.

The decay constants for the amplitude parameter M_0 are 0.50 msec and 0.96 msec, respectively, for Sodium Nitrite and 4-Picoline. For the more interesting parameter h, the decay constants are 0.96 msec and 1.7 msec, respectively. In both cases the rough 1:2 ratio which holds for thir spin-spin relaxation times seems to be approximately preserved. In the limit of zero τ, the parameter h becomes 0.79 Gauss and 1.3 Gauss for Sodium Nitrite and 4-Picoline, respectively. These values might appear to be comparable

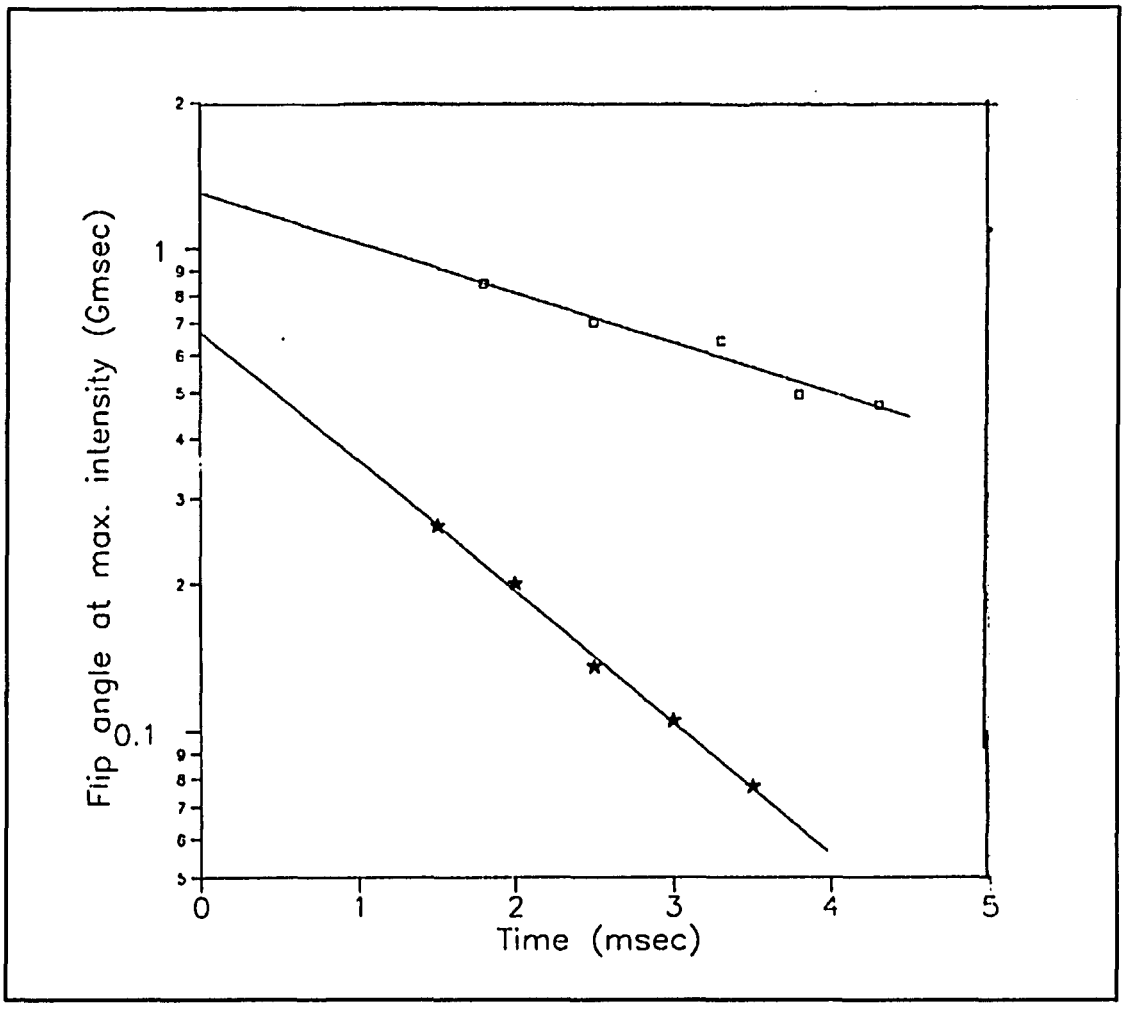

Figure 3.7 : The "flip angle" necessary to obtain maximum **SORC** response vs. the pulse spacing τ. In the limit of short τ the flip angle approaches the "$\pi/2$" value.

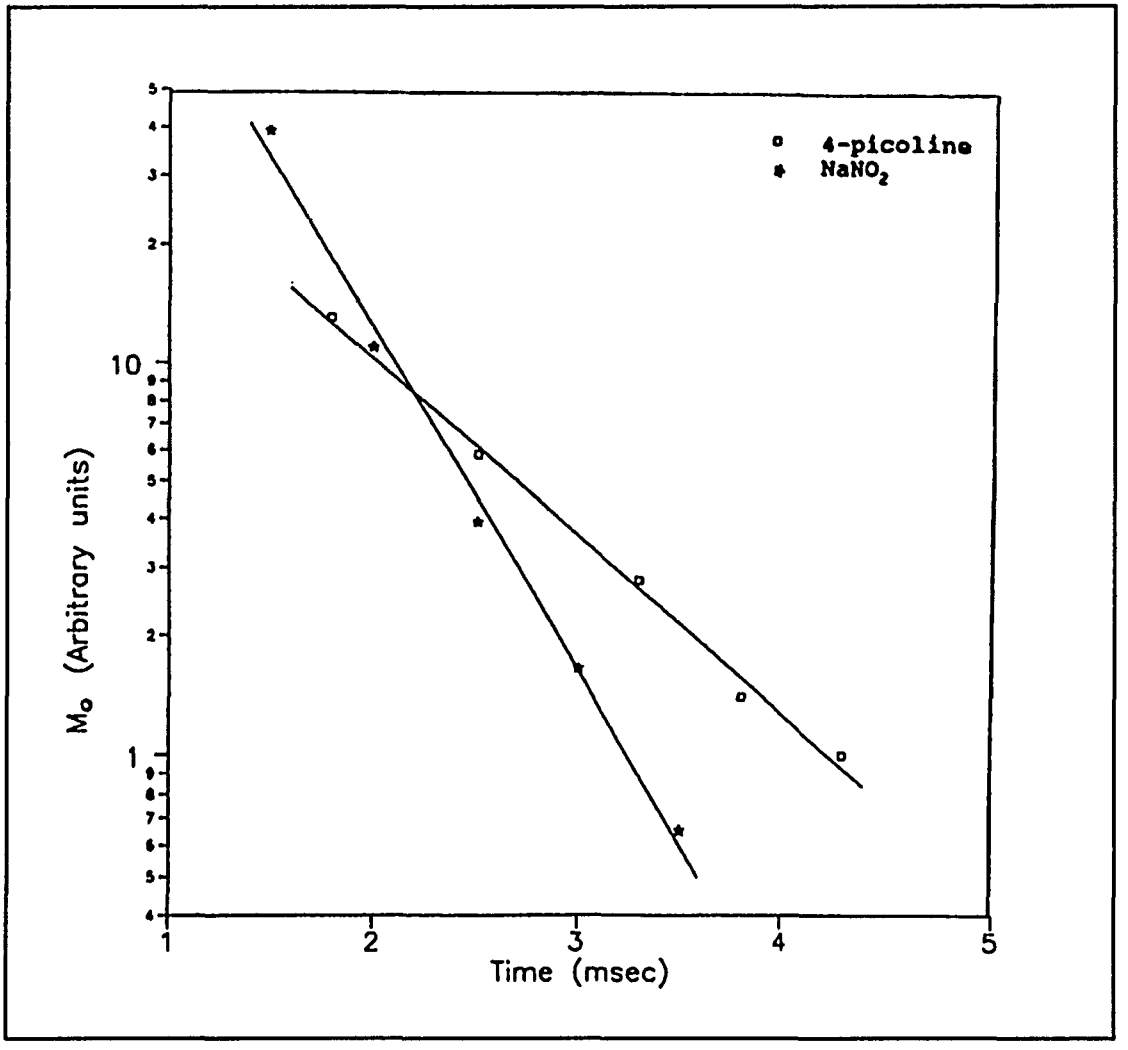

Figure 3.8 : The amplitude parameter M_0, defined in equation 3.4, and obtained from least square fits from figure 3.5a and 3.5b, vs. the pulse spacing τ. The decay time constants are 0.50 msec for $NaNO_2$ and 0.96 msec for 4-picoline.

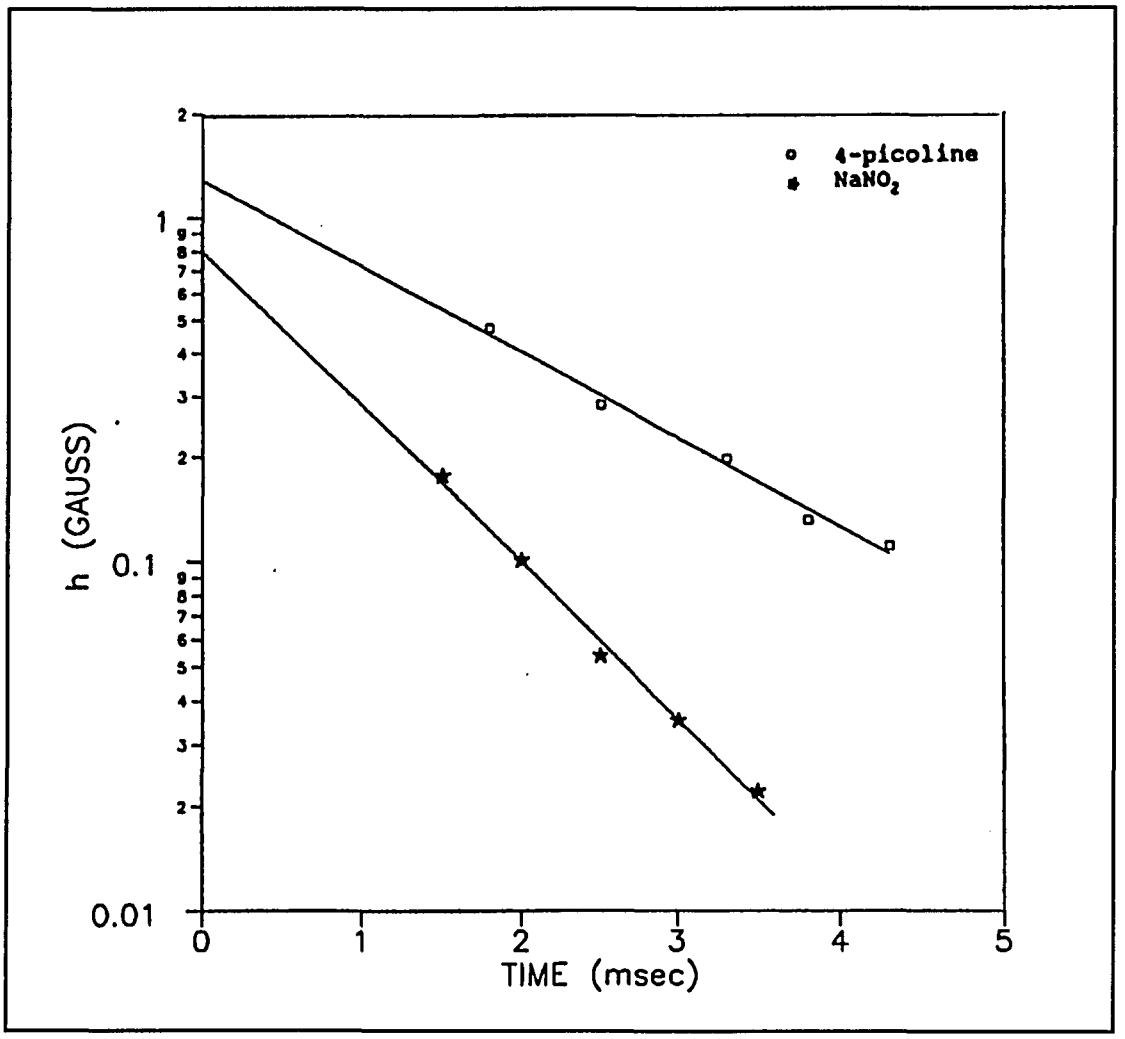

Figure 3.9 : The parameter h, defined in equation 3.4, and obtained from least square fits from figure 3.5a and 3.5b, vs. the pulse spacing τ. The data points are fit by the relations $h=0.79G.\ \exp(-\tau/0.96ms)$ for $NaNO_2$, and $h=1.29G.\ \exp(-\tau/1.71ms)$ for 4-picoline.

to possible local fields. However, the resonance offset $\Delta f = 1.5$ kHz in all these data, requires a minimum of 4.9 Gauss, (see equation 1). Clearly, then, the magnitude of the parameter h still remains to be explained, possibly by a higher order theory.

Conclusions

The following conclusions can be drawn from the experiments summarized above:

1. A sequence of strong rf pulses applied near-resonant, with no phase shifts, and with equal spacings τ of order T_2 or less, yields quasi steady-state signals repeated every τ seconds. For short τ, the signal intensity varies exponentially with τ.

2. The maximum signals obtained are comparable in magnitude to fully relaxed FID's.

3. The signal intensity is strongly modulated by the resonance offset, Δf. This can yield sharp maxima and minima as $\tau\Delta f$ is varied between integer and half-integer values.

4. To first order, signals are explained by considering the first Fourier component of the irradiation. This leads to signal strengths proportional to,

$$M_0(\tau,\Delta f)\frac{\langle H_1\rangle}{\langle H_1\rangle^2 + h^2(\tau,\Delta f)}.$$

5. The parameters M_0 and h, in the above equation show a clear exponential dependence on the pulse spacing τ, with decay constants about an order of magnitude smaller than corresponding values of the spin-spin relaxation times. It remains for further work on a higher order theory to explain this observation.

Chapter 4

Detection and Study of NQR signal in Cocaine Base using CW and Pulse technique

4.1 Introduction

Nuclear Quadrupole Resonance is one of the powerful techniques currently being considered by law enforcement agencies to detect drugs and explosive. In this work, Nitrogen-14 NQR signals from Cocaine Base have been observed with sensitivity sufficient to form the basis of a narcotics detector capable of scanning suitcases and unopened mail bags.

4.2 Experimental Details

A home built CW "Robinson" spectrometer [44] as modified by Gravina [45] and a Matec pulse spectrometer was used to detect the Nitrogen-14 NQR signal of Cocaine Base. A block diagram of the CW spectrometer is provided in Figure 4.1. The samples to be investigated are placed in the inductor coil of a Robinson oscillator (tank circuit), which is swept in frequency by means of a motor and gear train attached to the tuning capacitor. Robinson's circuit provides an output voltage which is proportional to the RF voltage level in the tank circuit. In order to use lock-in detection, some way of modulating the NQR signal is necessary. The modulation technique chosen for this spectrometer is Zeeman modulation using a bi-symmetric square wave [46]. If a small magnetic field is applied to the sample then the NQR resonance will be broadened by the zeeman effect. This broadening is used to modulate the NQR signal. The resonance

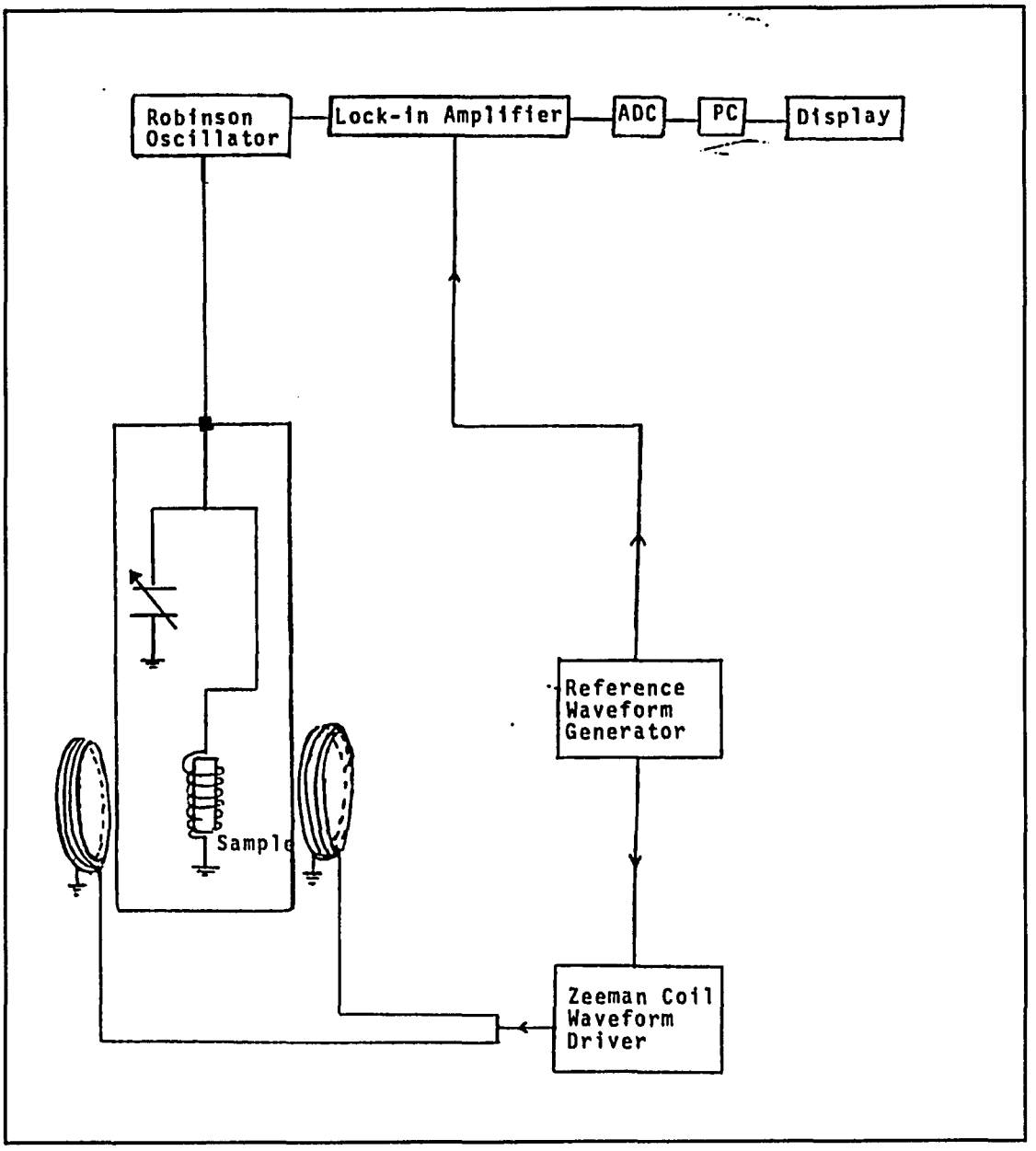

Figure 4.1 : Block diagram of the CW "Robinson" spectrometer

condition is thus revealed as an amplitude modulation of the radio-frequency oscillations. With lock-in detection, a set of Helmhols-coils with axis perpendicular to the RF field are used to modulate this field at audio frequencies. For data acquisition we use an IBM-PC with an Techmar Lab-Tender A/D plug-in board. The final product of an NQR measurement is a plot of NQR absorption signal vs. frequency, i.e., the output voltage from the lock-in amplifier vs. the frequency of the oscillator. Both the collection of the output voltage and the frequency counting are done with the computer.

The sample was recrystallized from alcohol and water solution by Dr. Julian Shaw of Quantum Magnetics, Inc.. About 30 g of sample was used for NQR measurement packed in 1-inch diameter, 4-inch height glass vials. The first signal search was conducted using the CW spectrometer. This instrument should be more sensitive at detecting broad NQR lines than the more conventional pulse spectrometers, whenever T_2^* is considerably smaller than T_2. Our Matec pulse spectrometer was also used to obtained relaxation times for ν_+ and ν_- lines at room temperature and 77K.

4.3 Results and Discussion

The Nitrogen-14 NQR signal of Cocaine Base was first observed by Garroway and Buess [47]. They reported room temperature NQR signals at two frequencies about of about 3718 and 3817 KHz. We have confirmed these results and measured the linewidths and relaxation times. Also we obtained the frequencies at 77K. The Nitrogen NQR signals of Cocaine Base at room temperature obtained using CW spectrometer shown in Figure 4.2a and 4.2b. The frequencies of ν_+ and ν_- lines are 3.816MHz and 3.7165MHz respectively. These results indicate that the results obtained from the indirect method

Figure 4.2a →

Figure 4.2b →

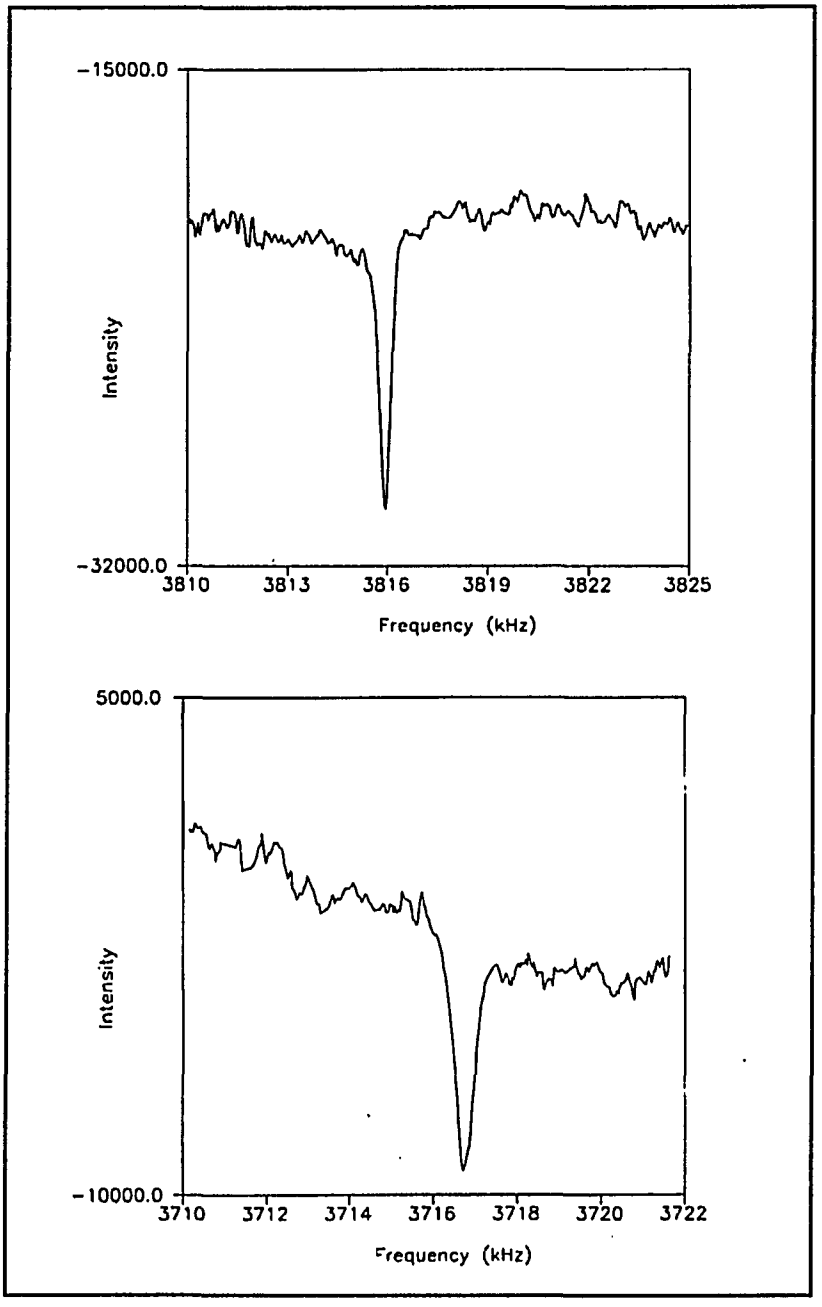

Figure 4.2 : ^{14}N NQR signals of Cocaine Base at room temperature obtained using CW spectrometer. 2a) ν_+ line at 3816 kHz. 2b) ν^- line at 3716.5 kHz.

(double resonance) in the literature may not be reliable. Note that the indirect detection frequencies of Cocaine Base were obtained to be 4260 and 4245 kHz.

The pulse spectrometer was used to obtain data on relaxation times and line width. Figure 4.3 and 4.4 shows the FID signals and their Fourier transform spectra for the upper and lower lines at room temperature. Signals were very strong. The spin-lattice relaxation time T_1 was measured for the ν_+ and ν_- lines using the method of progressive saturation. Figure 4.5a and 4.5b display the amplitude of the FID signal vs. the pulse repetition rate for ν_+ and ν_- line respectively. The spin-spin relaxation time T_2 was measured from the two-pulse spin echo decay, and the line-shape parameter T_2^* was estimated from the displayed FID signal. Figure 4.6 displays the spin-echo amplitude vs. the pulse spacing. The relatively long values of T_2 at room temperature made this substance very easy to detect by multiple pulse method like SORC. See Figure 4.7 for some SORC examples.

An NQR search was also conducted at 77K with the pulse spectrometer. Weak signals were detected at 3.829MHz for ν_+ line and at 3.7391MHz for ν_- line. See figure 4.8 and 4.9. It was found that T_1 values are much longer than the values at room temperature. Results are summarized in Table 4.1.

The NQR frequency, the strength of response and the response times of cocaine base has been measured and determined to be of sufficient sensitivity to form the basis of a narcotics detection device. Also the relaxation parameters of cocaine base are ideally suited to enhanced NQR detection with multiple sequence like SORC. Using the SORC sequence an NQR signal can be detected within a few seconds.

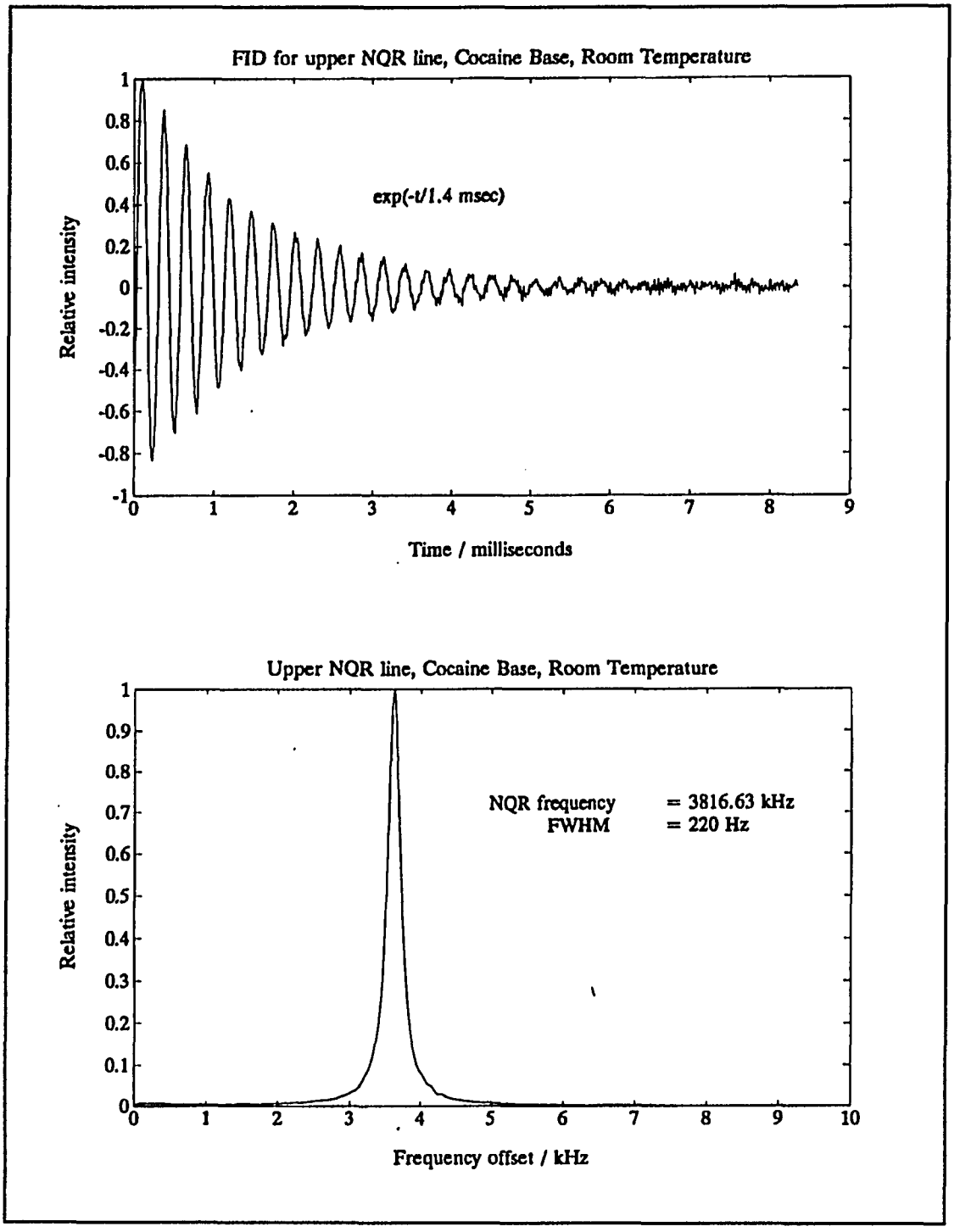

Figure 4.3 : ^{14}N NQR upper line of Cocaine Base obtained using a pulse spectrometer at room temperature.

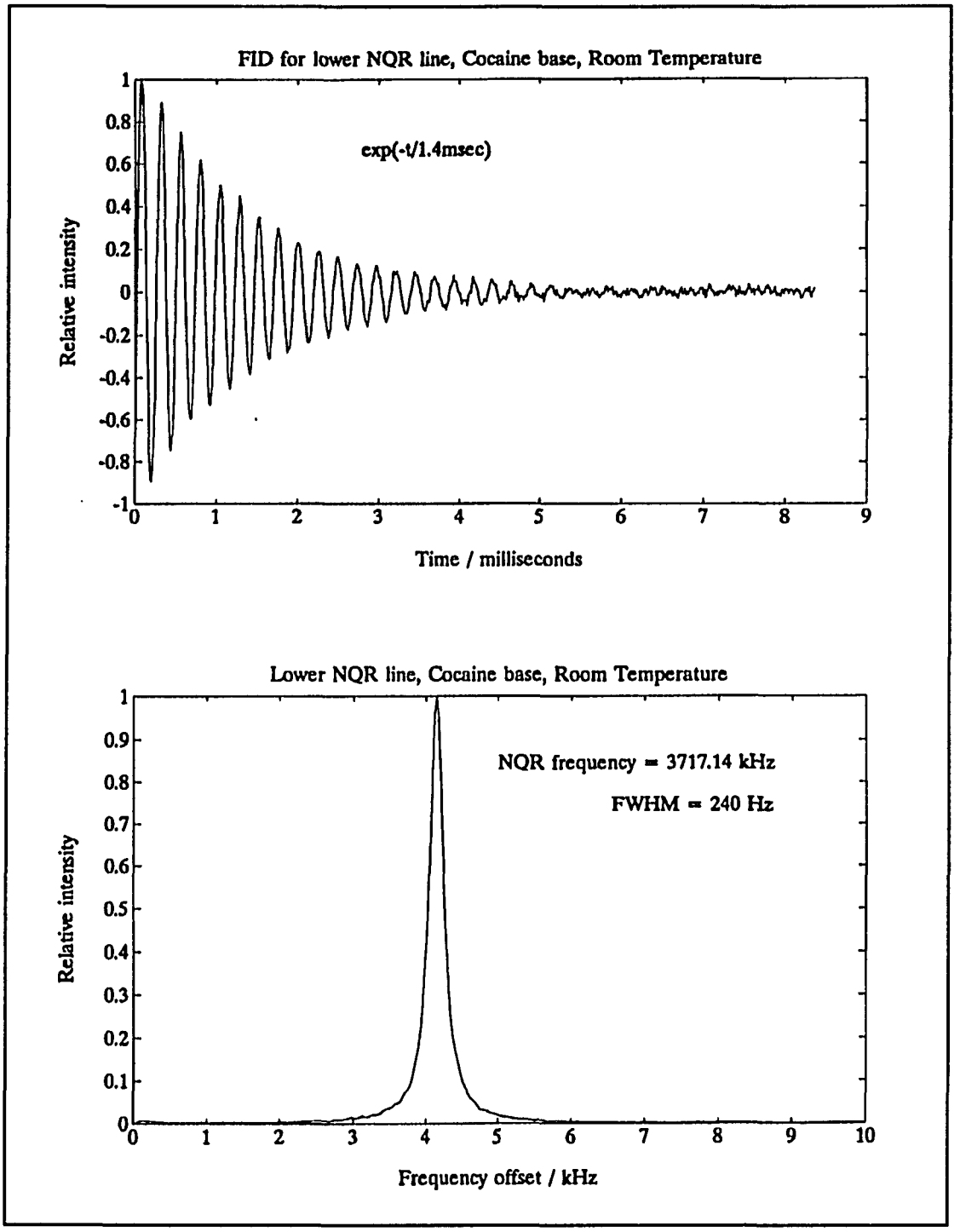

Figure 4.4 : ^{14}N NQR lower line of Cocaine Base obtained using apulse spectrometer at room temperature.

Fig. 5a →

Fig. 5b →

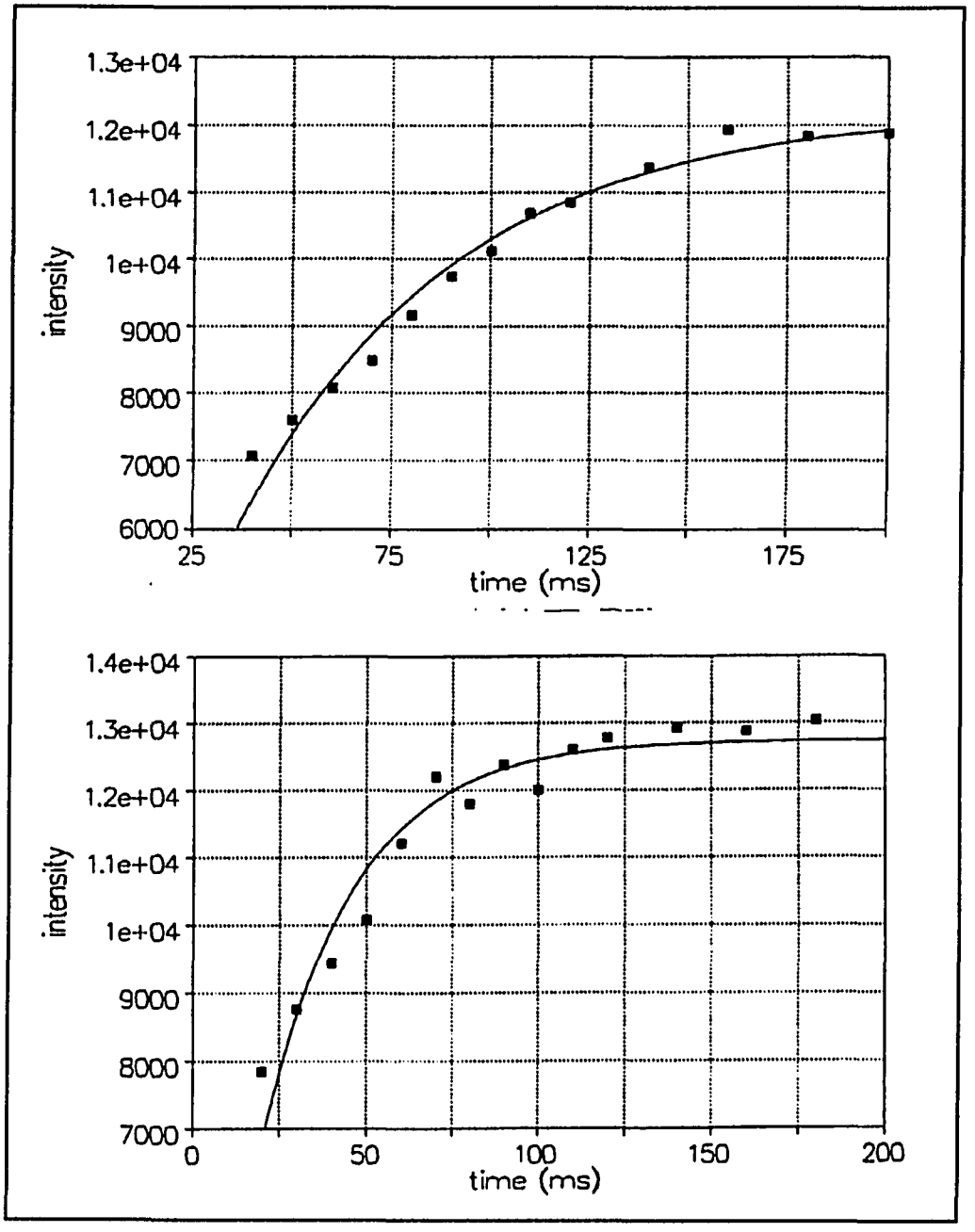

Figure 4.5 : Amplitude of FID signal vs. pulse repetition rate for Cocaine Base a) upper line b) lower line at room temperature.

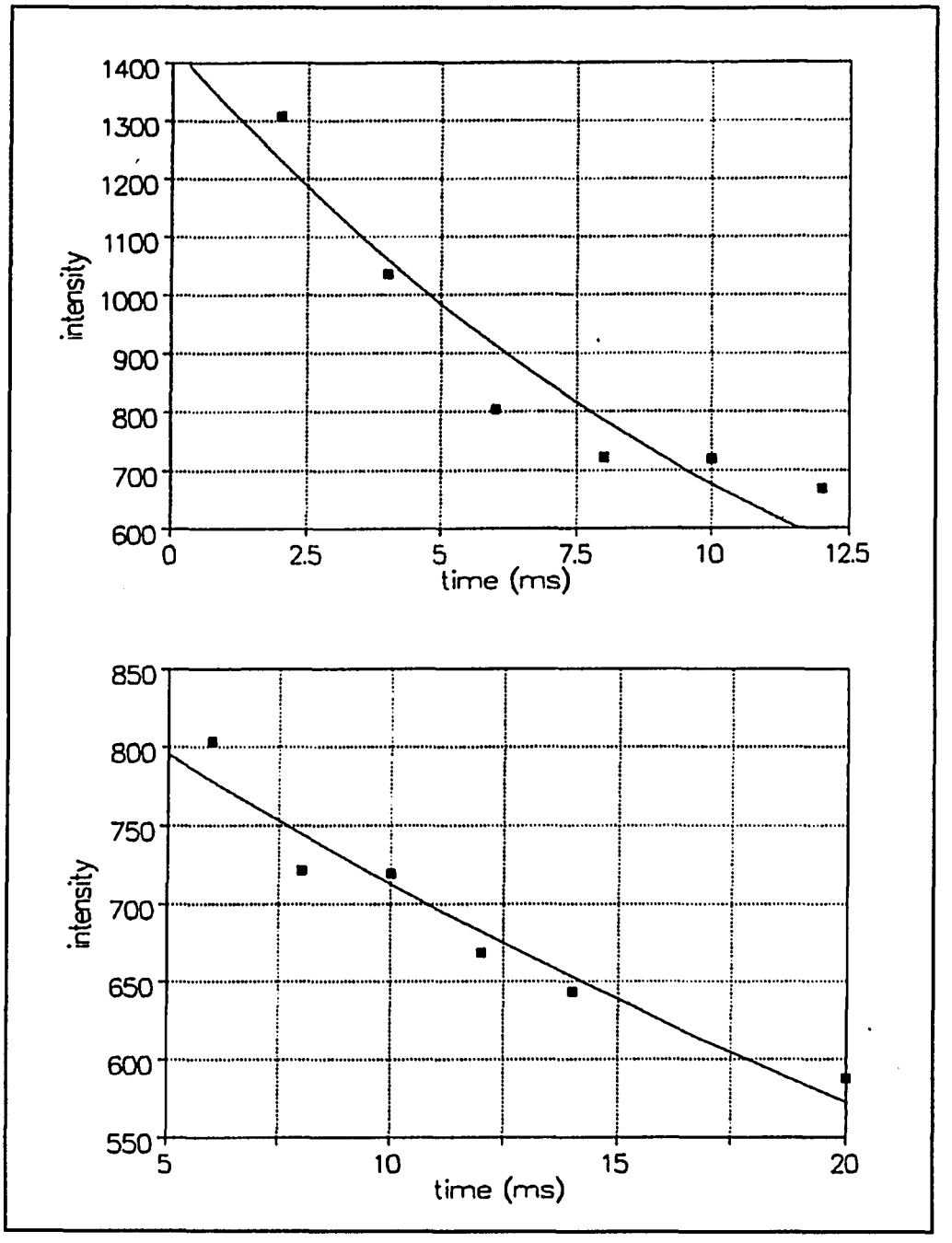

Figure 4.6 : Displays spin-echo amplitude vs. pulse spacing τ. Note that two curves represent two different ranges of τ.

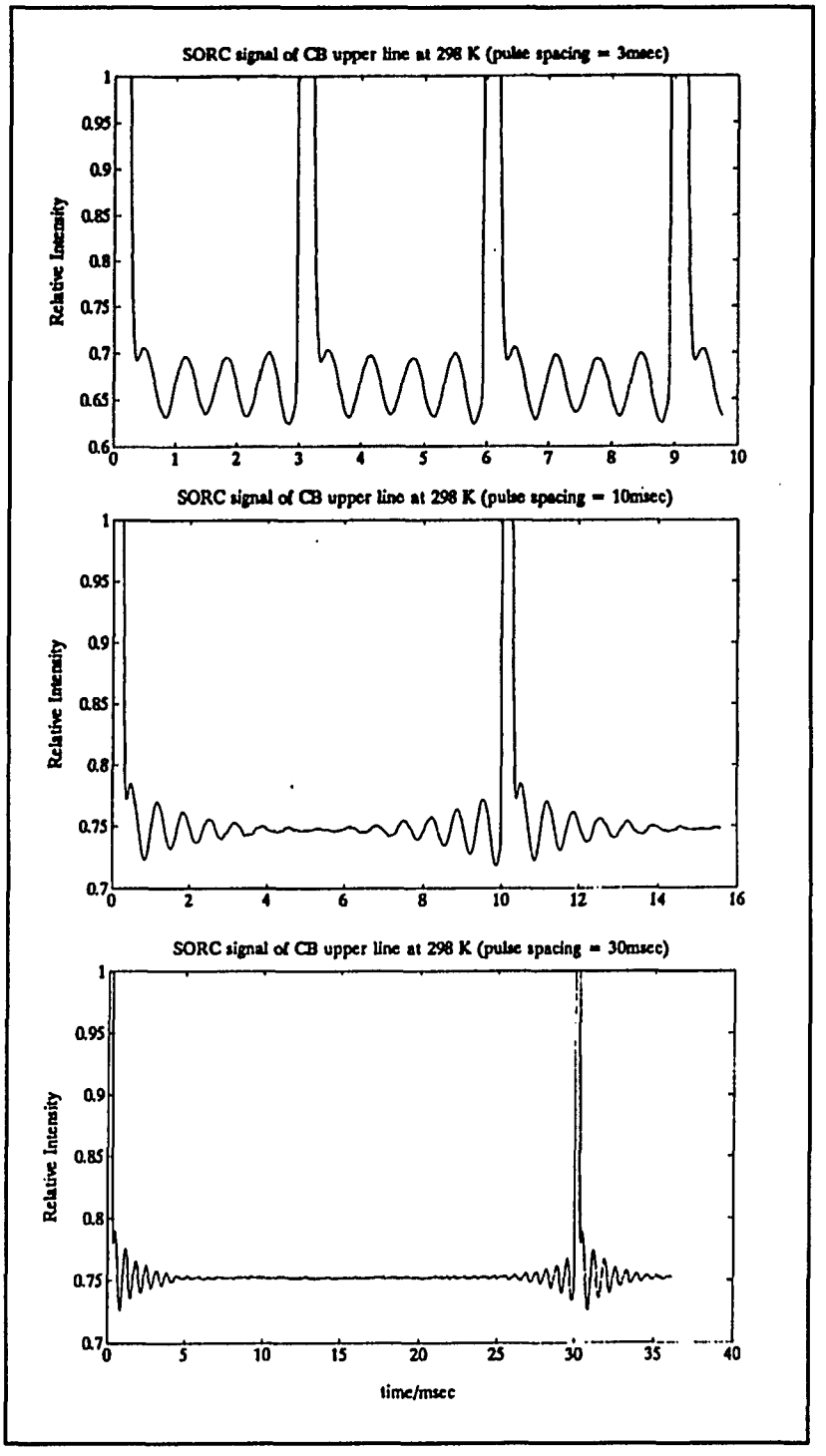

Figure 4.7 : Steady-state NQR signals in an SORC sequence for three different values of the pulse spacing τ. All data were taken on the ν_+ line of Cocaine Base at room temperature. Note that relatively long values of T_2 allowed this substance to give strong SORC signals even for the 30 msec region.

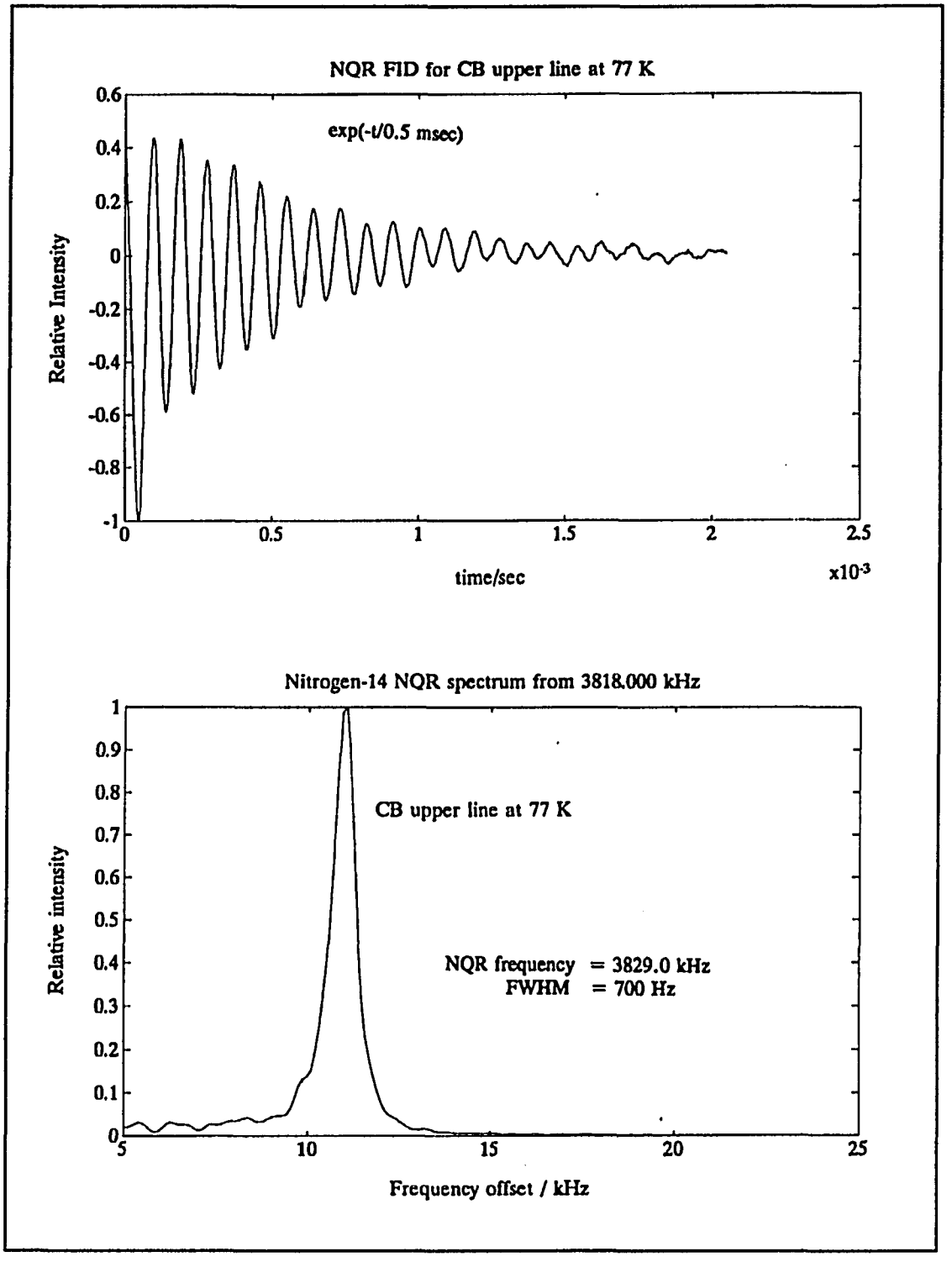

Figure 4.8 : ^{14}N NQR upper line of Cocaine Base obtained using a pulse spectrometer at 77K.

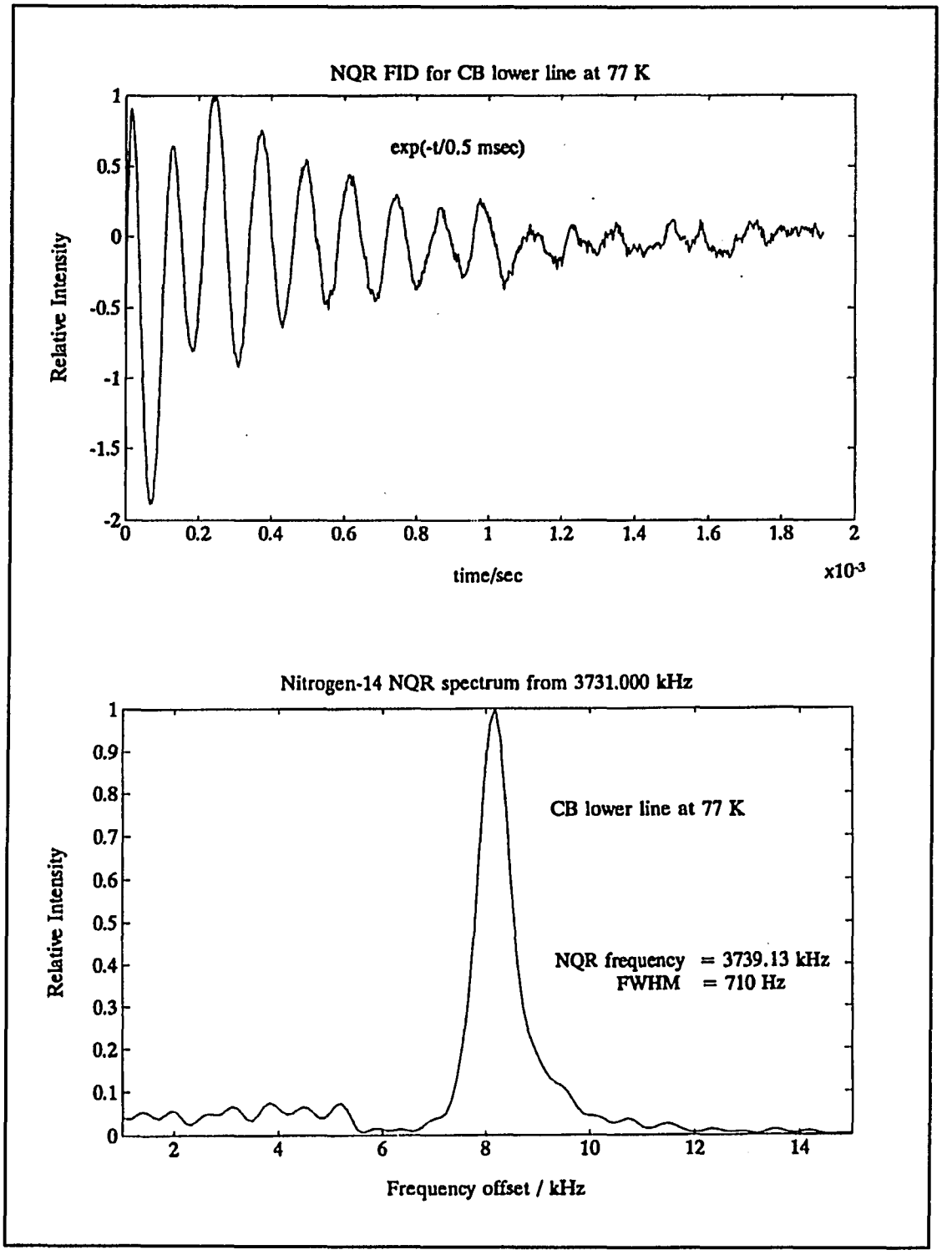

Figure 4.9 : ^{14}N NQR lower line of Cocaine Base obtained using a pulse spectrometer at 77K.

4.4 Conclusion

The experimental results show that detection can be of sufficient sensitivity to form the basis of narcotics screening devices for both mail and airline baggage. Some of the advantages of NQR detection are

1) NQR does not require a magnet, and therefore does not damage magnetic media, and is therefore less cumbersome.
2) Its uses non-hazardous radio-frequency waves.
3) It can be used on large packages. Since no magnet and low RF power are required, an NQR system to inspect unopened mail bags is possible.

TABLE 4.1 : Nitrogen-14 NQR data for Cocaine Base. **FWHM** is the full width at half maximum for the two transitions in slowly recrystallize samples. T_1 is the spin-lattice relaxation time measured by progressive saturation, and T_2 is the spin-spin relaxation time obtain from the spin-echo amplitude vs. pulse spacing. η is the asymmetry parameter calculated by Eq. $\eta=3\nu_d/(\nu_+ + \nu_-)$.

Temperature	Frequency	FWHM	T_1	T_2	η
300K	3816.63 kHz	220 Hz	54 ms	13 to 45 ms[*]	0.0394
	3717.14 kHz	240 Hz	26 ms		
77K	3829.00 kHz	700 Hz	500 ms		0.0357
	3739.13 kHz	710 Hz	500 ms		

Chapter 5

CORRELATION TIME FOR POLYMER CHAIN MOTION NEAR THE GLASS TRANSITION IN NITROCELLULOSE.[1]

5.1 Introduction

This work describes a nuclear magnetic resonance (NMR) technique, with several novel features, which can be used as a general method to obtain the correlation time τ of the random thermal motions of polymers at temperatures near the glass-to-rubber transition. The correlation time is interesting since it is the parameter that describes the time scale of the motion. Measurements of τ in nitrocellulose (NC) were undertaken as part of a project to understand the mechanical properties of this material at the microscopic level.

The method begins with Sook Lee's analytical theory [13,14,15] of anisotropic paramagnetic centers undergoing slow orientational diffusion. The NMR chemical shift anisotropy (CSA) has the required orientational dependence with respect to the externally applied magnetic field, and the theory can readily be expressed in terms of the CSA's natural variables from Lee's examples of dipole-dipole and quadrupole interactions. For this work, the choice of CSA interaction was dictated by the fact that it could be measured with considerably higher precision in nitrocellulose and other polymers than for either dipole-dipole or quadrupole parameters. For slow motions of a polymer chain at or near the glass transition, the CSA begins to decrease, with the characteristic powder

---

[1]This work is published with R. A. Marino and S. Bulusu

pattern features, shoulders and divergence, approaching one another. This motional narrowing can be interpreted to yield the correlation time of the thermal motions.

5.2 Theory

Anisotropic nuclear magnetic resonance centers, such as those involving nuclear quadrupole, dipole-dipole or the chemical shift interaction, undergo random tumbling motion due to thermal orientational diffusion processes in many polycrystalline-amorphous substances (e.g., polymers and glasses) over the temperature ranges of greatest interest. As a result of the tumbling motion nuclear-spin energy levels are modulated in such a way that the resultant NMR lines become broadened or narrowed, and their NMR frequencies shift from the rigid-limit values.

A few years ago a comprehensive analytical-theoretical treatment [13,14,15] was performed for the dynamic behavior of anisotropic nuclear or electron paramagnetic centers for slow-orientational motion in polycrystalline-amorphous condensed matter. Simple analytical expressions were derived for slow-motional line broadening and spectral line shifts for the important orientations of the NMR symmetry axes with respect to the external magnetic field H_0. The theory develops expressions which can be used to obtain the correlation time from experimental values of NMR frequency shifts.

In this work, the specific NMR fine-structure investigated is the first-order chemical shift anisotropy in nitrocellulose polymers. The first-order NMR CSA Hamiltonian in a coordinate system with the z axis parallel to the external field H_o is given by

$$\mathcal{H} = - \gamma\hbar H_o I_z(1-\sigma_{zz})$$

where σ_{zz} is the component of the CSA shift tensor along the direction of H_o. It can be

expressed in terms of the diagonal components σ_1, σ_2, and σ_3 of the shift tensor in its principal axis system. The unshifted NMR frequency for a nucleus of gyromagnetic ratio γ is $\omega_o = \gamma H_o$. Then the first-order NMR chemical shifted frequency can be written as

$$\omega(\theta,\phi) = \omega_o - \omega_o[\sigma_{ax}(3\cos^2\theta-1)+\sigma_{aniso}\sin^2\theta\cos2\phi + \sigma_{iso}]$$

$$= \omega_o - \omega_o\sigma_{iso} - \omega_o\sigma_{ax}[(3\cos^2\theta-1)+ \rho\sin^2\theta\cos2\phi]$$

where, $\sigma_{iso} = (1/3)(\sigma_1 + \sigma_2 + \sigma_3)$

$\sigma_{ax} = (1/6)(2\sigma_3 - \sigma_1 - \sigma_2)$

$\sigma_{aniso} = (1/2)(\sigma_1 - \sigma_2)$

$\rho = 3(\sigma_1 - \sigma_2)/(2\sigma_3 - \sigma_1 - \sigma_2)$.

θ and ϕ are the spherical angles between the external magnetic field H_o and the principal axes of the CSA tensor. The dynamic first-order chemical shifted NMR frequency under orientational diffusion motion can then be written as [13],

$$\omega(\theta,\phi,\tau) = \omega(\theta,\phi)\ [\tau/T_2][1\text{-exp.}(-T_2/\tau)]$$

where τ is the orientational correlation time and T_2 is the spin-spin relaxation time. At the slow tumbling limit, $T_2/\tau << 1$, valid for temperatures not too far above the glass-to-rubber transition, the above equation reduces to

$$\omega(\theta,\phi,\tau) = \omega(\theta,\phi)[1-T_2/2\tau].$$

Therefore, the slow motional NMR CSA frequency shift is

$$\Delta\omega(\theta,\phi,\tau) = -\omega(\theta,\phi)[T_2/2\tau].$$

The expression for the NMR spin-spin relaxation time T_2 along the three principal directions after inclusion of the tumbling motion can also be readily obtained. They are found to be

$$1/T_2(x,\tau) = 72^{-1/2}(109)^{1/4}\ \Delta^{1/2}\ \tau^{-1/2}$$

$$1/T_2(y,\tau) = 72^{-1/2}(62.5)^{1/4}\,\Delta^{1/2}\,\tau^{-1/2}$$

$$1/T_2(z,\tau) = 72^{-1/2}(201)^{1/4}\,\Delta^{1/2}\,\tau^{-1/2}$$

where Δ is the rigid-lattice chemical shift anisotropy.

Then, the frequency shifts of the principal features of the CSA spectrum obtained from the above equations, are,

$$\Delta\omega(1,\tau) = 0.284\,(\Delta\tau)^{-1/2}\,\Delta \qquad (1a)$$

$$\Delta\omega(2,\tau) = 0.176\,(\Delta\tau)^{-1/2}\,\Delta \qquad (1b)$$

$$\Delta\omega(3,\tau) = -0.376\,(\Delta\tau)^{-1/2}\,\Delta \qquad (1c)$$

where the indices 1, 2 and 3 denote, respectively, the principal directions x, y, and z.

5.3 Experimental Details

The experimental design was determined by the necessity to obtain spectra of sufficient signal-to-noise ratio at all temperatures before appreciable sample decomposition. For nitrocellulose, this forced timescales of minutes rather than hours or days. Nitrocellulose samples were prepared with 100% Nitrogen-15 isotopic enrichment by nitration of high quality cellulose fibers. The chemical structure of Nitrocellulose shown in Figure 5.1 . At room temperature, Nitrogen-15 broadband NMR spectra of 0.5 gram samples as shown in Figure 5.2 yielded typical CSA powder patters, with discernible shoulders and divergences. At higher temperatures, sufficient signal-to-noise could only be obtained in a timely fashion by using Magic Angle Spinning (MAS) techniques. In liquids, NMR resonances are very narrow by virtue of rapid isotropic tumbling which averages the anisotropic part of the shift, dipolar, quadrupolar and chemical. It was realized some time ago [35] that spinning a powder sample about an

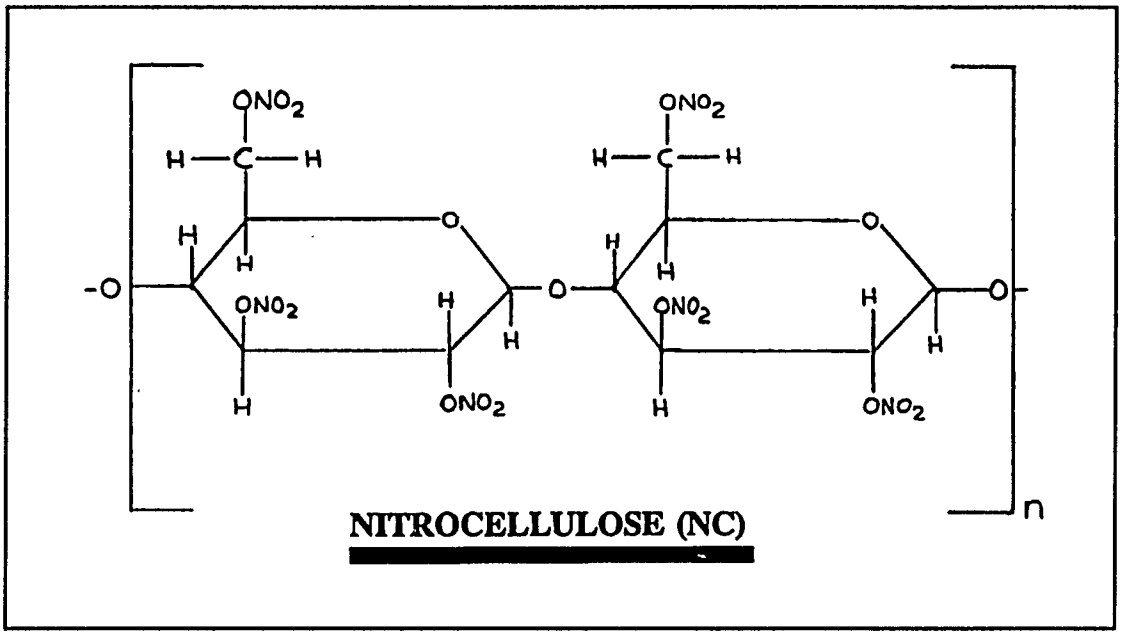

Figure 5.1 : Nitrocellulose (NC) repeat unit

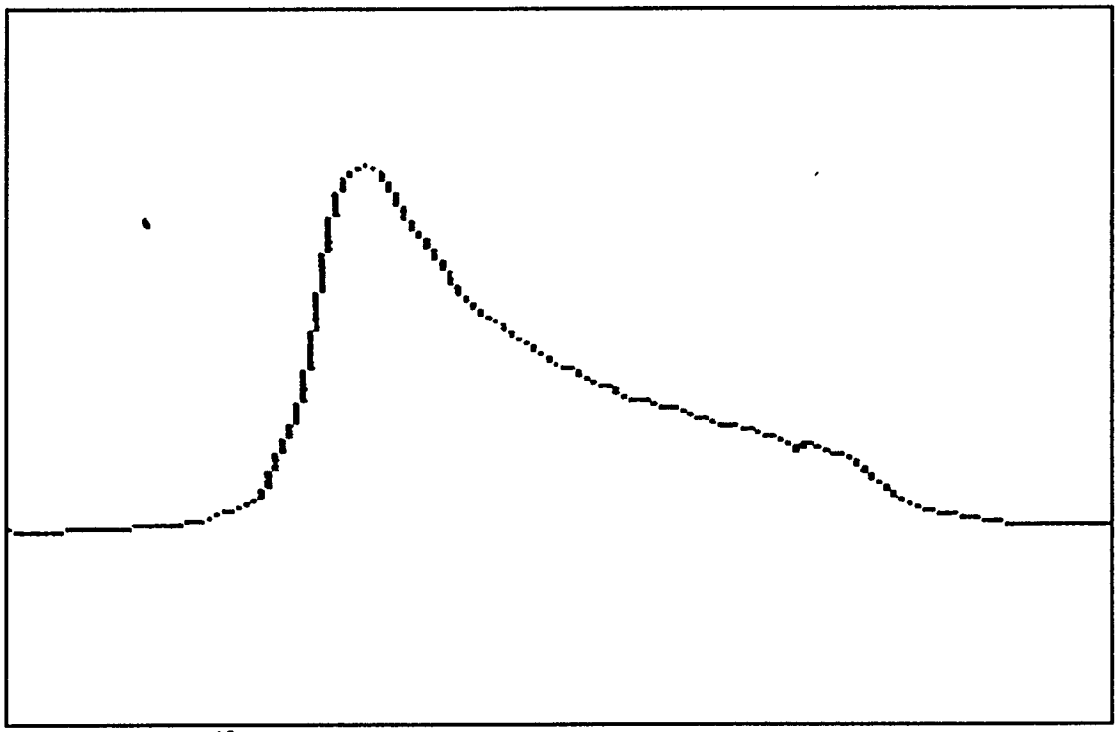

Figure 5.2. N^{15} NMR spectrom of NC at 25° C, taken at 30.9 MHz.

axis inclined at the so called Magic angle (54° 44') with respect to the applied field will average the shift anisotropy to zero. The general condition for complete averaging being that the spinning rate exceed the breadth of the shift anisotropy. When the spinning frequency is less than the Chemical shift anisotropy, this generates satellite spectra (sidebands) on either side of the central line at integer multiples of spinning frequency, as shown in Figure 5.3. The intensity of the spinning sidebands are related to the chemical shift anisotropy and provide an opportunity to recover the chemical shift parameters. As indicated by others [48], the individual sidebands intensities are very complicated functions of the chemical shift parameters given bellow.

Relative intensity of the Nth sideband is

$$I_N = (1/4\pi) \int \int |F|^2 \, d\alpha \sin\beta \, d\beta,$$

where $F = (1/2\pi) \int \exp[i\{-n\theta + \Delta_- \tau_-(\alpha,\beta,\gamma) + \Delta_+ \tau_+(\beta,\theta)\}]d\theta,$

$$\tau_-(\alpha,\beta,\gamma) = (1/24)\cos(2\alpha)[3+\cos(2\beta)]\sin(2\theta)$$
$$-(1/6)\sin(2\alpha)\cos\beta\cos(2\theta)$$
$$+(\sqrt{2}/6)\cos(2\alpha)\sin(2\beta)\sin\theta$$
$$-(\sqrt{2}/3)\sin(2\alpha)\sin\beta\cos\theta$$

$$\tau_+(\beta,\theta) = (1/24)[\cos(2\beta)-1]\sin(2\theta) + (\sqrt{2}/6)\sin(2\beta)\sin\theta$$

$$\Delta_- = \mu = (\omega_o/\omega_r)(\sigma_3-\sigma_1)$$

$$\Delta_+ = -\mu\rho$$

$$\rho = (\sigma_1+\sigma_3-2\sigma_2)/(\sigma_3-\sigma_1)$$

α,β and θ, described the orientation of the molecule relative to the principal axis of chemical shift tensor. σ_1,σ_2 and σ_3 are the principal values of chemical shift tensor.

However we used graphical and numerical methods of Herzfeld and Berger [49]

to extract the chemical shift parameters from the intensities of a few sidebands. The final values of the CSA parameters at each temperature were refined by matching simulated and experimental spectra (Figure 5.3).

5.4 Results and Discussion

At each temperature, three independent CSA parameters could be extracted from the experimental data, as shown in Figure 5.4 and 5.5. Since the absolute chemical shifts were not measured, only two independent parameters are available for analysis, namely $(\sigma_3 - \sigma_1)$ and $(\sigma_3 - \sigma_2)$. The discarded parameter, $(\sigma_2 - \sigma_1)$, also has the highest percent experimental uncertainty. The NMR results obtained at 27°C are taken to be the "rigid lattice" values, since the glass-to-rubber transition is reported [50] to be above 40°C. The data at the three higher temperatures were then used, with the aid of Eqs. (1), to calculate the corresponding correlation times, denoted τ_{31} and τ_{32}, respectively for the shoulder-to-shoulder parameter $(\sigma_3 - \sigma_1)$, and the divergence-to-shoulder parameter $(\sigma_3 - \sigma_2)$. The results are collected in Table 1. The last column in the Table lists the arithmetic average of τ_{31} and τ_{32}, and their percent difference shown as the uncertainty. Note that as the CSA shifts become larger, as the temperature increases, the agreement between the two independently calculated values, τ_{31} and τ_{32}, becomes substantially better. It is then presumed that their lack of complete agreement at the lower temperatures is a measure of our experimental uncertainty.

The final results obtained by this NMR technique are listed in the last column of Table 1 and also in Figure 5.6. They show that even at 100°C the correlation time for thermal orientational diffusion in nitrocellulose is an appreciable fraction of a second.

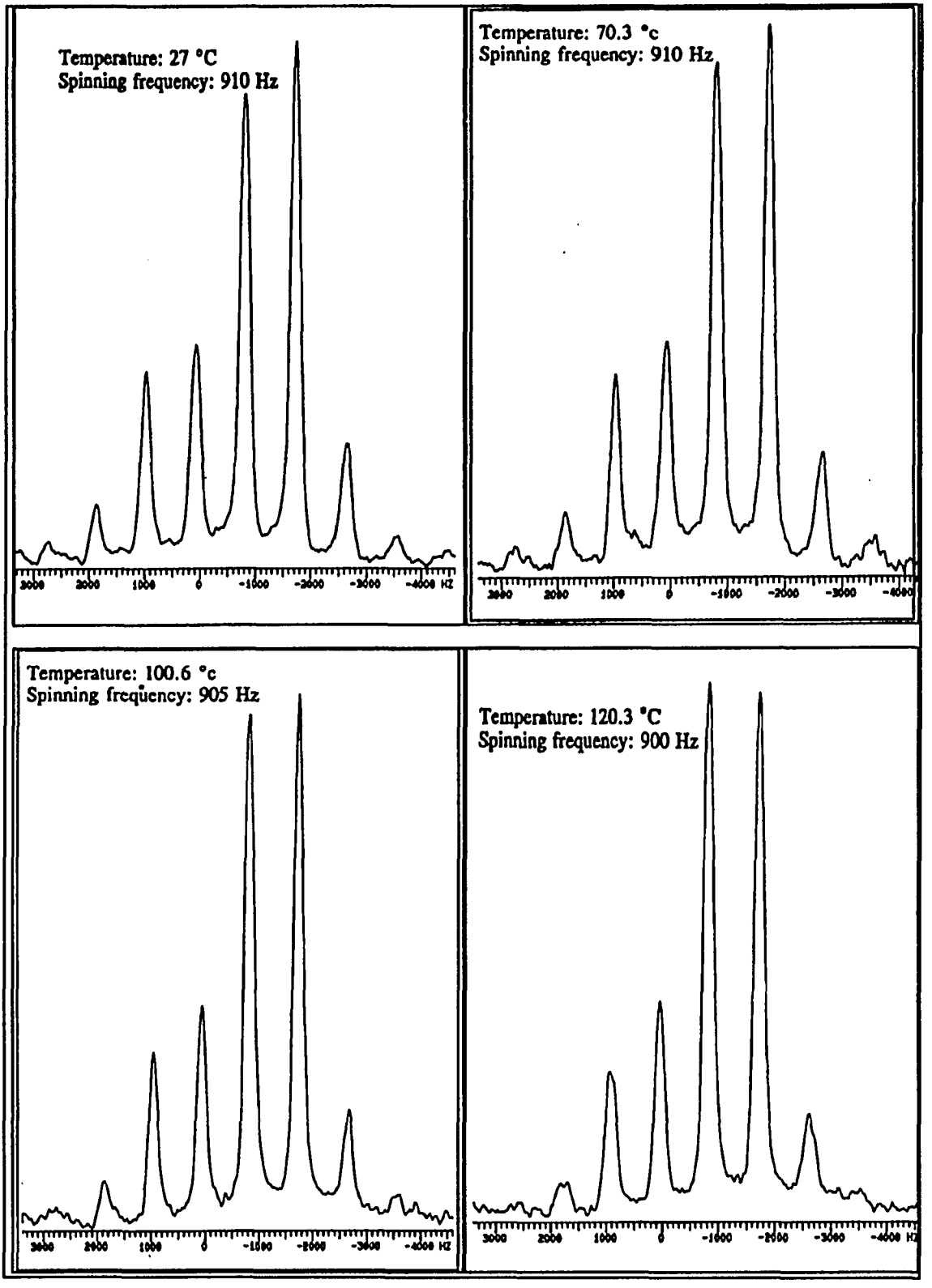

Figure 5.3. ^{15}N MAS/NMR spectrum of solid nitrocellulose at two different temperatures. Note the spinning sidebands, whose equal spacing is given by the spinning frequency, and whose relative intensities carry the chemical shift anisotropy information.

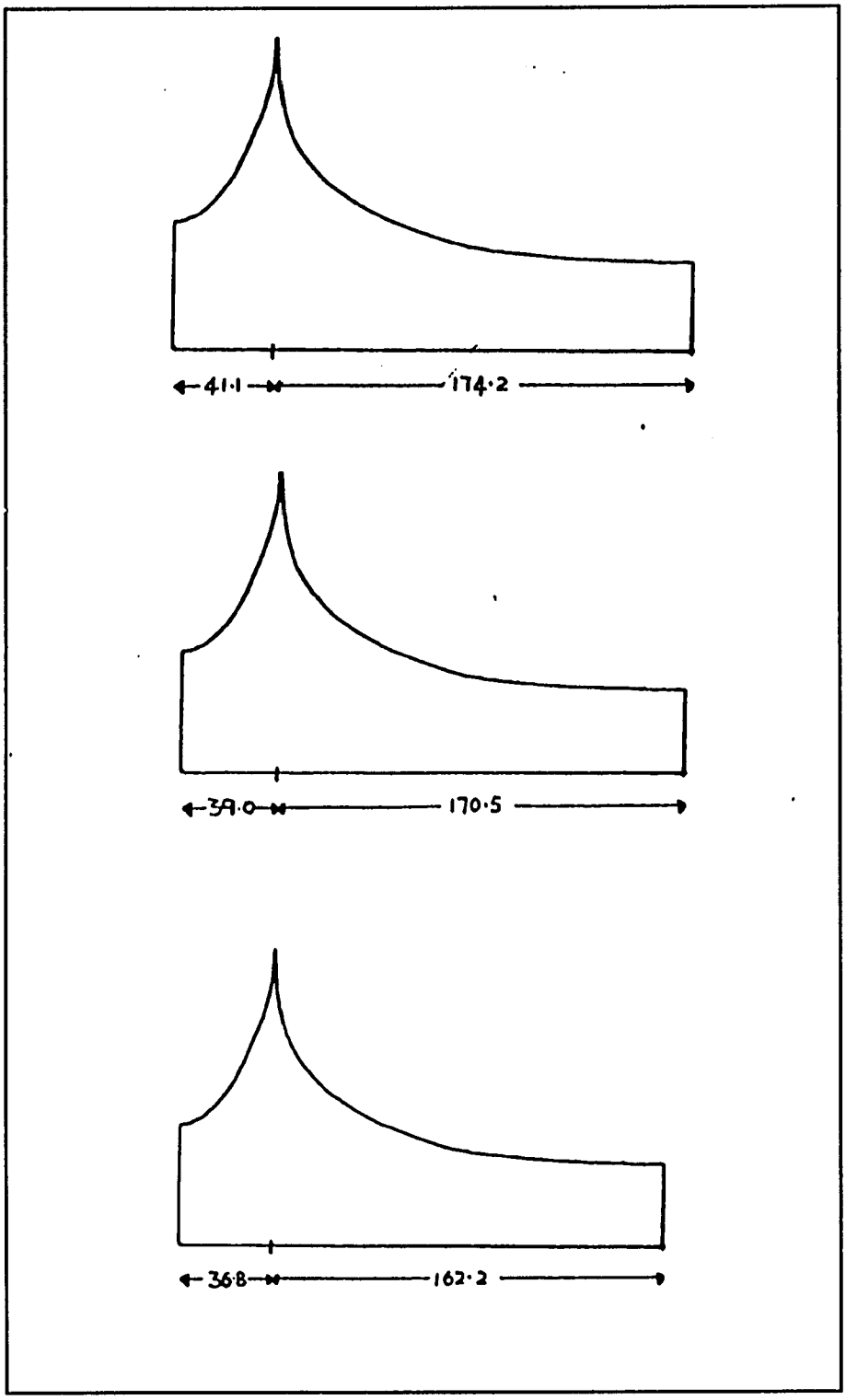

Figure 5.4. The ^{15}N chemical shift anisotropy of solid NC at three different temperatures reconstructed from MAS-NMR data.

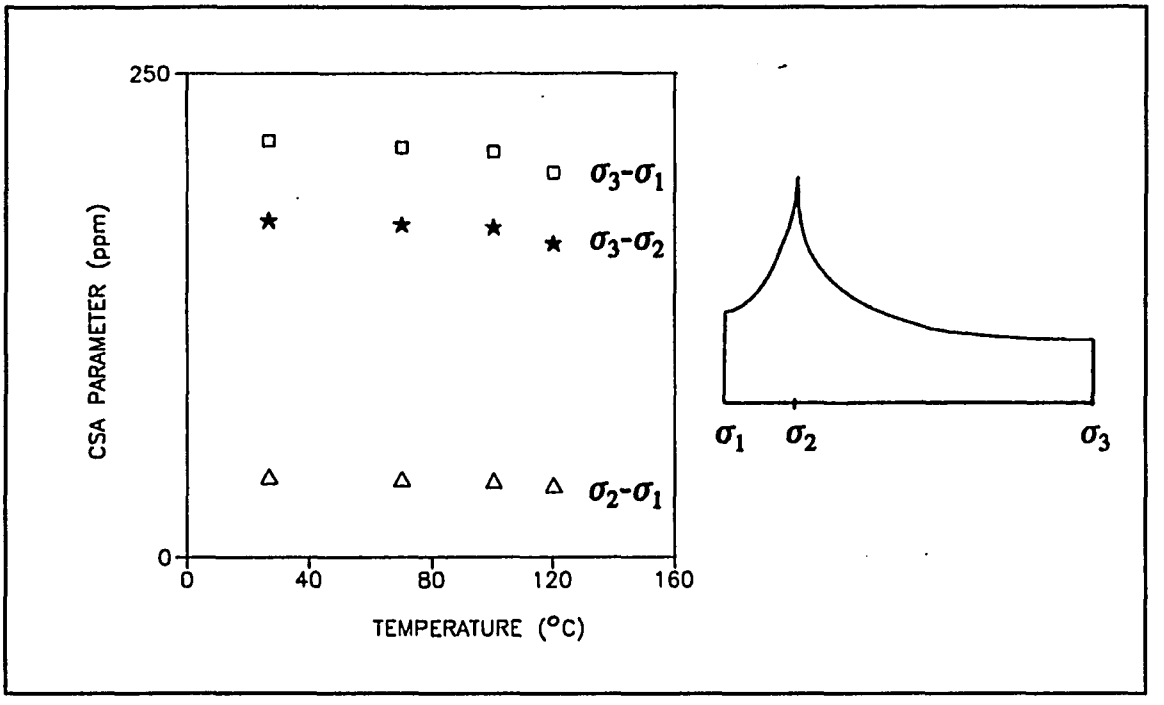

Figure 5.5. Experimental Chemical Shift Anisotropy (CSA) parameters vs. temperature in nitrocellulose. At right is shown a schematic of the broadband NMR line shape for polycrystalline/amorphous samples with asymmetric CSA. Note the definition of the frequency positions σ_1,σ_2, and σ_3, the principal values of the shielding tensor.

These results are consistent with the inelastic behavior of stretched 200 μm nitrocellulose films conducted in our laboratory. It is interesting to compare the results of Table 1 with the results obtained by Owens[ ] using ESR techniques in the same temperature region. Owens reports correlation times two orders of magnitude smaller, but they reflect the motion of small paramagnetic ions dissolved in nitrocellulose, not chemically bonded to the polymer chains. It is not surprising that the smallest ions are considerably more mobile.

The experimental method described in this paper differs substantially from traditional NMR methods relying on measurements of relaxation times vs. temperature, which for fixed-frequency NMR spectrometers are often inconclusive. It can easily be extended to other nuclei, like Carbon-13 or Fluorine-19. However, it is limited to slow motion, i.e., to temperatures below those where appreciable motional narrowing occurs.

Table 5.1. Temperature dependence of the ^{15}N chemical shift anisotropy Δ_{31}, Δ_{32}, frequency shift δ_{31}, δ_{32}, and the values of orientational correlation time τ_{31}, τ_{32}, for **NC.**

T (°C)	Δ_{31}(ppm)	Δ_{32}(ppm)	δ_{31}(kHz)	δ_{32}(kHz)	τ_{31}(ms)	τ_{32}(ms)	τ_{av}(ms)
27.0	215.3	174.2					
70.3	211.4	171.8	0.079	0.049	305	450	377±19%
100.6	209.5	170.5	0.118	0.075	138	189	163±16%
120.3	199.0	162.2	0.330	0.243	17	18	17.5±3%

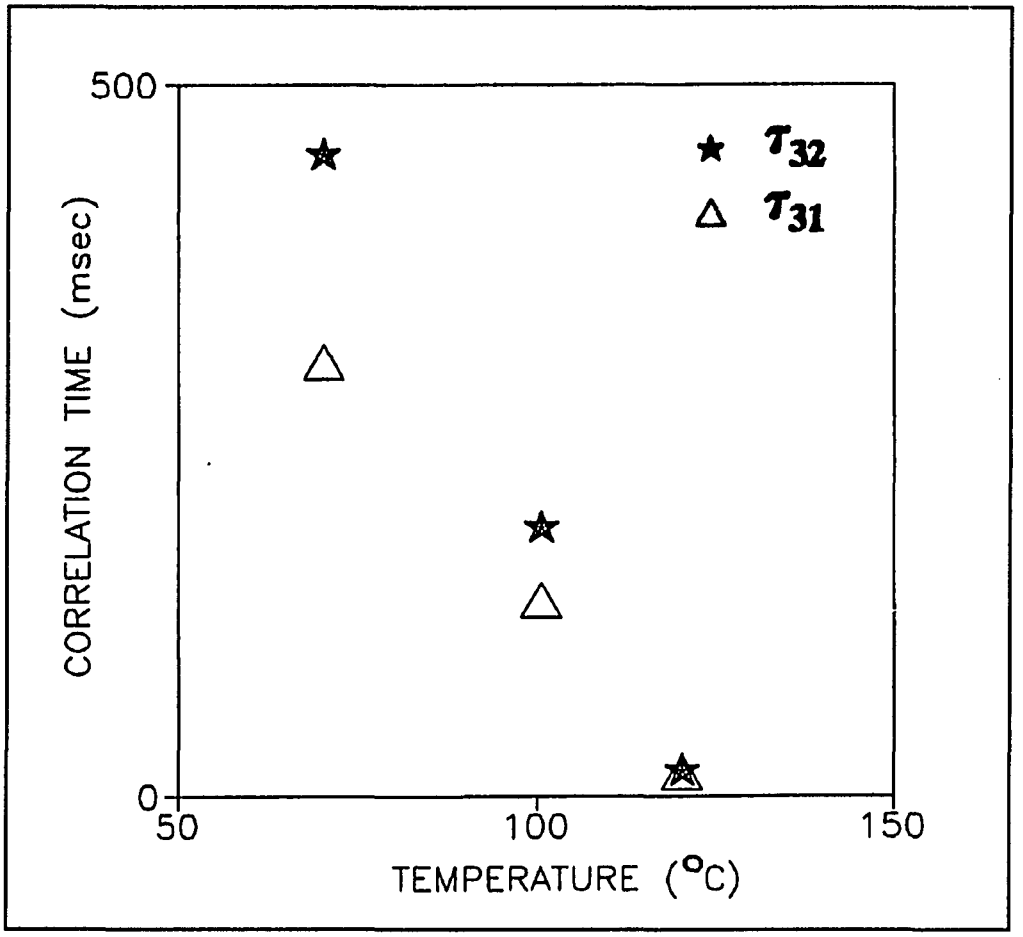

Figure 5.6. Correlation times for nitrocellulose polymer chain motion vs. temperature.

Chapter 6

NMR study of water in Nitrocellulose (NC)

6.1 Introduction

Polymers used in energetic materials formulations can transition between their brittle glass phase and their more supple rubber phase. Temperature and impurities can affect this property, and it is of interest to obtain a more fundamental understanding of the dynamics of the processes that contribute. We used Nuclear Magnetic Resonance (NMR) to understand impurity moisture dynamics in nitrocellulose-water system. We worked on the Nitrocellulose-water system by Deuterium NMR in samples of Nitrocellulose humidified with heavy water (D_2O).

6.2 Experimental Methods

Deuteron nuclear magnetic resonance (NMR) have been carried out with variable water content to investigate the nature of its behavior in nitrocellulose (NC). Two forms of NC were used: nitrated surgical cotton, which we shall refer as NC fibers, and nitrocellulose films. To prepare the films, NC fibers were first completely dissolved in acetone, and the resulting solution was then evaporated in a controlled environment in glass dishes yielding uniform films 75 to 200 μm thick.

To ensure complete dehydration, fibers and films were dried in a vacuum oven until no further weight loss was apparent. Samples were then exposed to a controlled D_2O humidity level until an equilibrium weight was established. For film samples, in order to obtain a reasonable filling factor without destroying the orientational

information, thin parallel strips were cut and stacked inside the 7 mm ID NMR sample tubes. The orientation of the sample relative to the NMR static magnetic field could be varied.

NMR spectra were obtained with a NOVEX variable-frequency spectrometer operating with a 7 Tesla superconducting magnet. Free Induction Decay (FID) signals were obtained by recording the nuclear induction signal immediately after a single narrow rf pulse, or from the peak of a quadrupolar echo evoked with a 90_x-τ-90_y sequence. The latter method is useful whenever the spectrometer pulse recovery time is an important fraction of the FID decay time. This was often the case at the lower temperatures studied. In addition to measuring spectrum line-shape parameters such as the linewidth or other powder-pattern features, we also used inversion-recovery methods [39] to measure the spin-lattice relaxation time (T_1) in our samples as a function of temperature, moisture and film thickness.

6.3 Results and Discussion

6.3.1 Cellulose

Cellulose in the form of surgical cotton is well known to be able to absorb appreciable amounts of water. We were able to easily obtain samples with D_2O weight percents up to 21. Figure 6.1 shows the deuterium NMR lineshapes in cellulose for several water contents. The spectra exhibit clear quadrupolar splitting, $\Delta\nu_Q$, which decreases with increasing water content.

Table 6.1 collects the values of $\Delta\nu_Q$ and the linewidths measured from Figure 6.1. The resolved quadrupolar splitting in the upper three traces indicates that water molecules

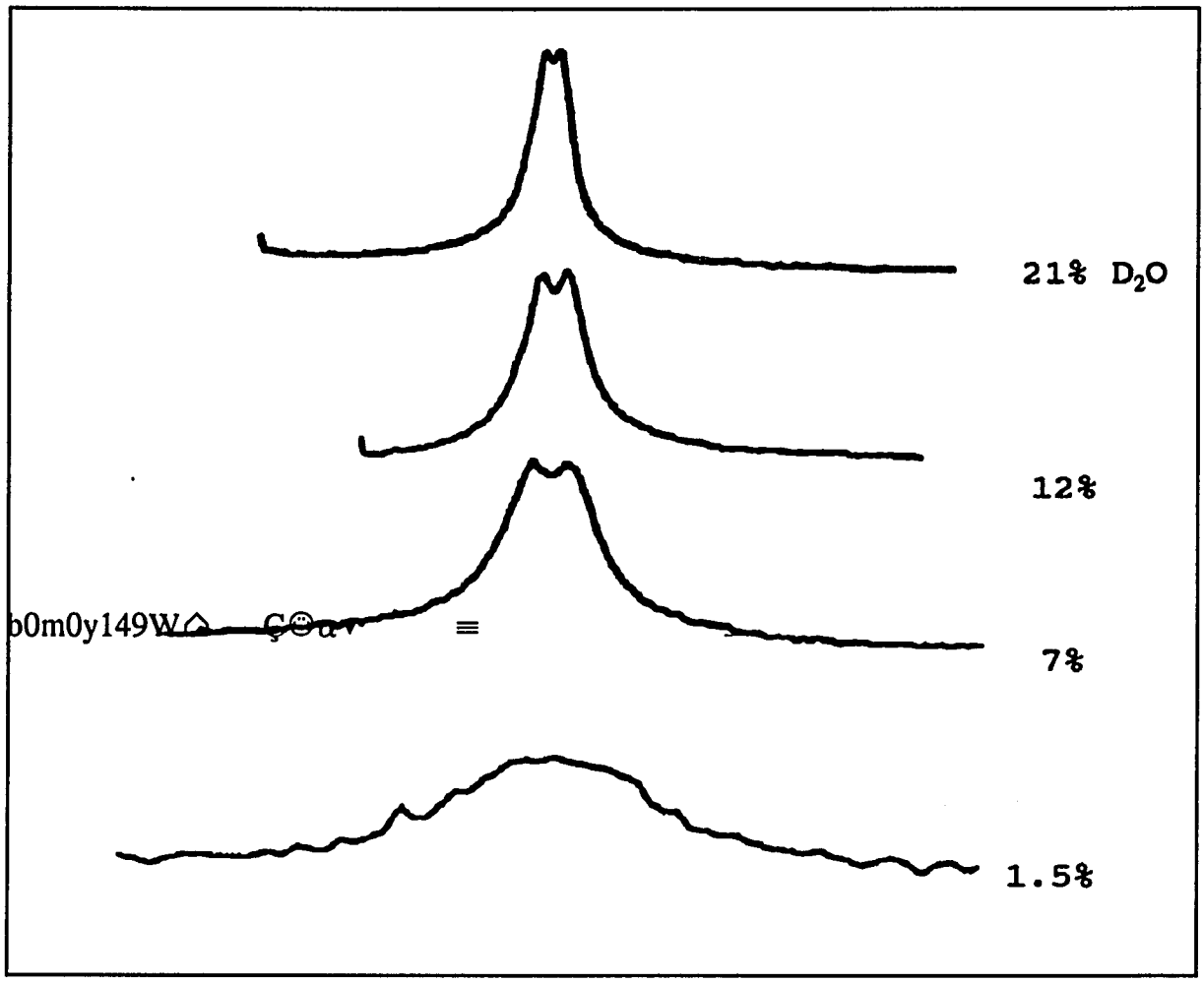

Figure 6.1. Deuterium NMR spectra of cellulose as a function of water content (wt % D_2O, shown to right of each spectrum). The scale of the horizontal axis is 5 kHz/cm.

Table 6.1: NMR line width and spin-lattice relaxation time as a function of water content.

Water content (wt%)	Line width ($\Delta\nu$)kHz	Separation ($\Delta\nu_Q$)kHz	T_1 (msec)
1.5	10.0		7
7.0	4.6	1.44	10
12.0	3.0	1.0	16
21.0	1.8	0.5	26

in different physical states exchange rapidly among themselves, on the NMR timescale. At the lowest water content, which is much less than one D_2O molecule per polymer repeat unit, the quadrupolar splitting is not clearly resolved. Water-water exchange is not as effective here, indicating that this is the regime where the water-polymer interaction predominates. When the water content is increased to about 7 wt. %, exchange becomes dominant and a resolved quadrupolar powder-pattern doublet emerges. For still larger water content the additional water, which is clearly increasingly more mobile, contributes to a net smaller average value of quadrupole coupling. However, even for the largest water content, about four D_2O molecules per cellobiose repeat unit, the presence of resolved quadrupolar splitting indicates that the D_2O is far from "liquid" on average. Water-polymer interactions still determine the NMR lineshape.

Spin-lattice relaxation data, shown in Table 1, indicate that T_1 increases with increasing water content, consistent with the BPP [37] theory. We conclude that while water-polymer interactions are important in all of our samples, at least some fraction of the total water in cellulose will approach an isotropically "free" state, and that rapid exchange, on the NMR time scale, between nearly free water and more bound water

yields an average response.

The cellobiose monomer which is the repeat unit of cellulose has six lateral hydroxyl groups. The presence of these sites goes a long way toward the explanation of the hygroscopic properties of cellulose. In addition, however, we must also consider the possibility that our deuterium NMR spectra arise from the deuteration of the polymer backbone hydroxyl groups. To study this possibility we dried completely the cellulose sample which had given the 21 wt % D_2O data. The resulting signals, FID and spectrum, are shown in Figure 6.2. Note that the horizontal scale of the spectrum is an order of magnitude larger than in the previous figure. The weak broad line of Figure 6.2 arose from a poorly averaged out (little motion) quadrupolar interaction. The NMR spectra in Figure 6.1 are sufficiently different from that of Figure 6.2 that there can be no mistaking the D_2O signals from the deuterated hydroxyl groups on the polymer backbone. This point is important for the subsequent nitrocellulose study, because it assures that any hydroxyl groups that failed to be nitrated but are then subsequently deuterated will not be confused with bound or free D_2O.

6.3.2 Nitrocellulose

Nitrocellulose (NC) was found to be much less hygroscopic than cellulose. Maximum moisture content was 2% in films and 3.5% in fibers. The latter translates to very nearly one D_2O molecule per cellobiose unit. The degree of nitration of NC in military formulations (comparable to that of our NC samples: 13.5 wt. % nitrogen) indicates that the number of un-nitrated hydroxyl sites is the same order of magnitude as the number of D_2O molecules taken up. Therefore, we conclude that the hydroxyl sites

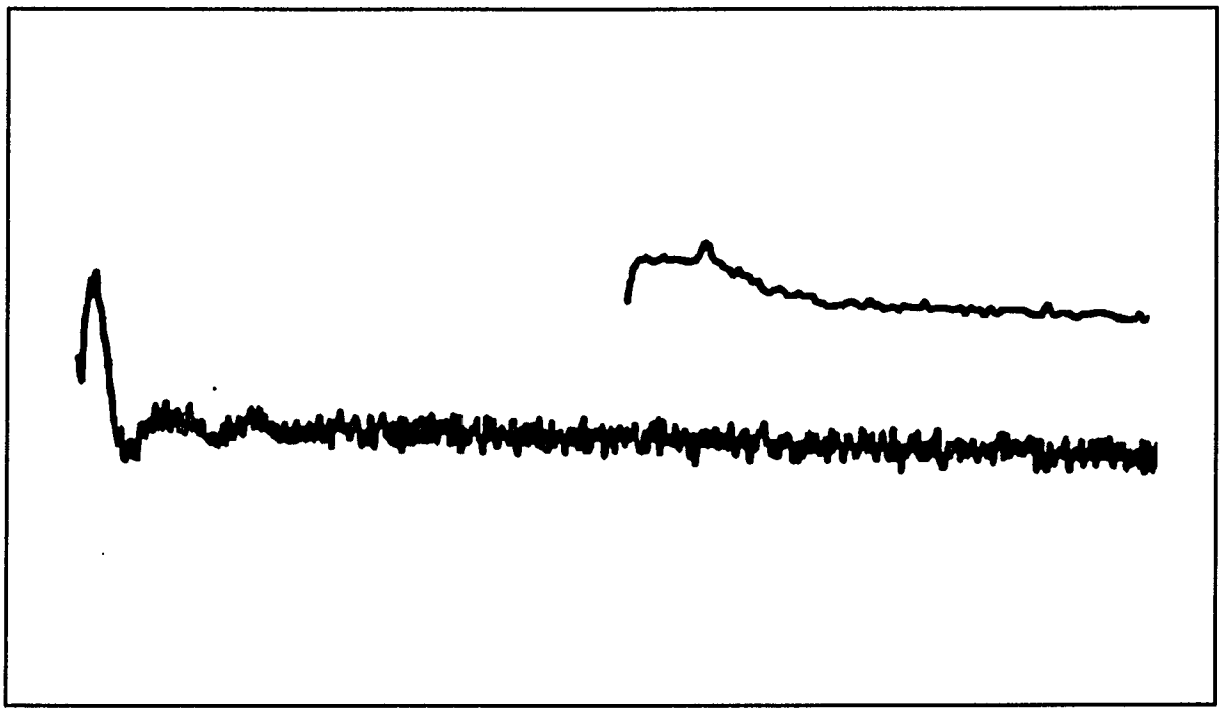

Figure 6.2. Deuteron NMR spectrum (time-domain FID and its Fourier transform) for a cellulose sample which was first saturated in D_2O moisture and then completely dried. The scale for the horizontal axis is 50 kHz/cm.

which fail to be nitrated may play a crucial role in water uptake in NC.

Deuterium NMR spectra for D_2O humidified NC taken for various temperatures are shown in Figure 6.3 for NC fibers and Figure 6.4 for NC film. Note that, in contrast to cellulose, no doublets are discerned. Furthermore, the linewidths are much narrower than in cellulose for comparable water content. Together, these results show that water molecules in NC are more mobile, i.e., less rigidly bound, than in cellulose. The remaining un-nitrated sites are the least polar, so water-polymer interactions are weaker in NC than in cellulose. The temperature dependence of the spin-lattice relaxation times should reveal important details of the D_2O motion. Figures 6.5 and 6.6 show Arrhenius plots of these data. Assuming a BPP relaxation process along with the fast motion approximation $\omega \tau_c << 1$, one can obtain the result,

$$1/T_1 \propto \tau_c = \tau_0 \exp(-E_a/kT)$$

where τ_c is the correlation time, and E_a is the activation energy. The data in Figures 6.5 and 6.6 yield $E_a = 4.1$ kcal/mole for both forms of NC, fibers or film. This value of the activation energy is about an order of magnitude larger than was reported in ESR results[ ] for Cu^{2+} ions in polymer binders.

A plot of the NMR linewidths, shown in Figure 6.7 and 6.8, respectively for NC fibers and film, indicates the presence of two kinds of water molecules, one more mobile than the other. Again, we are led to the conclusion that at the lower temperatures studied, there is little exchange between the two water sites. We note that this effect is more clearly pronounced in the film data, especially the lineshape details shown in Figure 6.4. While it may be premature to speculate about the nature of these two water sites,

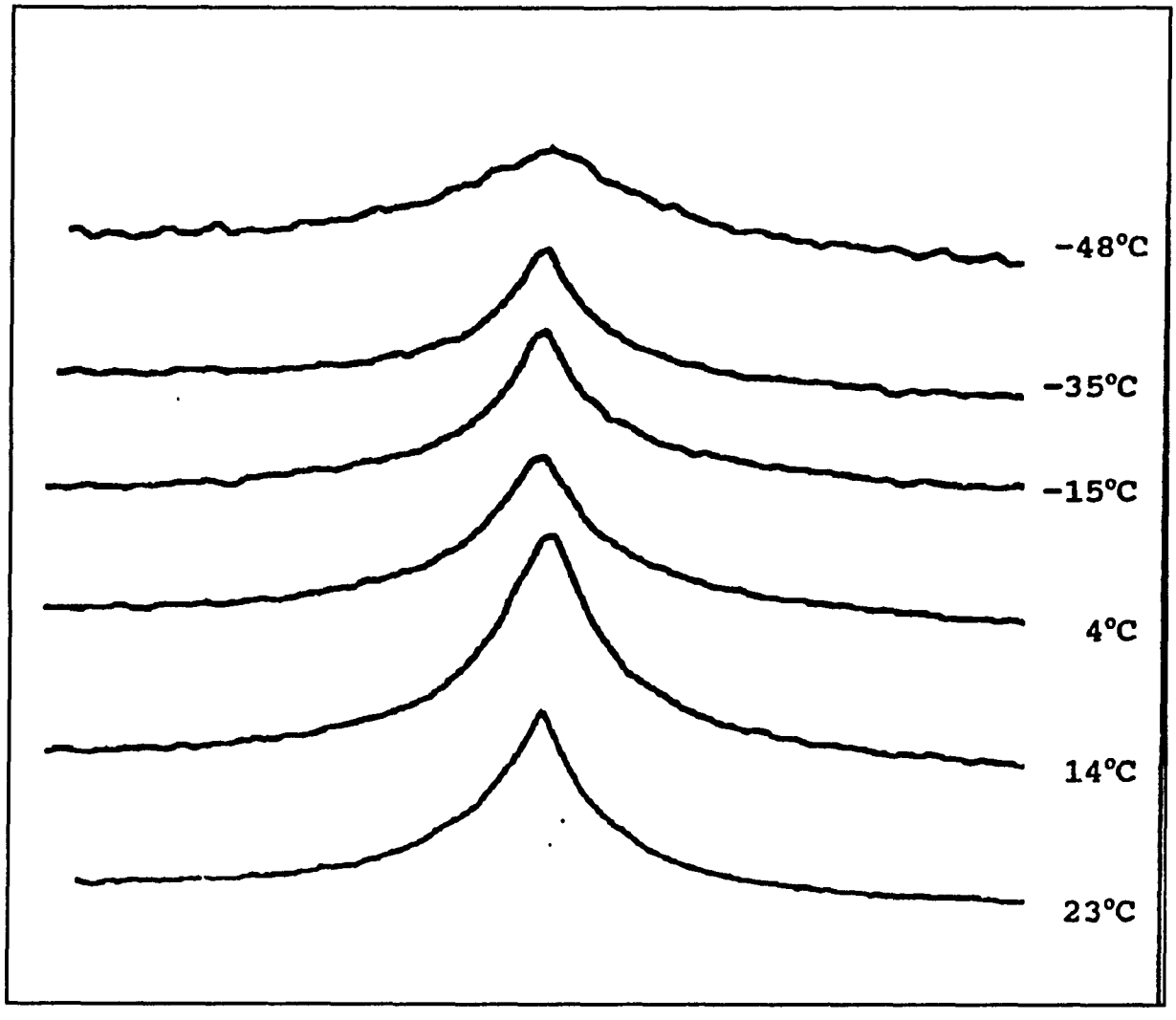

Figure 6.3. Temperature dependence of the Deuterium NMR lineshape in 3.5% D_2O nitrocellulose fibers. The scale for the horizontal axis is 2 kHz/cm.

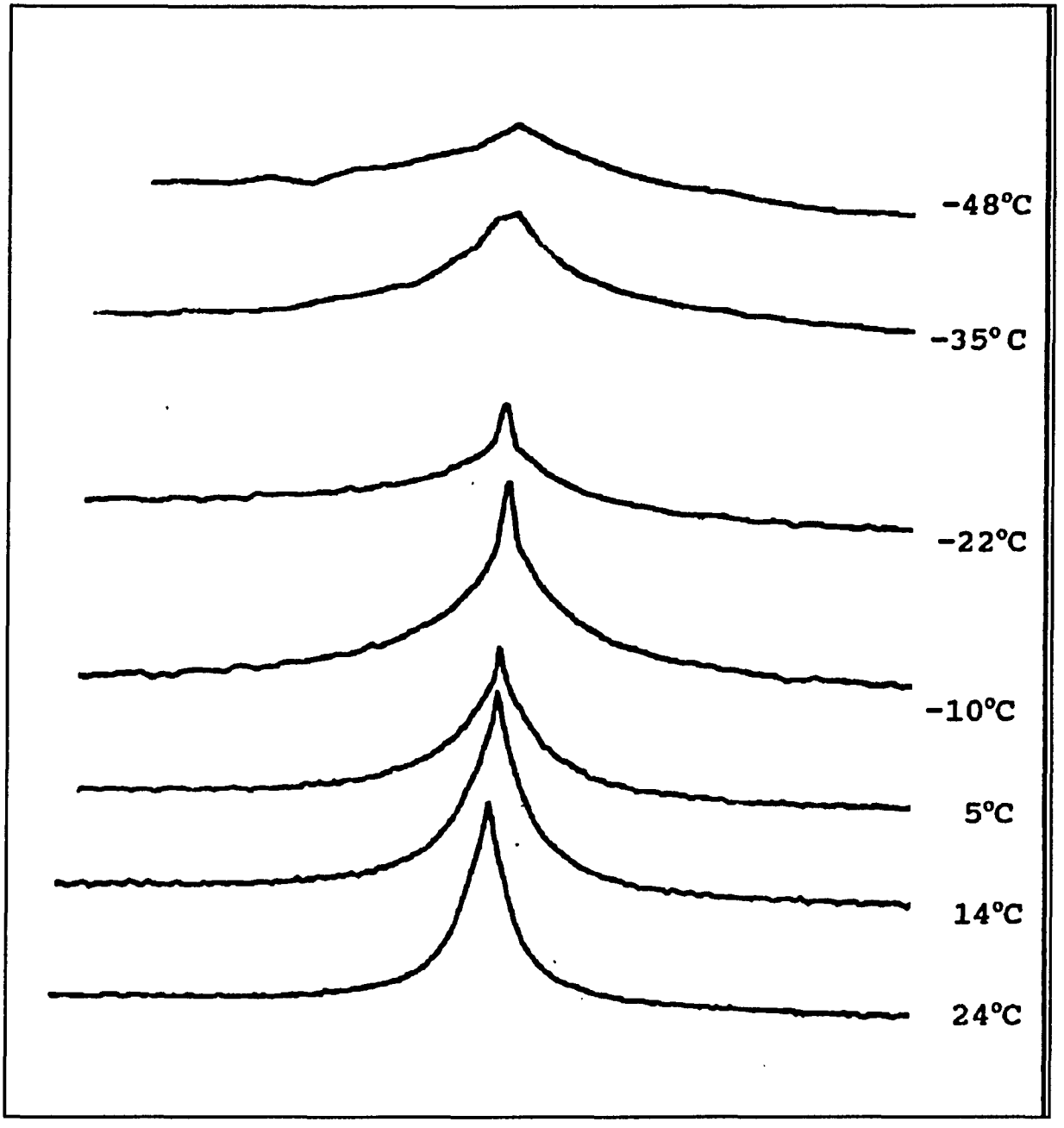

Figure 6.4. Temperature dependence of the Deuterium NMR lineshape in 2.0% D_2O nitrocellulose film (75 μm). The scale for the horizontal axis is 1.6 kHz/cm.

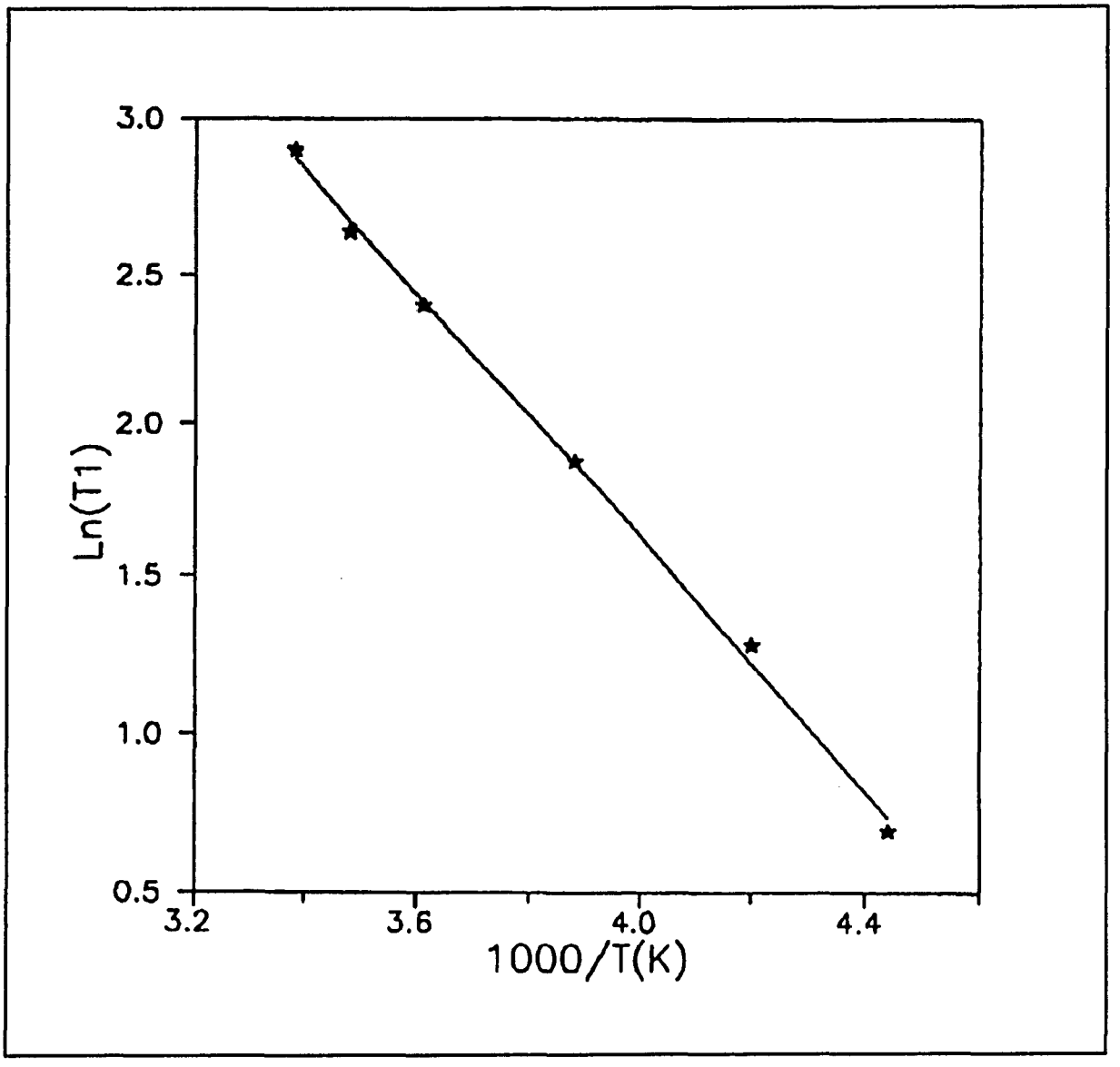

Figure 6.5. Temperature dependence of the Deuterium NMR spin-lattice relaxation time, T_1, for 3.5% D_2O nitrocellulose fibers.

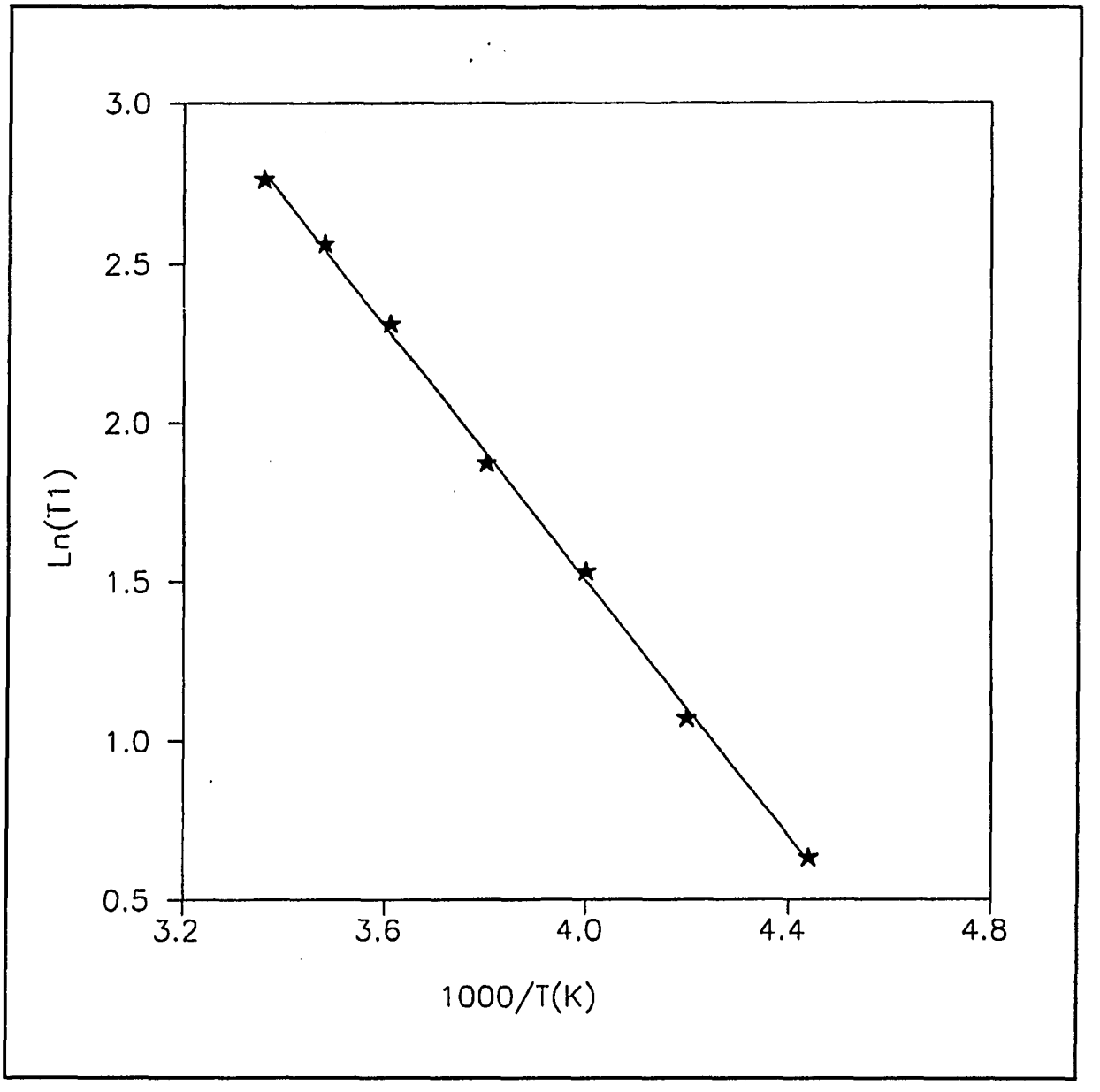

Figure 6.6. Temperature dependence of the Deuterium NMR spin-lattice relaxation time, T_1, for 2.0% D_2O nitrocellulose film (75 μm).

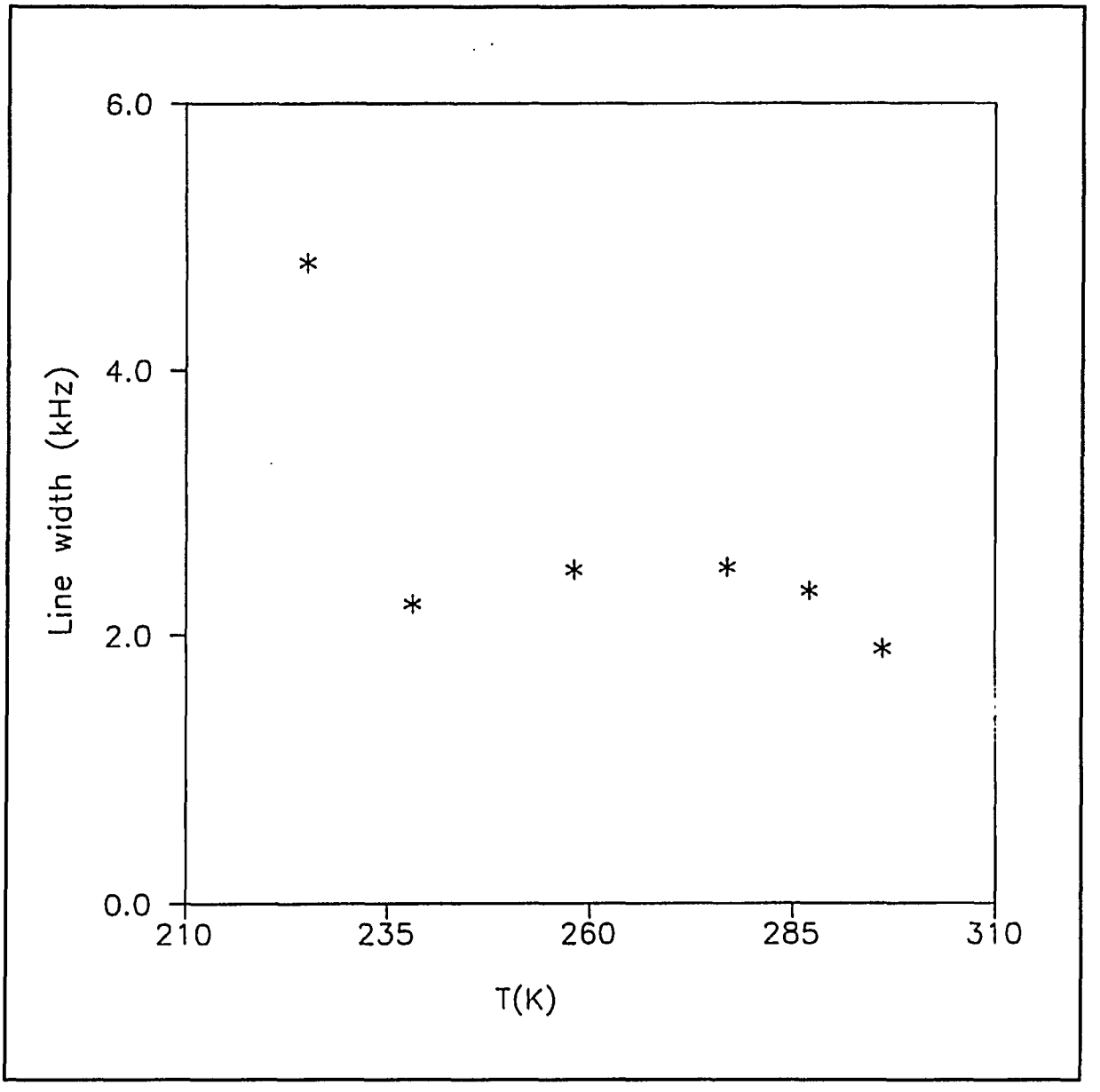

Figure 6.7. Plot of the Deuterium FWHM linewidth of 3.5% D_2O nitrocellulose fibers vs. temperature.

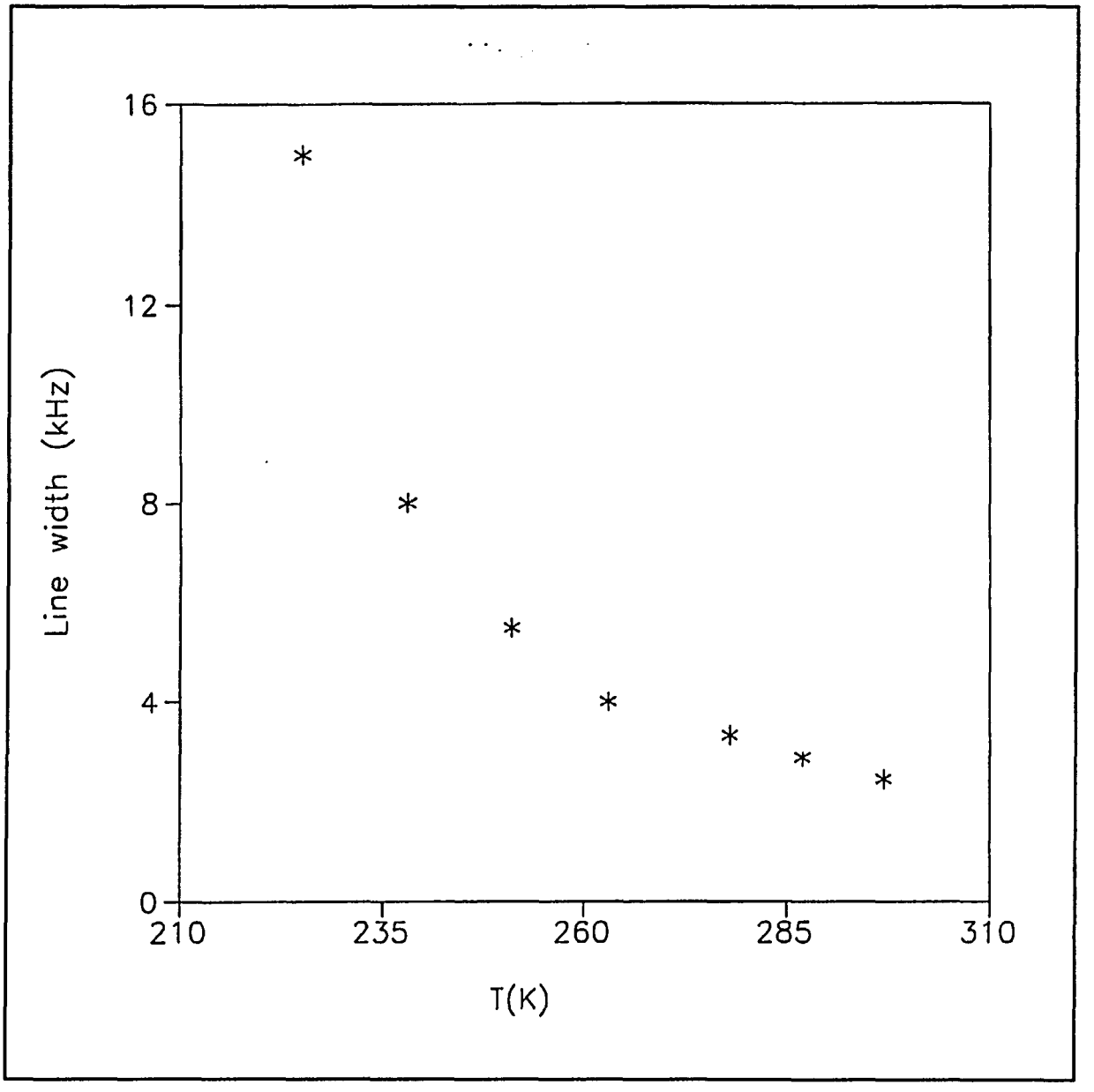

Figure 6.8. Plot of the Deuterium FWHM linewidth of 2.0% D_2O nitrocellulose 75 μm film vs. temperature.

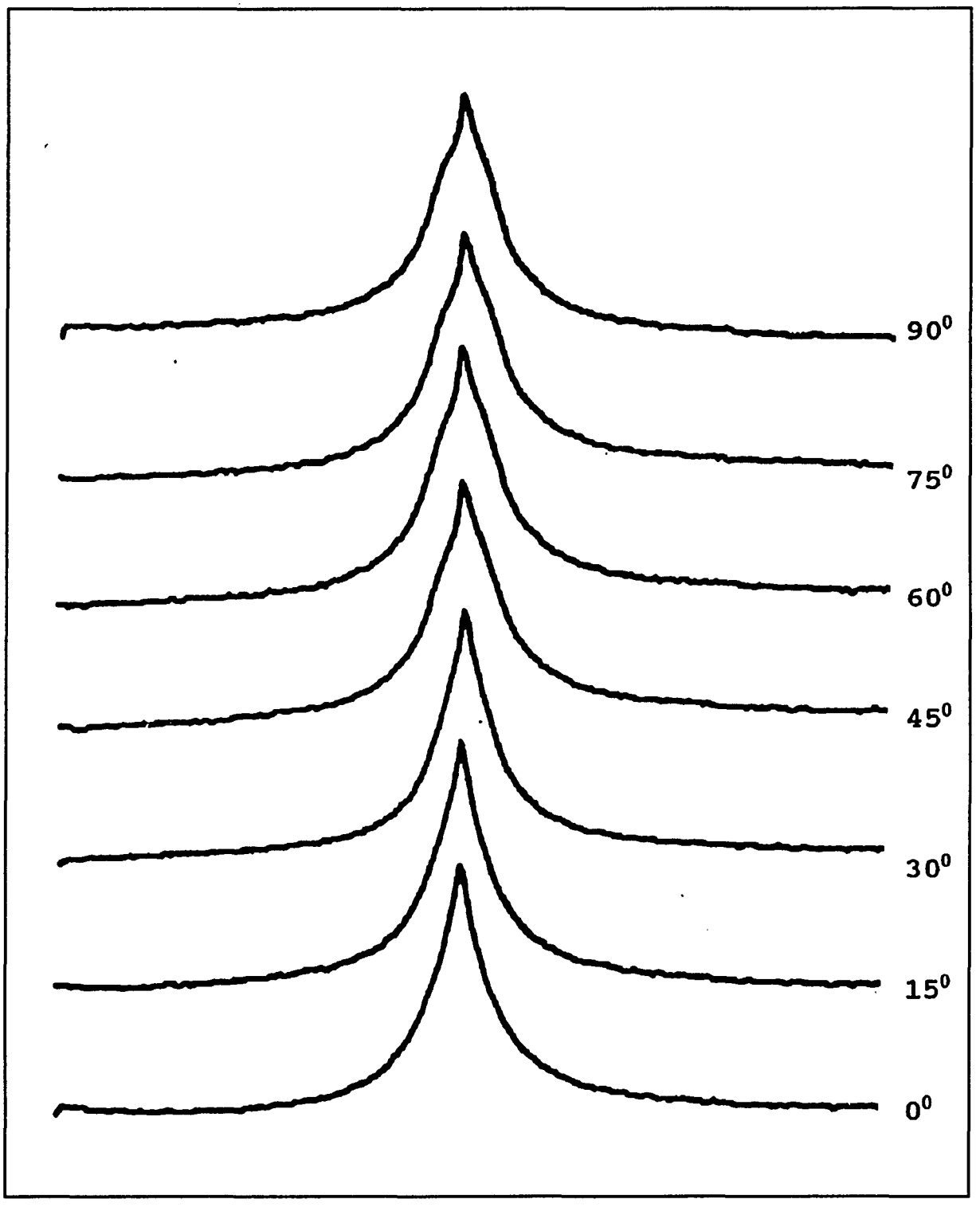

Figure 6.9. Orientational dependence of the Deuteron NMR room-temperature lineshape in 2% D_2O nitrocellulose film (75 μm).

we note that in the region between -22° and +5° they clearly differ in linewidth, and therefore, mobility.

The benefit of preparing thin NC films is that a partial orientation is thereby obtained. Presumably, very few polymer strands will be found with their long axis perpendicular to the film plane. NMR spectra from film samples can then be obtained with a known and variable angle between the static magnetic field and the normal film axis. Figure 6.9 shows the deuterium spectra at room temperature for a 75 μm film for seven different orientations between 0° and 90°. Very clearly there is an anisotropy, indicating that the axis of symmetry of the residual quadrupole coupling is (partially) ordered with respect to the polymer long axis. We could speculate that we are detecting a directed bonding to a specific structural feature of the polymer, such as the residual hydroxyl groups. However, more work is necessary, particularly lineshape simulations, to follow up on this conjecture.

In Table 6.2, we collect and compare the data obtained for films of thickness 75 and 200 μm. Narrower lines are observed in thicker films, indicating more exchange with more mobile water. Also, increasing water content results in smaller linewidths and longer spin-lattice relaxation times, consistent with the data and the discussion of cellulose Section (3.2.1).

6.4 Conclution

*NMR is shown to be able to offer unique and specific insights into the dynamics of polymer chains and in the behavior of impurity moisture.

Table 6.2 : NMR line width and T_1 values as a function of water content and film thickness

Film thicknesses	Water content (wt%)	Line width (kHz)	T_1 (msec)
75 μm	1.8	3.2	11.5
75 μm	2.0	2.3	15.8
250 μm	0.8	2.8	11.5
250 μm	1.3	2.3	13.8

*Two water sites were identified in moistened nitrocellulose. They have different temperature-dependent lineshapes showing that their motions "freeze out" at different temperatures.

*One of the water sites in nitrocellulose films is shown to be partially oriented with respect to the chain long axis, and is conjectured to be closely associated with un-nitrated hydroxyl sites. In order to follow up on these preliminary results, it would be useful to conduct further NMR studies, especially as a function of pressure, and it is very important to do a thorough lineshape simulation study to obtain more qualitative conclusions.

*Oxygen-17 NMR (via H_2O^{17} moisture)' could add additional insights into this general problem. Oxygen-17 has a much larger quadrupole moment than deuterium, and is not subject to the chemical substitution problems of D_2O with nitrocellulose, which would become severe at low moisture concentrations.

Chapter 7

Studies of water and methanol in NAFION membranes using Deuteron and Oxygen-17 NMR[1]

7.1 Introduction

Perfluorosulfonic acid ionomer membranes, a commercial example of which is Nafion (DuPont), are currently receiving a great deal of attention with regard to their ion exchange properties, especially in electrochemical applications such as fuel cells [26]. Nafion films readily incorporate water (up to 25% by weight) whose presence greatly facilitates ion transport. A number of studies have been directed at examining the specific role that water plays in proton transport, and related work has addressed the degree of water molecular diffusion through Nafion membranes [51,52,53].

The physical nature of water in Nafion has been characterized by several techniques and found to be significantly different than in the bulk state. Deuteron NMR has been shown to be a powerful technique in studying structural and dynamical aspects of polymers [18], owing to its selectivity and the nuclear quadrupole moment of the deuteron, which produces information-rich spectral and relaxation features. Part of this work consists of deuteron and ^{17}O NMR measurement on Nafion-117 films treated in D_2O and 20% enriched $H_2{}^{17}O$ respectively. These measurement were performed as a function of water content in order to examine the effect of water concentrate on proton and ^{17}O or water molecular mobility. These studies will include lineshape and spin-lattice

---

[1]This portion of the thesis concerns experimental work performed jointly with Mr. R.Chen, Physics Department, Hunter College

relaxation measurements as a function of water content and temperature. In addition, the presence of orientation effects were considered. For example, one of the main results of this study was the observation of anisotropic molecular motion in the film plane, with dramatic enhancement of the anisotropy in modestly stretched films.

The prospect of employing methanol directly as a fuel in low temperature fuel cells has obvious appeal, but there are some problems that must be addressed. Principal among these are the choice of a suitable catalyst to facilitate oxidation at the anode, and finding a membrane in which the methanol itself is inhibited from diffusing. In the latter case, methanol transporting across the membrane would be spontaneously oxidized at the cathode, leading to a chemical "short-circuit" in the fuel cell [32]. In other part of this work we employ NMR to investigate issues related to methanol molecular mobility in Nafion containing CH_3OD and $CH_3{}^{17}OH$ (15% ^{17}O-enrichment).

7.2 Experimental Details

Samples of Nafion-117 were obtained from E. I. du Pont Co. The samples were measured as received after having been dried in vacuum at about 340 K for several days. For the measurements, the Nafion film was cut into parallel strips which were stacked and placed in an open ended 7mm o.d. NMR tube. The sample was then treated in water (either D_2O or 20% enriched $H_2{}^{17}O$) or methanol (either CH_3OD or 15% enriched $CH_3{}^{17}OH$) vapor in a sealed bottle for several days, with various water contents of the Nafion being achieved by adjusting the relative humidity in the bottle through suitable choices of saturated salt solutions. Stretched Nafion samples were prepared by gradually (over period of several minutes) increasing the tension of a film clamped at both ends,

to a maximum elongation of about 20%, and maintaining this position for couple of days. The films were then released and were found to relax to about 115% of the original length after a few days, maintaining this length for about a week before further contraction was observed. The stretched film was dried under vacuum at room temperature and treated in the same manner as the unstretched samples.

Deuteron and oxygen-17 NMR data were obtained at a field of 7.2 Tesla with a Novex NMR spectrometer interfaced to a LeCroy 9400 digital oscilloscope and a microcomputer. A block diagram of the spectrometer is shown in Figure 7.1. Both single-pulse and quadrupole-echo (solid-echo) sequences were employed, the latter primarily for measurement of broad spectra at low temperature. Deuteron spin-lattice relaxation times (T_1) were measured by inversion recovery.

7.3 Result and Discussion

7.3a Deuteron NMR

Deuteron NMR linewidths of D_2O-containing Nafion film rolled into a cylinder (to suppress anisotropy) as a function of water content at 295K are displayed in Figure 7.2a. As water content increases the line width decreases, approaching the "liquid" deuteron line width of 40 Hz in this Magnet. Spin-lattice relaxation times (T_1) as a function of water concentration at 295K are shown in figure 7.2b. The T_1 values exhibit an approximately linear increase with increasing water content, approaching the value of free D_2O, 400ms [54]. The data in Figure 7.2a and 2b are consistent with the expectation that some fraction of the total water in the film approaches an isotropically free state, and that rapid exchange, on the NMR timescale, between these nearly free water molecules

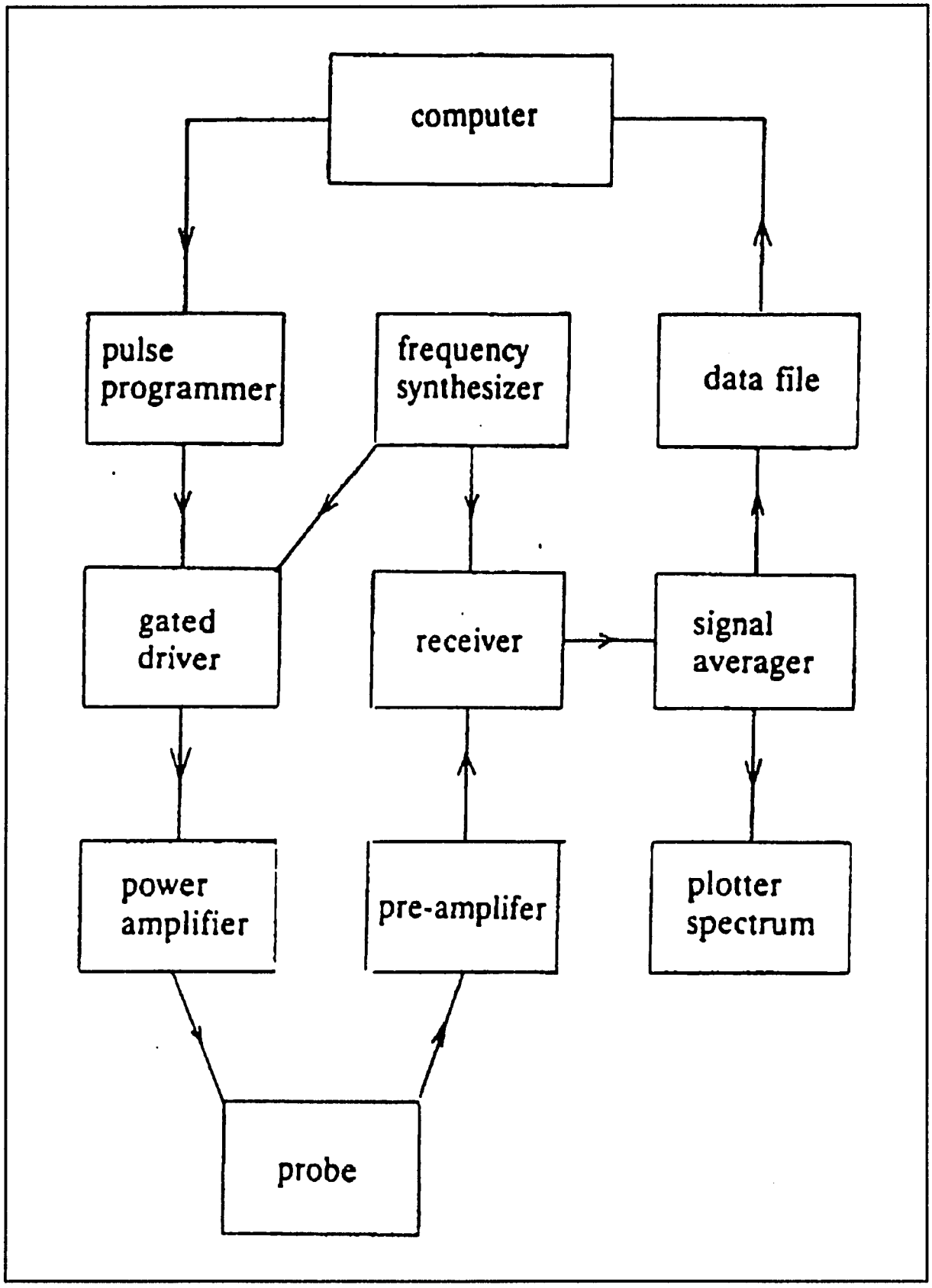

Figure 7.1: Block diagram of Novex NMR spectrometer.

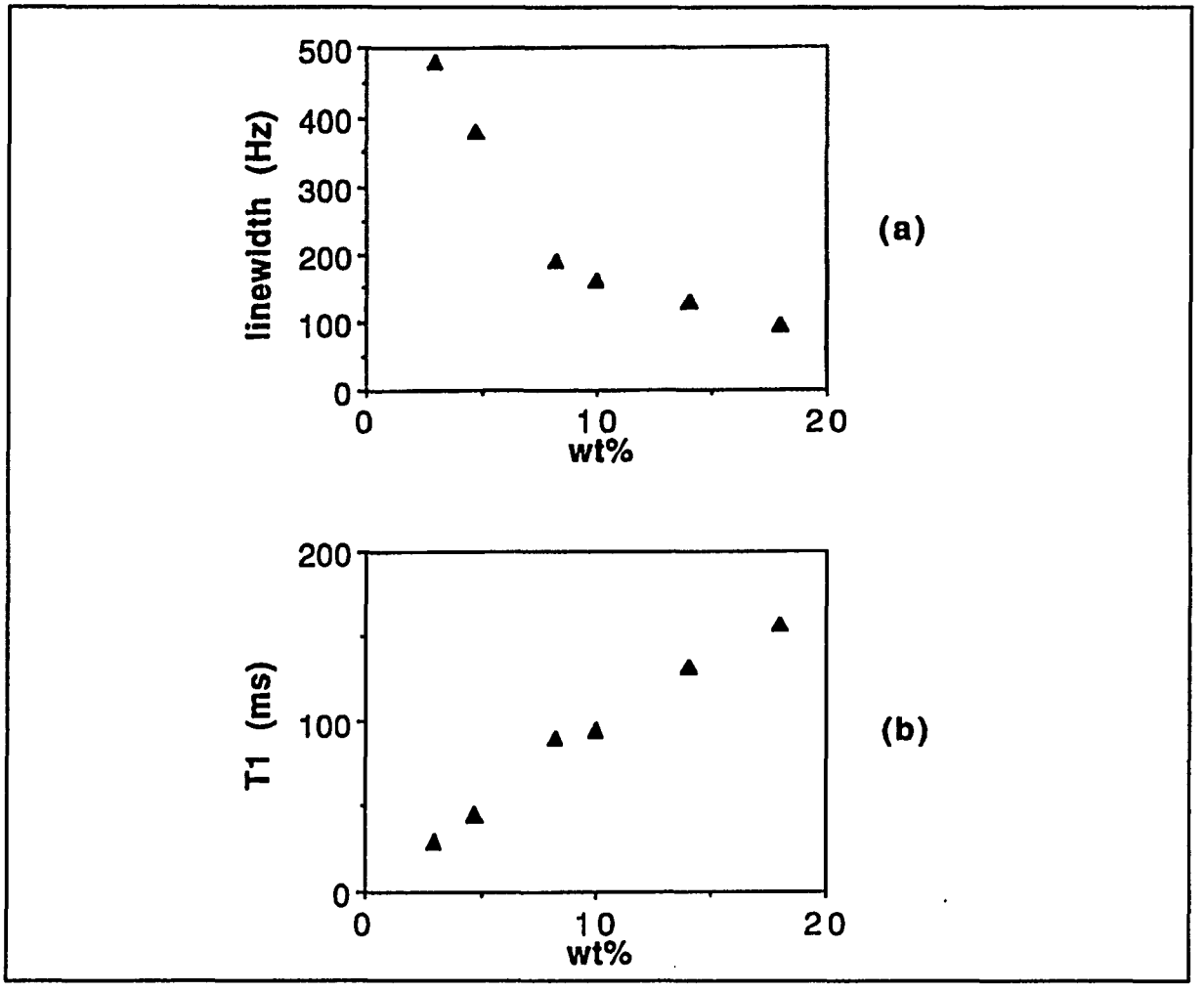

Figure 7.2: Deuteron NMR parameters as a function of D_2O water content at 295 K. (a) The linewidth vs. water concentration (b) The spin-lattice relaxation times vs. water concentration.

and those that are more motional restricted (by interaction with the polymer host) yield an averaged response. Such behavior, discussed previously in connection with water in NC, is commonly observed in organic membranes containing large amounts of water [55].

Deuteron spin-lattice relaxation times as a function of temperature were obtained by inversion recovery. Recovery profiles were observed to be exponential from room temperature down to 190 K. Figure 7.3 shows recovery curves of four different temperatures for Nafion with 10 wt% D_2O. Arrhenius plots of deuteron T_1 in Nafion at four different water concentration (4.7, 10, 14, and 18%) are shown in Figure 7.4. All sample exhibit a T_1 minimum at about 205K. Activation energies for deuteron motion have been obtained from the high T (with respect to the T_1 minimum) data in Arrhenius plots and are listed in Table 7.1. In the calculation of activation energy an exponential relaxation process was assumed along with the fast motion approximation $\omega\tau_c << 1$, as

Table 7.1. Activation energy from Figure 7.4.

Water content (w/o)	Activation energy (eV)
4.7	0.20
10.0	0.22
14.1	0.25
18.3	0.27

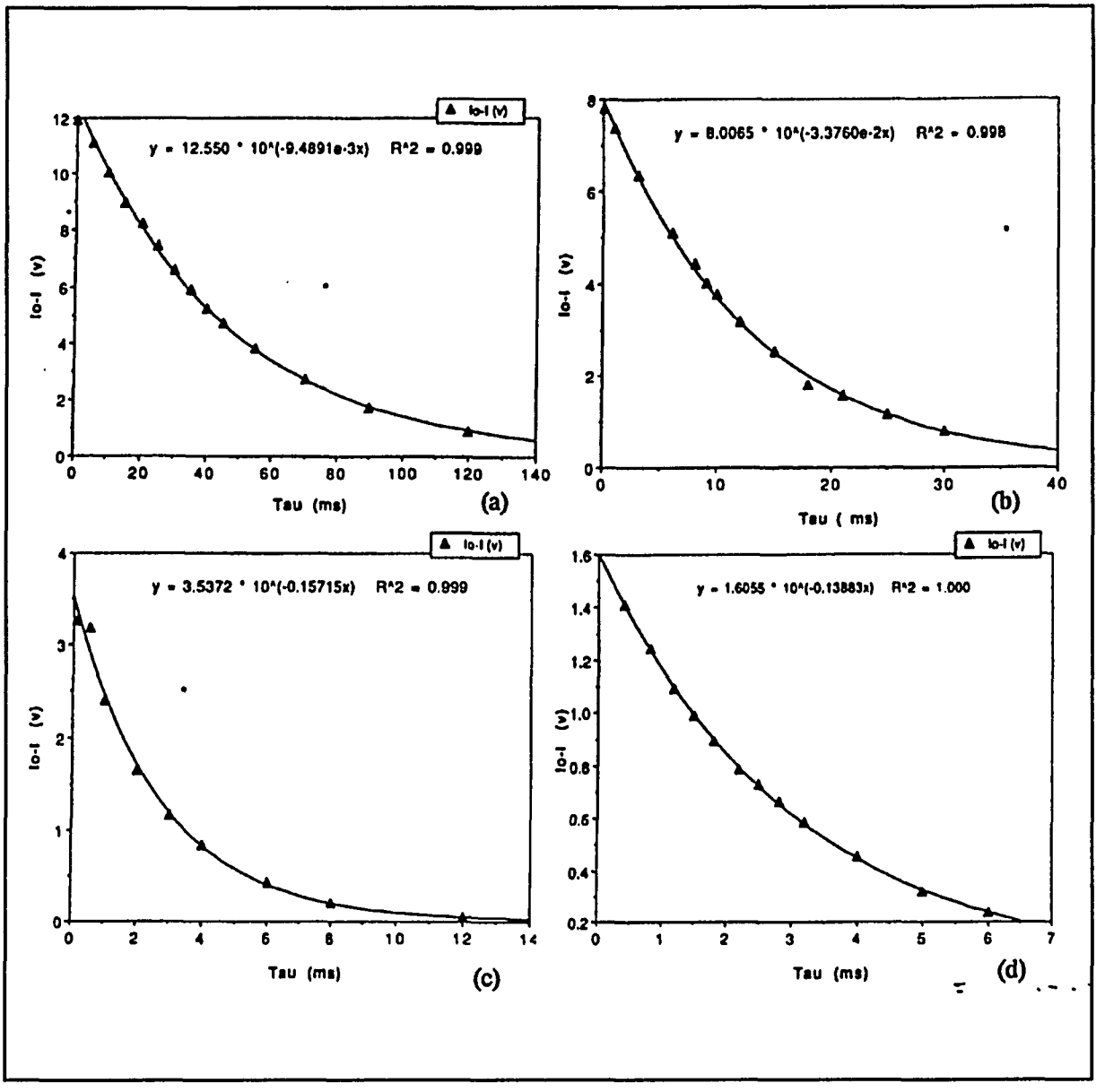

Figure 7.3: T_1 recovery curves for NAFION with 10 wt% D_2O at different temperature (a) T = 268 K, (b) T = 243 K, (c) T = 213 K, (d) T = 193 K. It can be easily seen that the data fits an exponential relation very well.

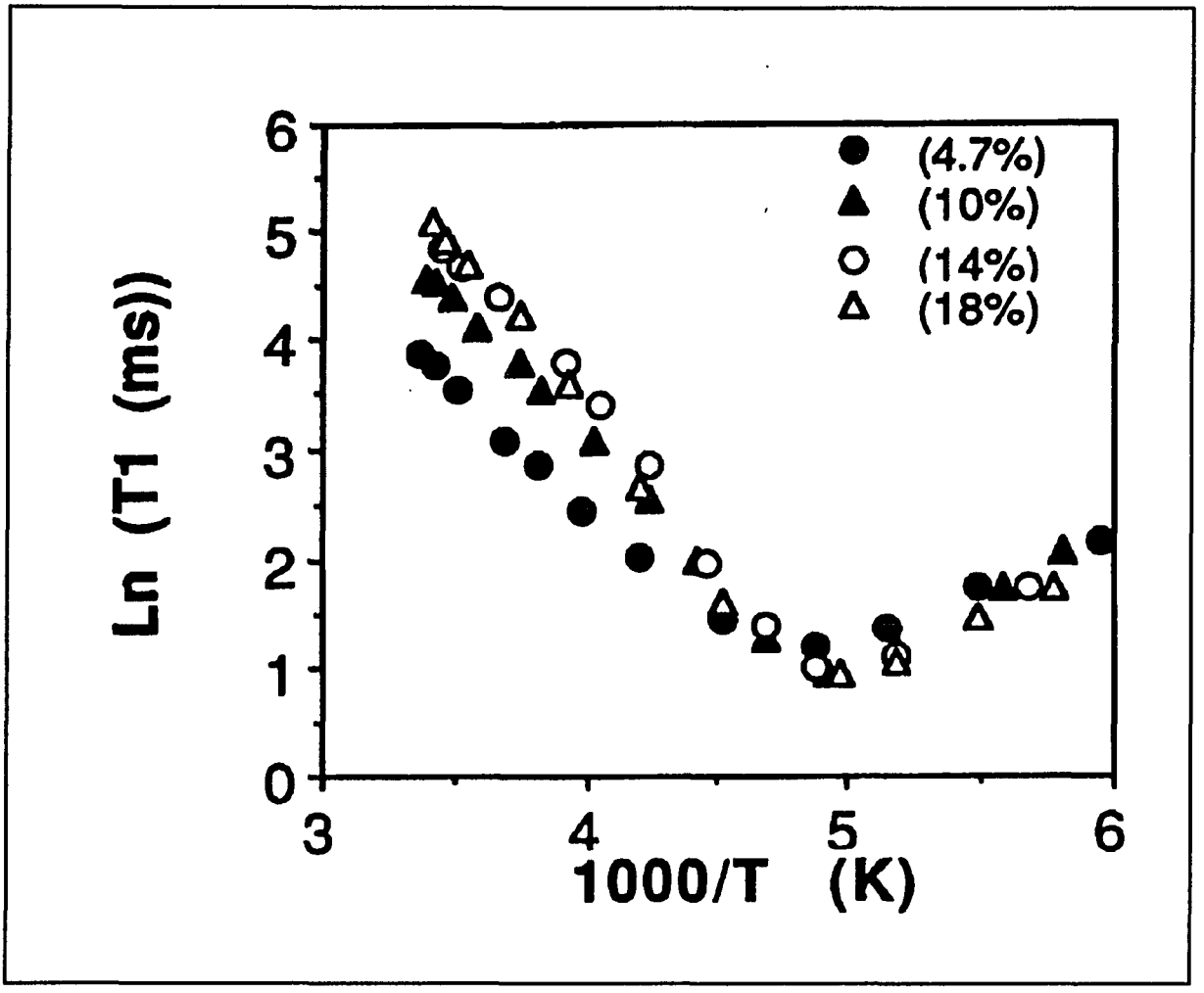

Figure 7.4: Arrhenius plots of deuteron T_1 in NAFION at four different water concentrations (4.7, 10, 14 and 18%). The activation energies extracted are listed in Table 1.

as described on page 84 (NC-work). Again this approximation yields

$$1/T_1 \propto \tau_c = \tau_0 \exp(-E_a/kT)$$

where ω is the NMR frequency, τ_c is the motional correlation time and E_a is the activation energy [38]. Although the true relaxation process is undoubtedly more complex than given by the BPP approximation, the rationale for using the above equation is that comparisons are being made between samples in which only one parameter (water content) is varied. Thus it is the relative change in activation energy that is physically significant. From Table 7.1, we see that E_a increases with increasing water content. The values of Table 7.1 are somewhat larger than the corresponding activation energy for free molecular rotation in liquid D_2O (0.14eV) [54]. This observation is consistent with earlier proton NMR results which suggested that thermally activated motion of water molecules is somewhat impeded by interactions with the host polymer [55].

Glassy behavior at low temperature, reported by previous investigators [30], can be inferred from the deuteron NMR line shape. Figure 7.5 shows spectra for both D_2O ice at 233K and Nafion containing 10% D_2O at 193K. The ice spectrum exhibits the well known divergence associated with a spin 1 powder pattern [18]. The Nafion spectrum, while being comparable in width to the ice spectrum, shows no clear divergence. Although averaging due to molecular motion is partly responsible for this effect, the Nafion line shape is also attributed to the glassy arrangement of water molecule, in which the associated distribution of deuteron quadrupole coupling parameters smears out the divergence.

Oriented Nafion films containing 8% D_2O at 295K and at several angles θ between the film plane and the static field were observed. The film set up is shown in Figure 7.6.

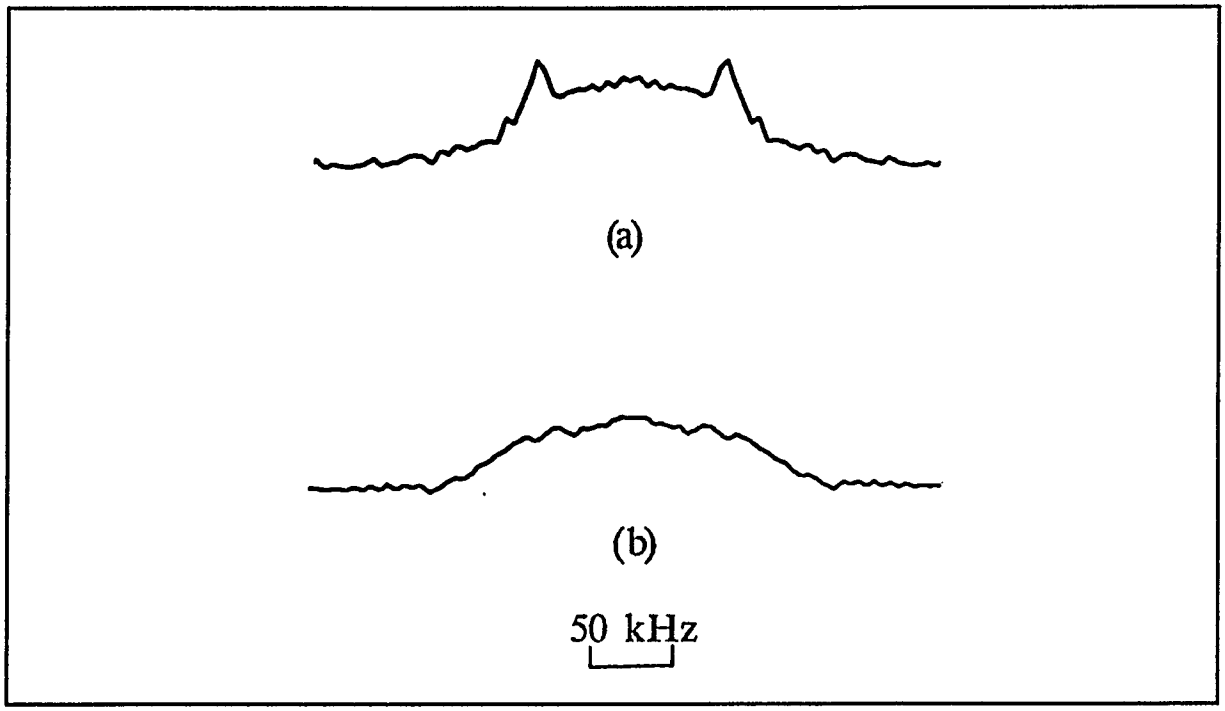

Figure 7.5: Deuteron powder pattern shows glassy behavior at low temperature, (a) D_2O ice at 233 K. (b) NAFION containing 10 wt% D_2O at 193 K.

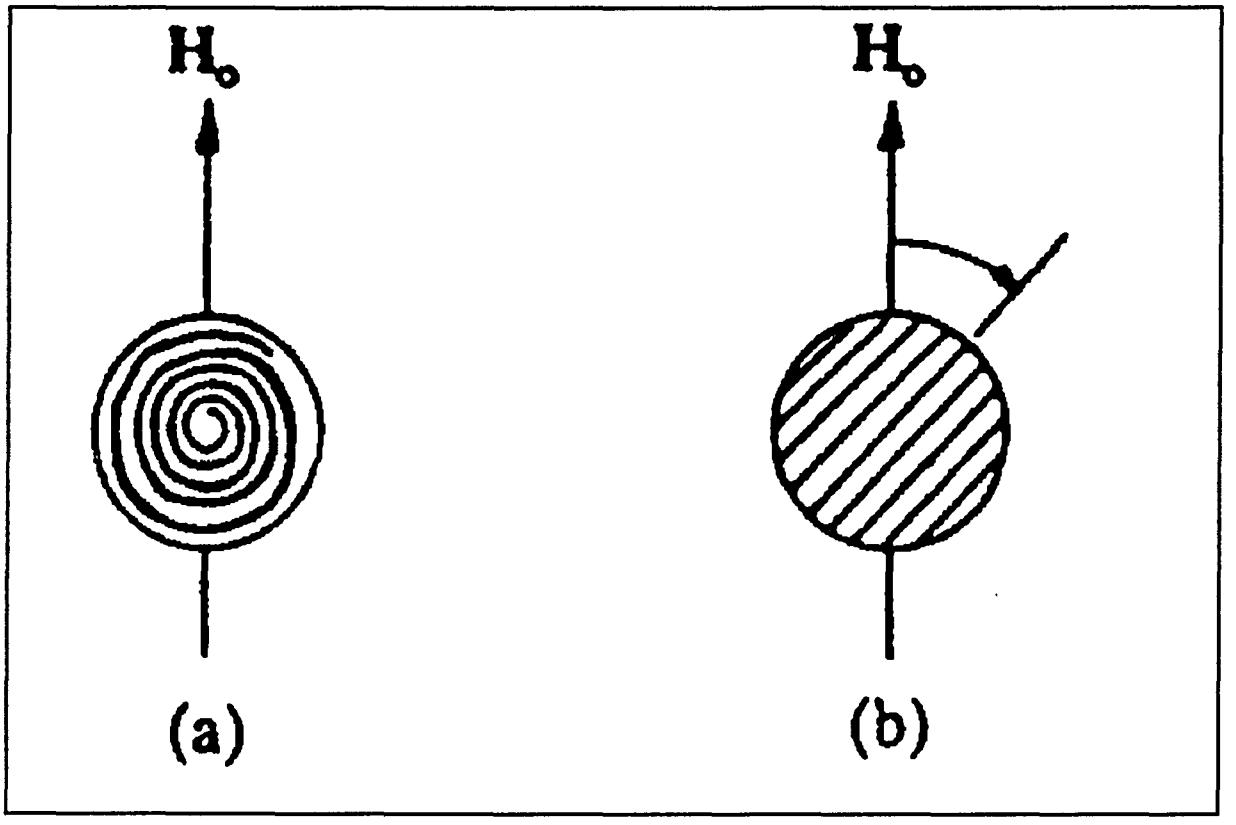

Figure 2.6: Sample configuration of a) the rolled films and b) the stacked films.

Deuteron NMR spectra of an oriented stack of Nafion films containing 8 wt% D_2O at 295 K and at several angles θ between the film plane and the static magnetic field are displayed in Figure 7.7a. The observed angular dependence indicates that the deuteron motion, while rapid on the NMR time scale, is anisotropic. That is, although much of the quadrupole interaction is average out by molecular motion, residual molecular orientation persists approximately in the plane of the film. Figure 7.7b shows the angular dependence for a film of 8% D_2O that was stretched by 13%. The largest splitting occurs when the static magnetic field is parallel to the stretched direction. In addition the angular dependence follows the $3\cos^2\theta$-1 dependence of the quadrupole splitting, given that the average principal axis of the electric field gradient (EFG) tensor is along the stretch direction [55]. This conclusion is most evident by observing that the splitting reaches a minimum at the 60° orientation, which is close to the angle at which the quadrupole splitting vanishes. The 0° spectrum in Fig. 7.7b suggests the presence of two inequivalent deuteron sites in the stretched film. Whether this inequivalence is generated or merely resolved by stretching is not known.

Deuteron NMR spectra at room temperature of Nafion-117 films containing 24 wt% CH_3OD are shown in Figure 7.8a and 8b, for both unstretched and 11% stretched samples respectively. The angles listed between the spectra correspond to the relative orientation of the external magnetic field and the stretched direction. Comparison of the spectra in 8a and 8b clearly show that some molecular anisotropy is generated by stretching. The splitting in 8b appears to follow the $3\cos^2\theta$-1 angler dependence of a

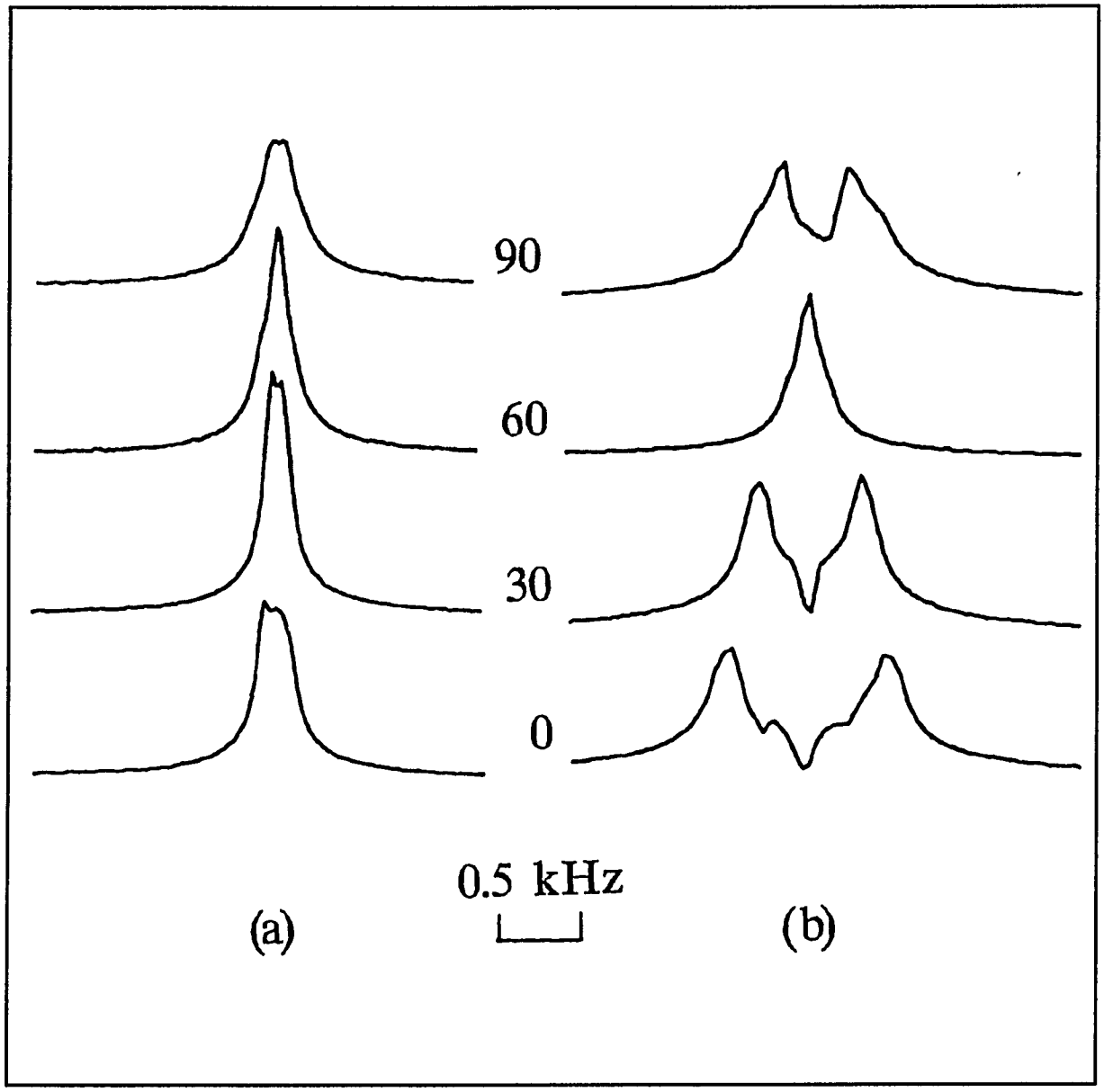

Figure 7.7: Deuteron NMR spectra of NAFION film with 8.2 wt% D_2O at θ=0°,30°,60°,90°.(a) unstretched, (b) stretched to 13% elongation.

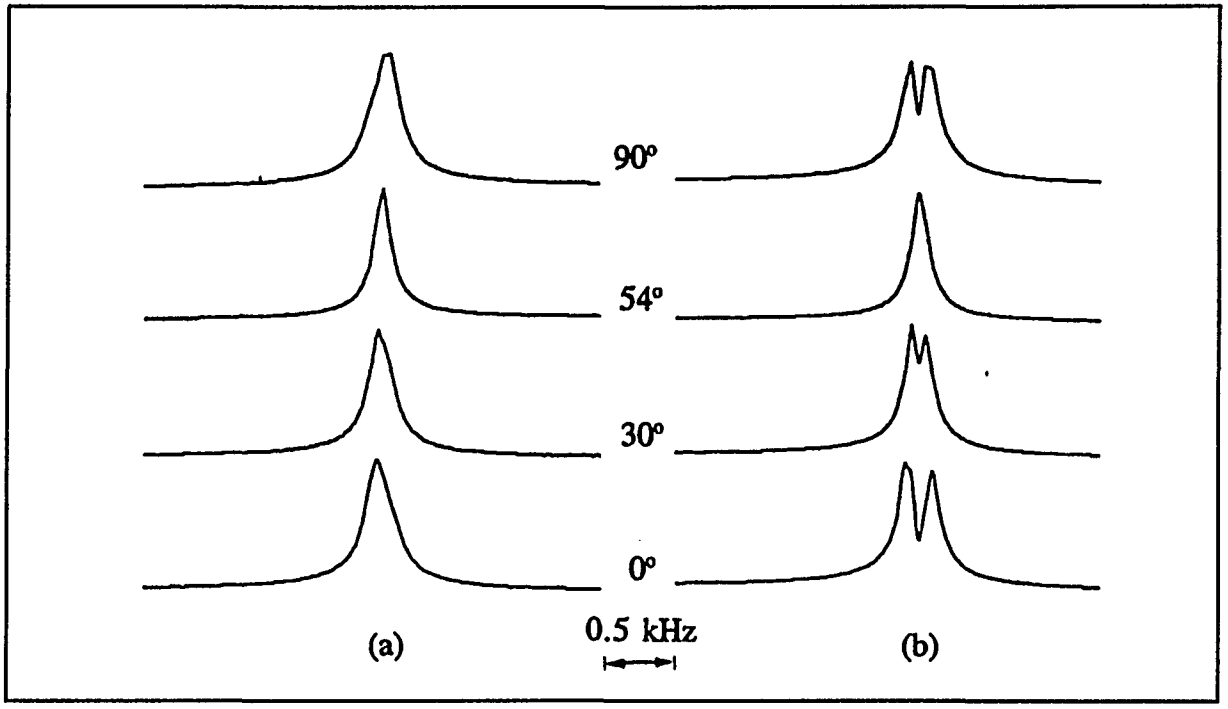

Figure 7.8: Deuteron NMR Spectra Nafion containing 24 wt% CH_3OD. (a) unstreched; (b) 11% stretched.

quadrupole-perturbed Zeeman Hamiltonian. Close examination of the spectra in 8a also shows some anisotropy, even though much smaller than 8b, according to the minimum line width being observed at the angle 54° ("magic angle") at which the quadrupole splitting vanishes. However, it is necessary to point out that stretched films containing a comparable molecular concentration of D_2O (15 wt%) exhibited (Fig. 7.7b) splitting an order of magnitude larger than shown in 8b. In order to appreciate the degree of anisotropy exhibited here it is useful to mention that the full splitting that would result from the quadrupole interaction of a rigid O-D bond is on the order of 200 kHz [54]. Thus nearly all of the anisotropy is averaged out by molecular motion, more so for CH_3OD than for D_2O.

In order to obtain additional information regarding the dynamics of methanol in Nafion, variable temperature linewidth and T_1 measurements were performed. For linewidth measurements, unstretched samples oriented close to the magic angle were utilized in order to suppress the small anisotropy shown in Figure 7.8. Arrhenius plots of deuteron linewidth of two samples, one saturated with CH_3OD (24 wt%) and the other containing 17 wt%, are displayed in Figure 7.9. The linewidth of the 17 wt% sample is characterized by a low activation energy ($\sim$0.05 ev) region above 240 K, steepening to $\sim$ 0.20 ev between 180 and 240 K. The sample exhibits a highly unusual line-narrowing phenomenon as T is decreased below 170K. The origin of this line-narrowing is presently unknown, but could possibly be attributed to a subtle phase transition. The 24 wt% sample follows the same kind of behavior as the unsaturated one, but all of the features are shifted to lower temperature by some 5 - 10 K. It is interesting that at the lowest temperature at which measurements were made (140 K), the linewidth was still observed

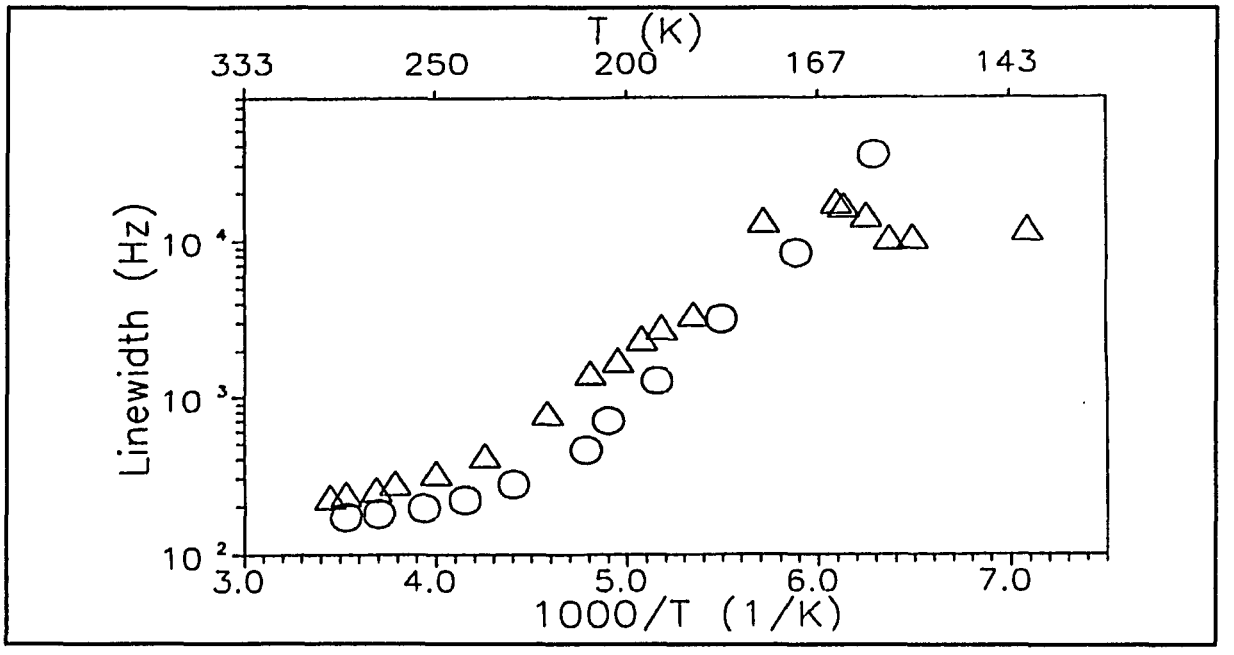

Figure 7.9: Arrhenius plots of ^2H NMR linwidth in Nafion containing 17 wt% (triangles) and 24 wt% (circles) CH_3OD.

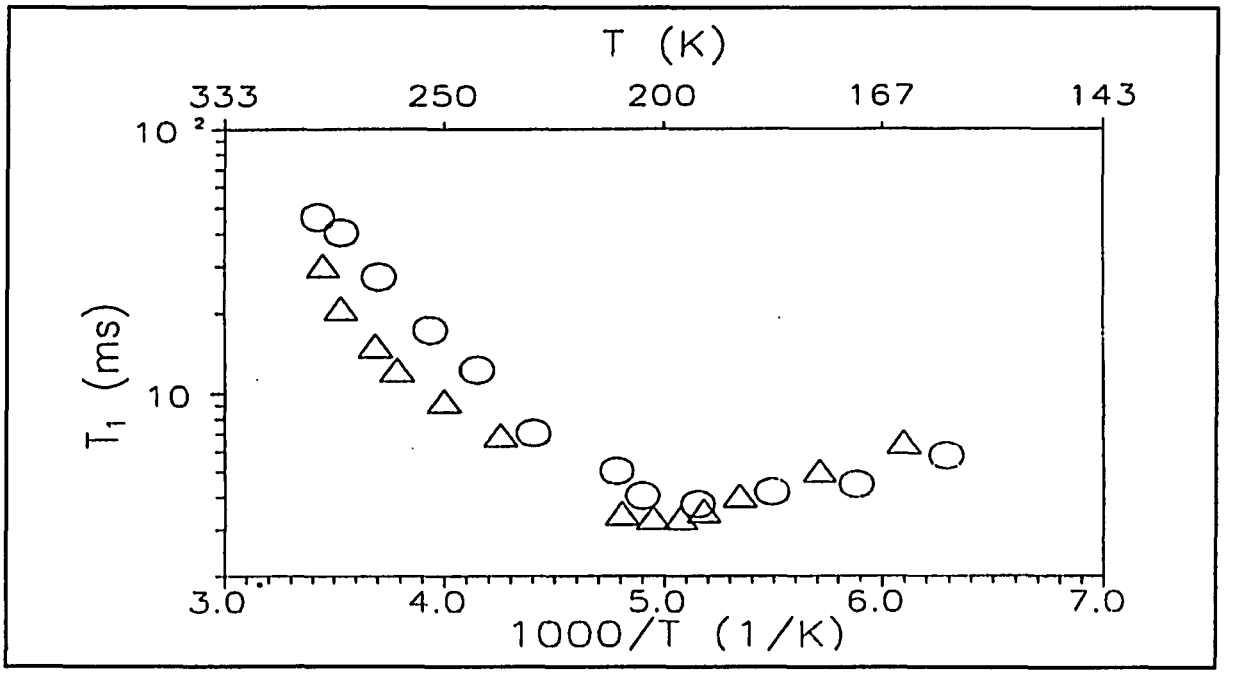

Figure 7.10: Arrhenius plots of deuteron spin-lattice relaxation time T_1 in Nafion containing 17 wt% (triangles) and 24% (circles) CH_3OD.

to be an order of magnitude smaller than that corresponding to a rigid quadrupole interaction for an O-D bond. In Nafion containing D_2O, the full rigid deuteron linewidth was observed at around 190 K [31]. Thus molecular motion is frozen out at much higher T in the Nafion-water system than in Nafion-methanol. Arrhenius plots of T_1 of these samples are shown in Figure 7.10. Again, the two curves exhibit similar behavior with the features, most notably the T_1 minimum, of the 24 wt% sample shifted to lower T (by 5 - 10 K) relative to the 17 wt% sample.

7.3b Oxygen-17 NMR

Since ^{17}O has a central as well as satellite transitions (with different relaxation times) while ^{2}H has only a single effective resonance frequency, the recovery profiles were exponential only at large water content and high temperature, where the high speed molecular motion averages the quadrupole interaction. Several recovery plots with curve fitting are shown in Figure 7.11. As we can see, the recovery profiles are exponential when the temperature is not so low (287 K, 270 K) while at 201 K and 183 K, the experimental curves can no longer be fit by a single exponential.

Oxygen-17 spin-lattice relaxation times (T_1) as a function of water content were obtained by fitting the inversion recovery data to an exponential,and from the relation $\tau_0 = T_1/\ln 2$ where τ_0 is the time separation between two pulses corresponding to a null signal. The resulting value are plotted in figure 7.12. It can be seen, at the high water content (> 10 wt%), the T_1 data obtained by both methods are in good agreement. At low water content there are some deviations because of non-exponential profiles. The T_1 value of 0.26 ms for 6.0 wt% increases to 1.8 ms for 15.7 wt%. Oxygen-17 lineshapes

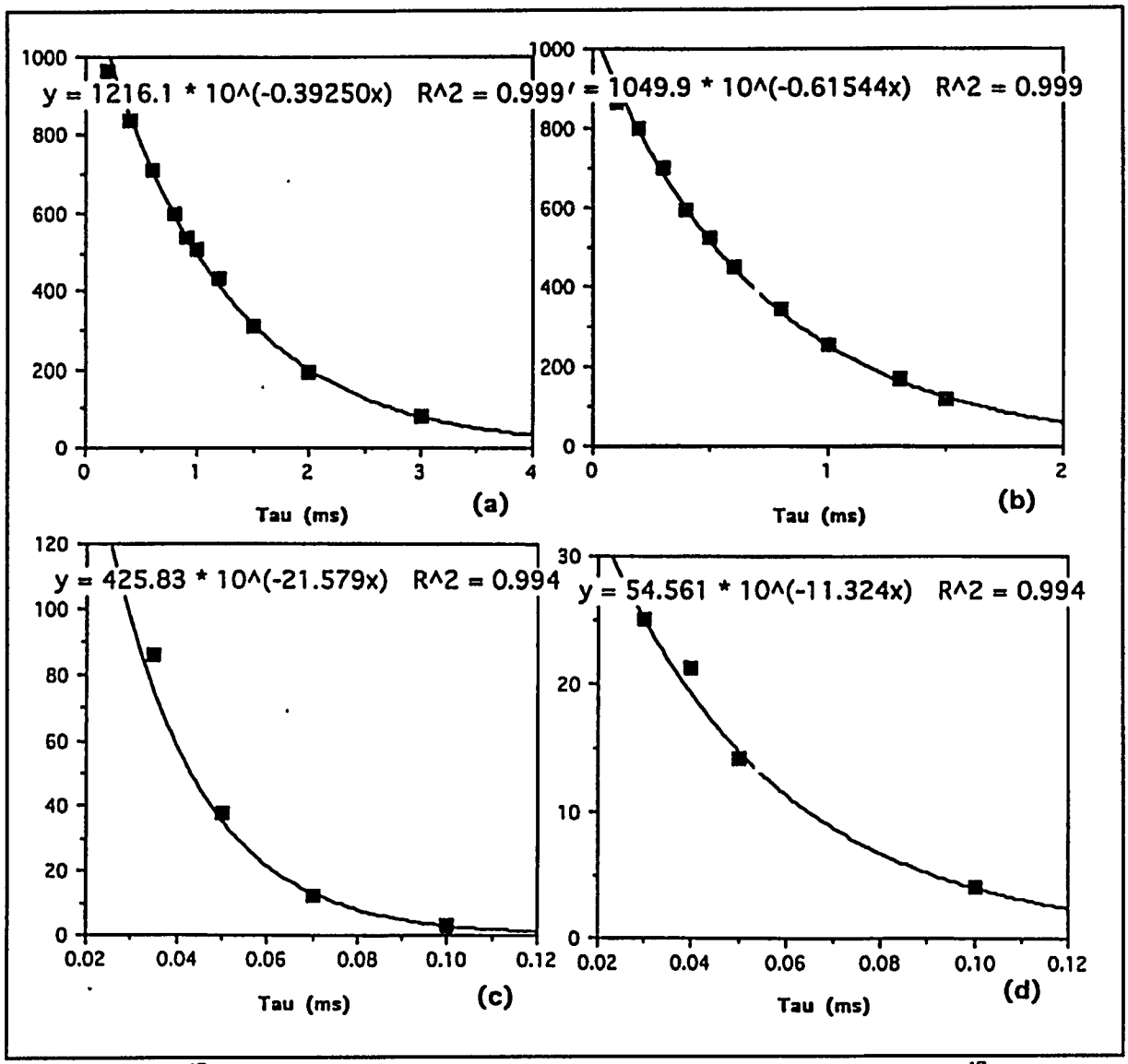

Figure 7.11: ^{17}O T_1 recovery profiles for NAFION with 13.2 wt% H_2O^{17} at several different temperature, (a) T = 287 K, (b) T = 270 K, (c) T = 201 K, (d) T = 183 K.

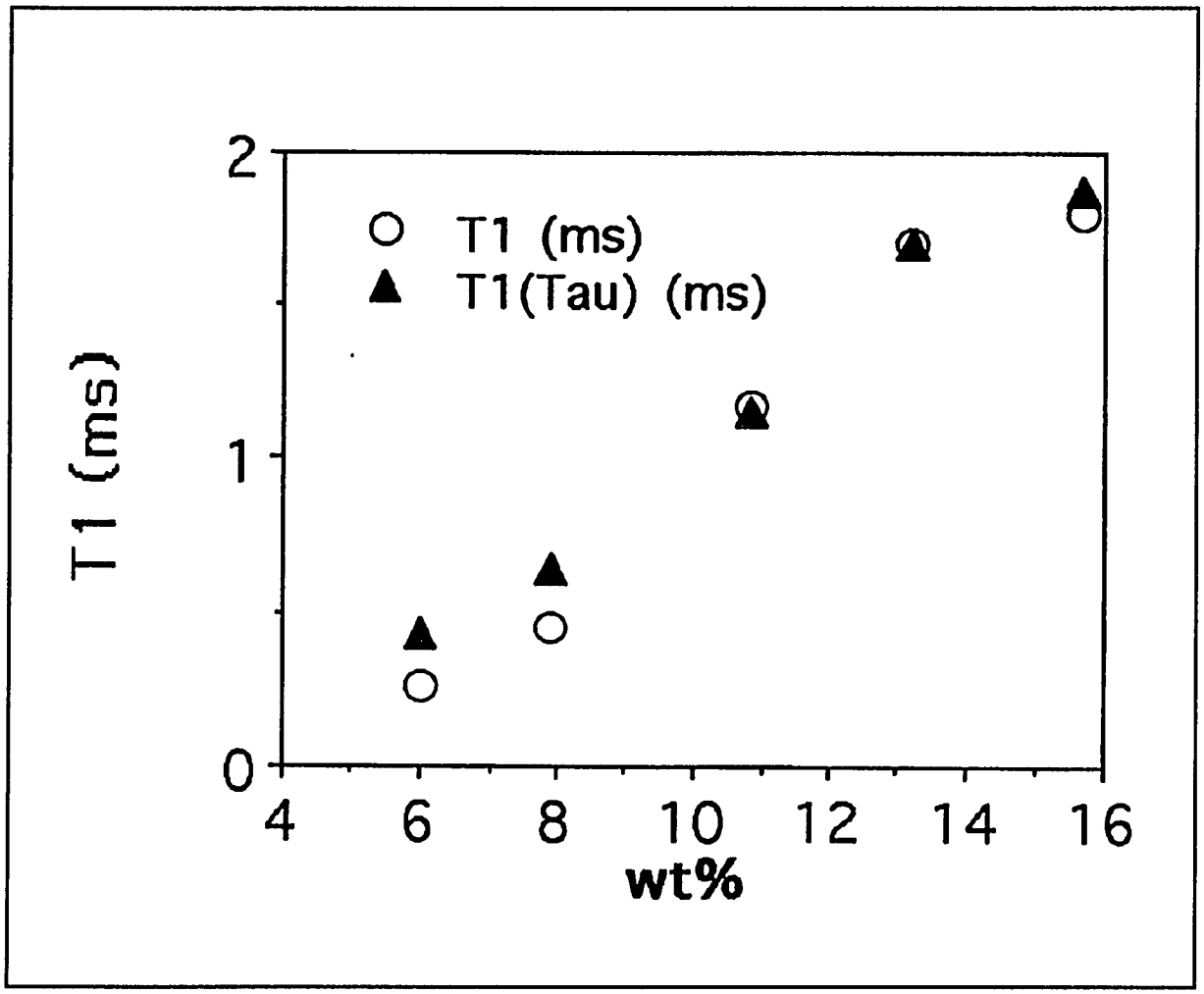

Figure 7.12: Oxygen-17 T_1 as a function of water content in NAFION membranes.

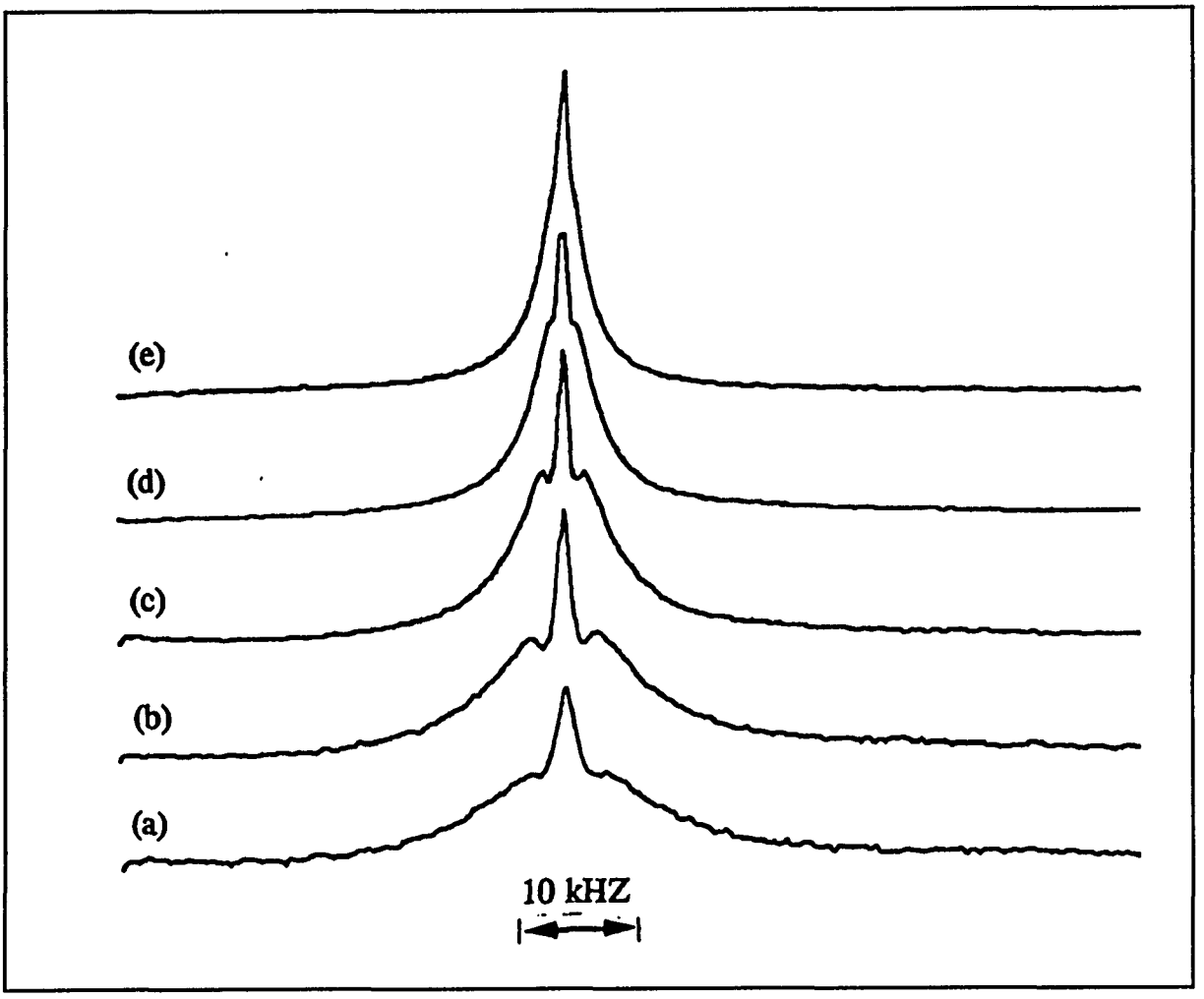

Figure 7.13: Oxygen-17 lineshapes vs. water content in NAFION, (a) 6.0 wt%, (b) 7.9 wt%, (c) 10.9 wt%, (d) 13.2 wt%, (e) 15.7 wt%.

vs. water content are displayed in Figure 7.13. The Nafion film plane is parallel to the external field $\mathbf{H}_0$. Unlike deuteron, it has a central transition peak and two inner satellites when the water content is low. The outer satellites are unresolved.

The separation of two satellites (Δf) at 0° degree orientation as a function of water content is plotted in Figure 7.14a, the separation decreases from 6.7 kHz to 1.5 kHz as the water content increases from 6.0 wt% to 15.7 wt%. The linewidths ($\Delta\nu$) for central transition at 54.7° orientation and the linewidth of two satellites (ΔF) at 0° orientation are plotted in Figure 7.14b. The linewidth $\Delta\nu$ at 54.7° shows a decrease from 4.1 kHz to 1.9 kHz, and the linewidth for the two satellites also shows a decrease though the value is about four times $\Delta\nu$. All of these results provide evidence for rapid exchange and motional effects at higher water content.

An Arrhenius plot of T_1 in NAFION at 13.2 wt% water is shown in Figure 7.15a. The curve shows a T_1 minimum at about 201 K. Activation energy for oxygen motion extracted from the high T side was 0.24 eV, this is consistent with the deuteron NMR results. The Arrhenius plot of ^{17}O linewidth for 15.7 wt% water is displayed in Figure 7.15b. Note that there is a broadening peak at about 201 K, which corresponds to the T_1 minimum. The second order quadrupole interaction for the central transition has been studied in detail [56,57], and the linewidth behavior shown in Figure 7.15b is predicted by calculations and borne out by other experiments [56,57].

^{17}O NMR spectra of an 13 wt% H_2O film stack (20% enriched ^{17}O) are shown in

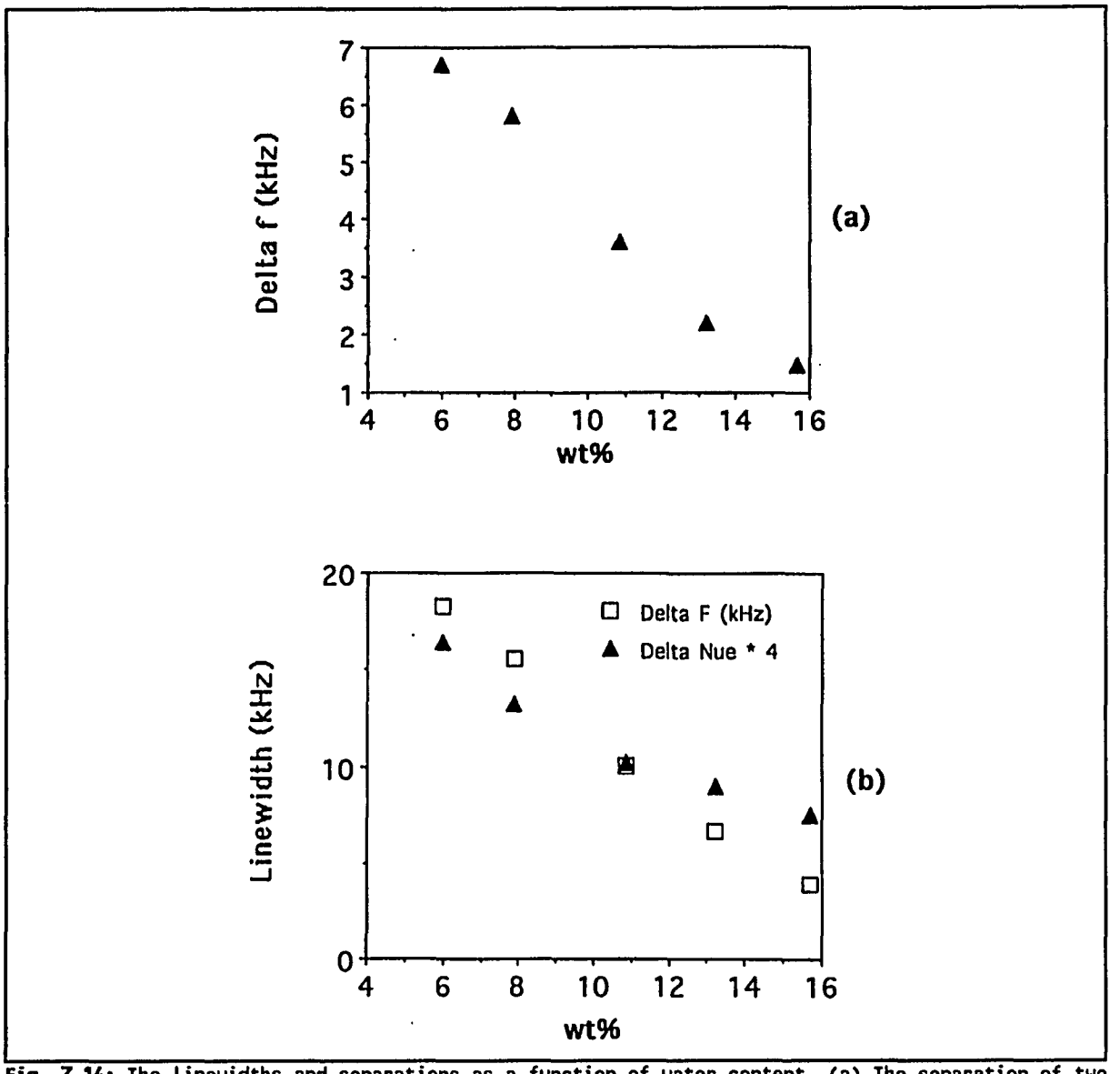

Fig. 7.14: The linewidths and separations as a function of water content, (a) The separation of two satellites (Δf) at 0°, (b) The linewidths (Δν) at 54.7° and the linewidth of satellites (ΔF) at 0° orientation.

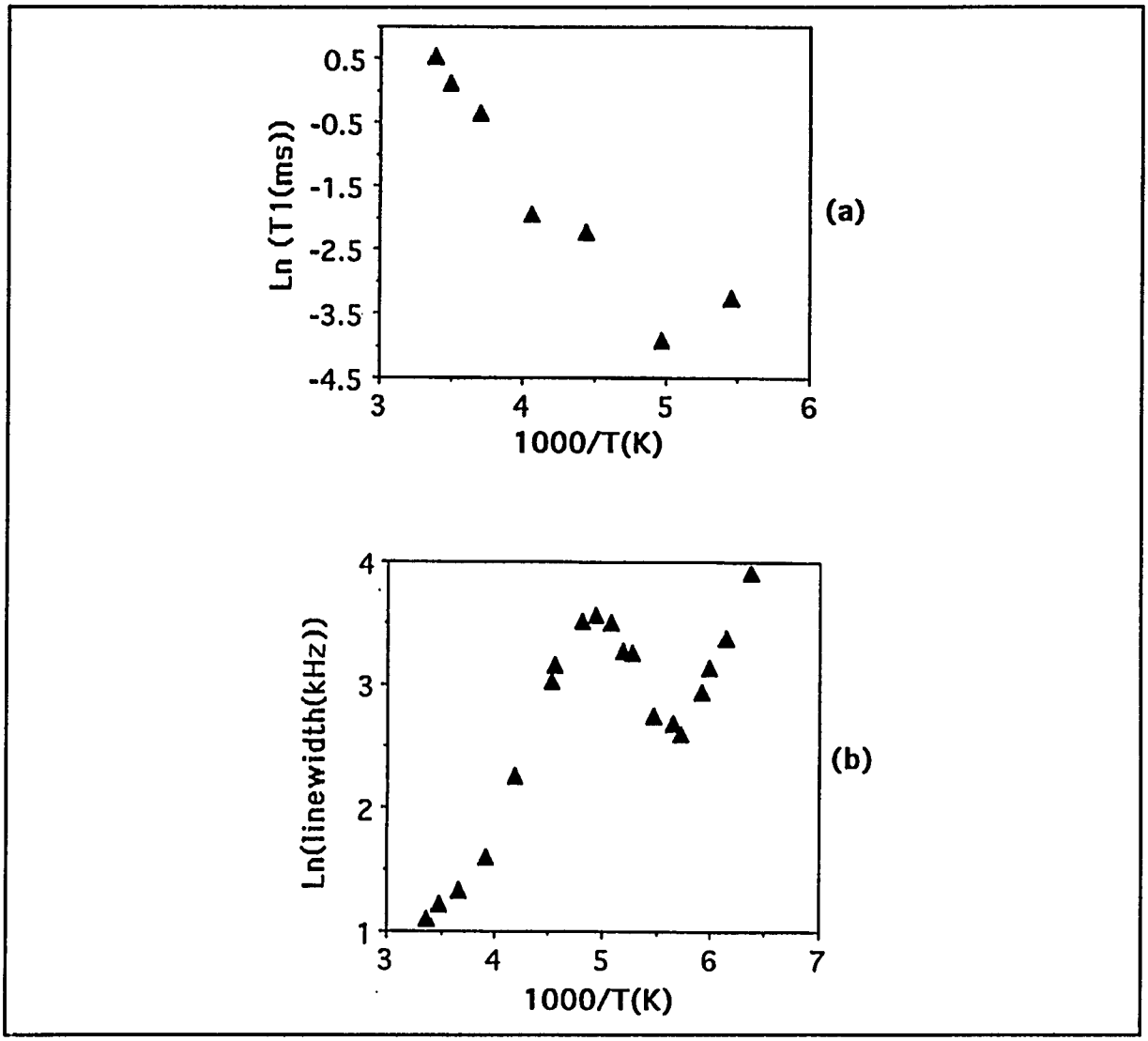

Figure 7.15: Oxygen-17 T_1 and linewidth temperature-dependence: (a) T_1 vs. temperature for 13.2 wt% water in NAFION, (b) linewidth vs. temperature for 15.7 wt% water in NAFION.

Figure 7.16a. Because of the large quadrupole interaction of ^{17}O relative to deuteron, the spectra are considerably broader. The spectra show one clear set of satellite transitions with an angular dependence providing the clear evidence that the EFG principal direction is in the plane of the film. Thus both ^{2}H and ^{17}O results indicate that residual molecular orientation for unstretched films resides in the plane of the film.

Figure 7.16b displays ^{17}O spectra of a 19% stretched film containing 13% ^{17}O enriched H_2O. The resolution of the satellite transitions and their angular dependence for the anisotropy enhanced by the 19% elongation are very clear. The appearance of only one set of quadrupole split ^{17}O resonances in figure 7.16b, as opposed to two sets of ^{2}H lines in Figure 7.7b, suggests that the site inequivalence explanation of the latter spectrum is unlikely. Thus ^{17}O NMR results do not confirm the previously referenced IR study which found two different water molecule environments [28]. However, depending on the timescale of molecular exchange between the two inequivalent sites, it is plausible for effects observed in IR not to be directly detectable by NMR.

Room temperature oxygen-17 NMR spectra of unstretched (a) and stretched (b) Nafion-117 films containing 22 wt% $CH_3{}^{17}OH$ are displayed in Figure 7.17. No angular dependence is apparent, even in the stretched samples. This is in stark contrast to the situation observed in stretched samples containing 13 wt% $H_2{}^{17}O$, in which well-defined satellite transitions, with an overall spectral width of about 10 kHz, were observed as discussed above. Although some of the anisotropy could be masked by lifetime broadening of the rapidly relaxing ^{17}O nuclei, it is clear that methanol molecular motion retains almost none of the anisotropy generated in the stretched perfluoropolymer host, again in contrast to the situation concerning water molecular motion.

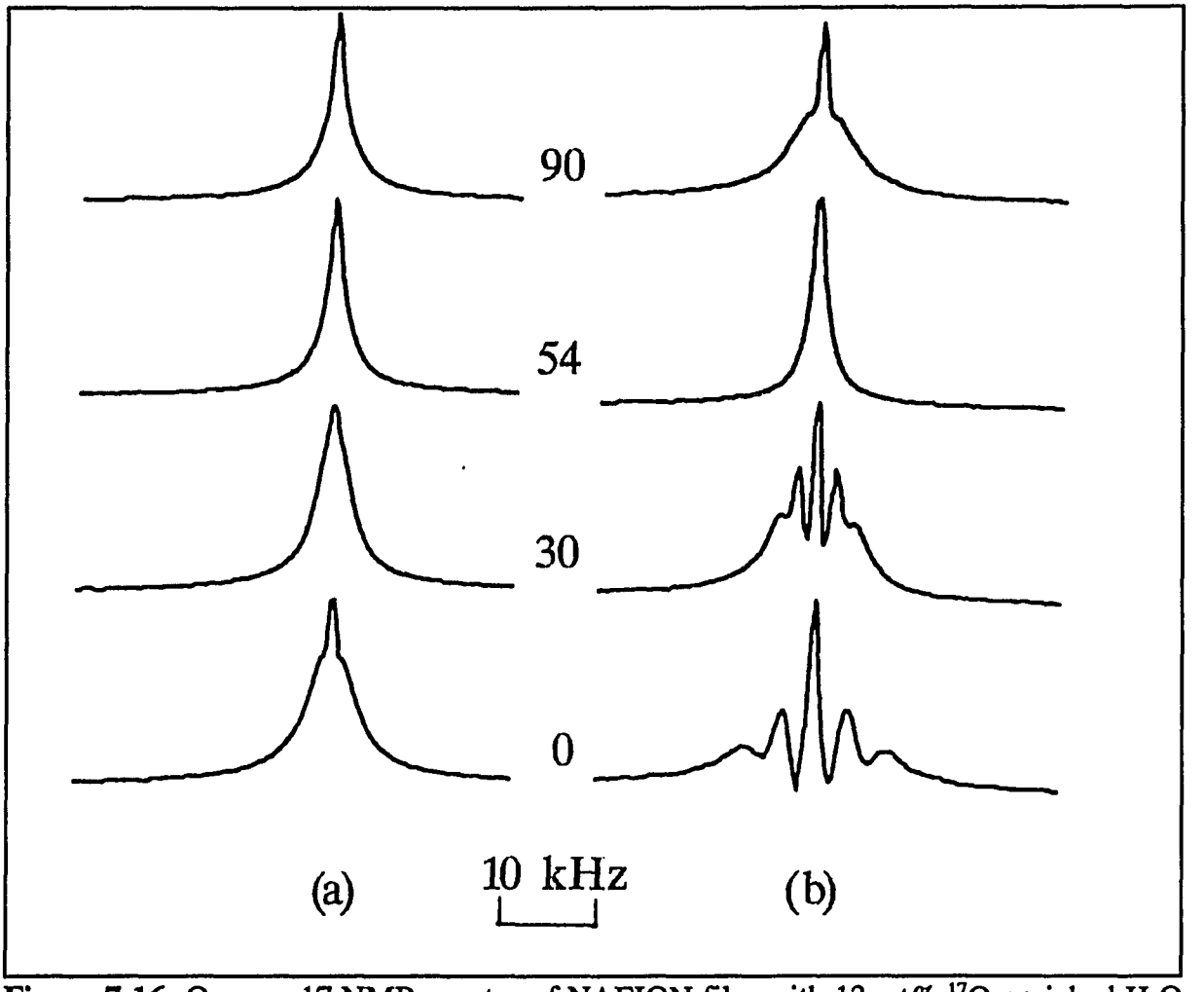

Figure 7.16: Oxygen-17 NMR spectra of NAFION film with 13 wt% ^{17}O-enriched H_2O at θ=0°,30°,54°,90°. (a) unstretched, (b) stretched to 19% elongation.

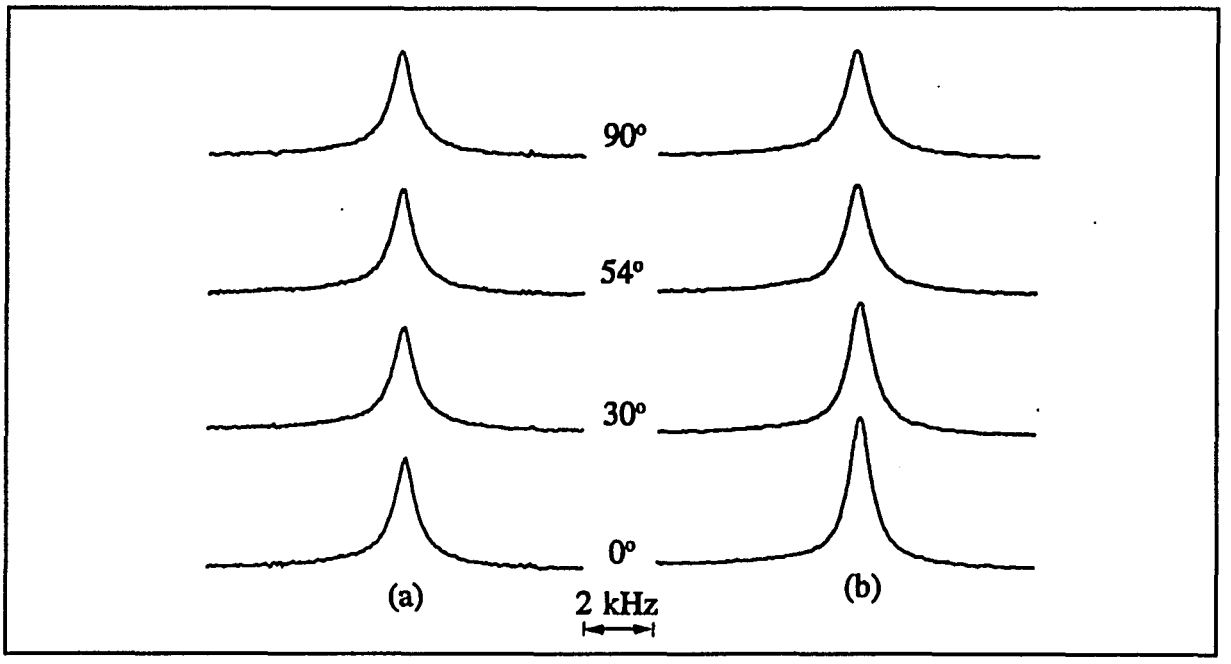

Figure 7.17: Oxygen-17 NMR spectra of unstreched (a) and streched (b) *Nafion* films containing 22 wt% of 15% enriched $CH_3{}^{17}OH$.

Although the molecular motion time-scale probed by linewidth and T_1 are considerably different (10^{2-5} Hz in the former and 10^{7-8} Hz in the latter), the dominant motional process responsible for both linewidth and T_1 behavior is assumed to be molecular rotation, as in the case of liquid CH_3OD [58]. Molecular rotation provides an even more efficient relaxation pathway for $CH_3{}^{17}OH$ because of the considerably larger (than deuterons in the same molecule) quadrupole interaction experienced by the ^{17}O nucleus. Figure 7.18 displays Arrhenius plots of ^{17}O T_1 in Nafion-117 samples containing 22 wt% and 18 wt% CH_3OH enriched 15% in ^{17}O. At temperatures below ~220 K, T_1 cannot be measured reliably because it becomes comparable to the width of the inverting pulse (~20 μs). Oxygen-17 linewidths of the same samples are plotted in Figure 7.19. It is interesting to note that the ^{17}O linewidths are determined, in large part, by lifetime (i.e. T_1) effects. For example, the T_1 contribution to the linewidth, which can be estimated as $(\pi T_1)^{-1}$, is approximately half of the total linewidth at 295 K. This is at least partly responsible for the absence of ^{17}O spectral anisotropous in Figure 7.17. Not surprisingly, the activation energies which characterize the T_1 and linewidth temperature dependencies are quite similar (~0.20 ev). The general shapes of the linewidth curves in Figure 7.19 follow the temperature dependence predicted for a second-order quadrupole broadened central transition (lifetime effects are included), shown schematically in Figure 7.20 [59]. The high-T region, equivalent to short motional correlation time τ, corresponds to the extreme narrowing limit $\omega_L\tau << 1$, where ω_L is the Larmor frequency. As T is lowered (or τ increased) the linewidth reaches a maximum associated with the T_1 minimum occurring at $\omega_L\tau = 1$. This represents the lifetime contribution to the linewidth discussed above. Lowering T further reduces the

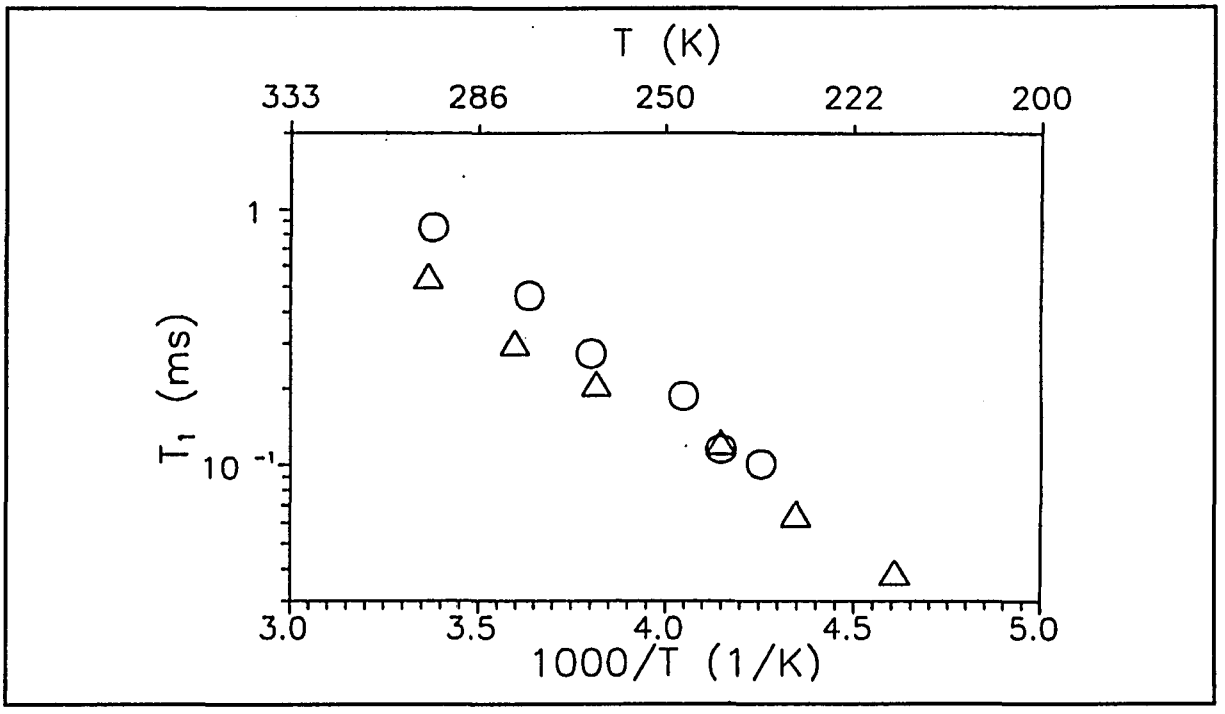

Figure 7.18: Arrhenius plots of ^{17}O T_1 in Nafion containing 18 wt% (triangles) and 22 wt% (circles) of 15% ^{17}O-enriched CH_3OH

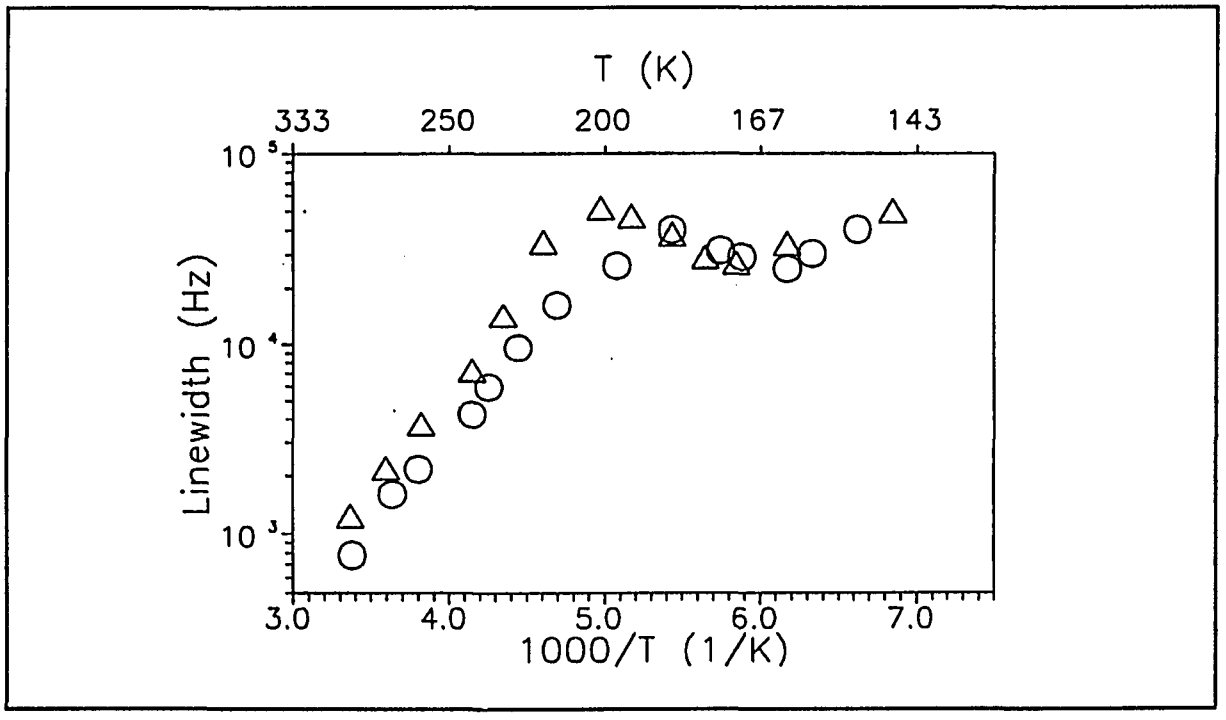

Figure 7.19: Arrhenius plots of ^{17}O linewidth in Nafion containing 18 wt% (triangles) and 22 wt% (circles) of 15% ^{17}O-enriched CH_3OH

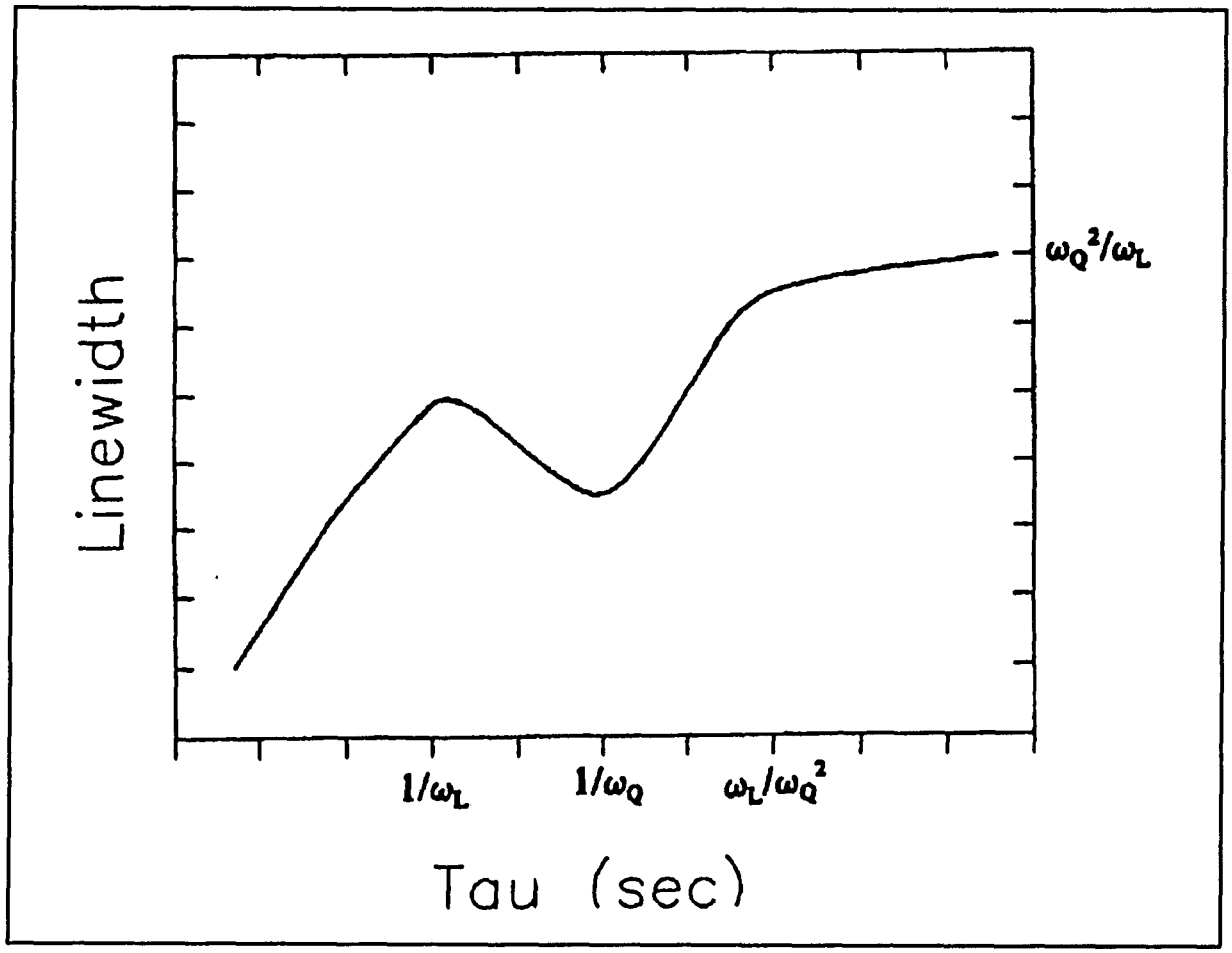

Figure 7.20: Predicted behavior of the linewidth of the central transition for a half-integer spin quadrupolar nucleus, as a function of molecular correlation time.

linewidth untill a minimum is reached, corresponding to a τ value of the order of $1/\omega_Q$, where $\omega_Q$is the strength of the quadrupole interaction (order of several MHz at lower T). Further reduction in T broadens the line until the rigid limit of the second-order linewidth, ω_Q^2/ω_L is reached. As in the case of the deuteron NMR results, the oxygen-17 linewidths of the two samples follow similar trends, with the main features of the higher methanol-content sample shifted to lower temperature. Thus the molecular dynamics at a given temperature are somewhat faster in the saturated sample.

Although there is no simple and direct relationship between relaxation processes dominated by molecular rotation and methanol diffusion across the membrane, the results reported here clearly suggest that methanol is highly mobile in Nafion-117, considerably more so than water. A brief summary of the experimental evidence supporting this conclusion is given: (i) near absence of anisotropic molecular motion in stretched films; (ii) deuteron linewidth at 140 K is still an order of magnitude smaller than that corresponding to a rigid O-D bond; (iii) molecular dynamics are somewhat faster at higher methanol content.

Finally, high pressure deuteron spin-lattice relaxation time T_1 for NAFION film containing 6, 12, 20 wt% D_2O are shown in Figure 7.21. The activation volume can be determined from the data in Fig.13 from the relation

$$\Delta V^* = -kT\frac{d(\ln T_1)}{dp} \qquad (3)$$

yielding the results 2.0, 2.8, and 4.6 cm^3/mol for 20, 12, 6 wt% D_2O samples, respectively.

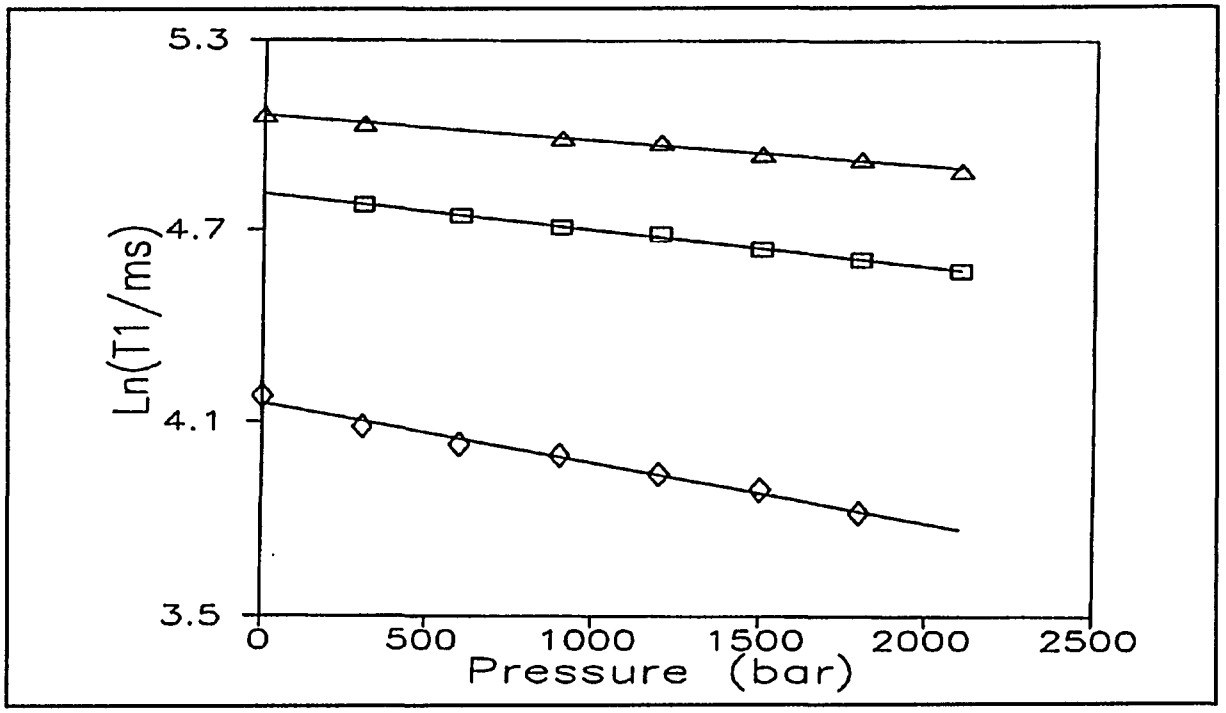

Figure 7.21: Deuteron spin-lattice relaxation time pressure dependence for Nafion containing 20(triangles), 12(squares), 6(diamonds) wt% D_2O.

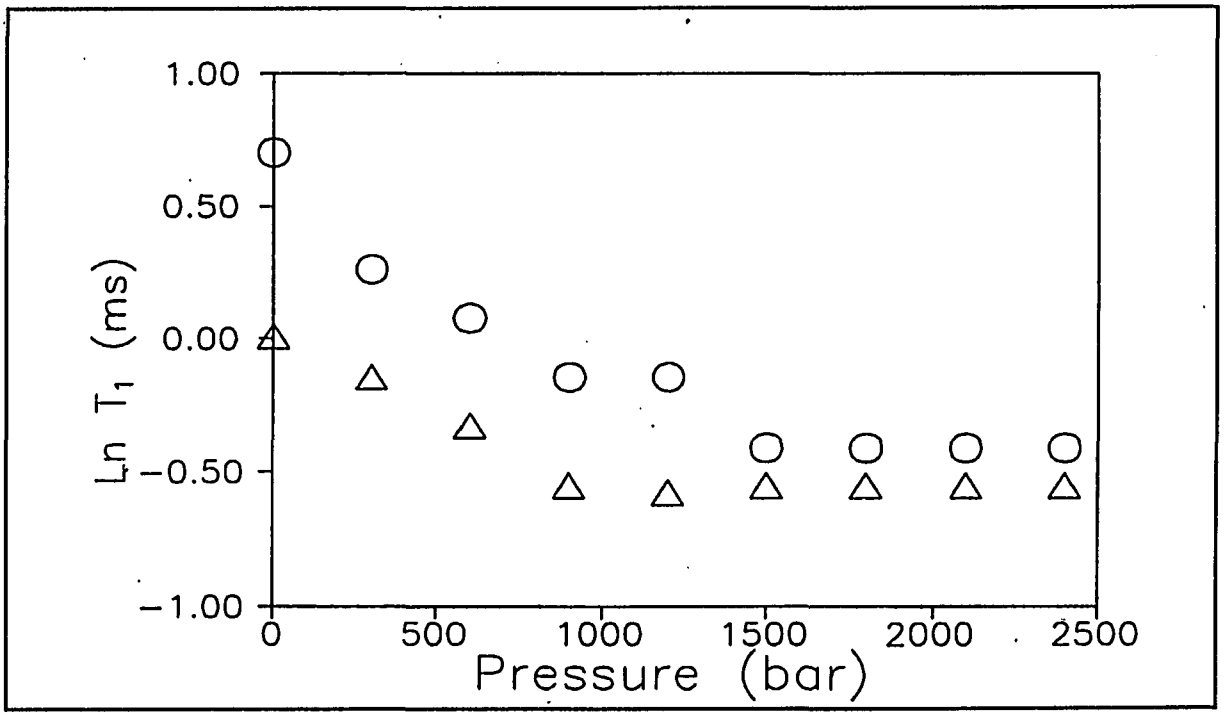

Figure 7.22: Oxygen-17 spin-lattice relaxation time pressure dependence for *Nafion* containing 22(circles), 12(triangles) wt% $H_2{}^{17}O$.

Figure 7.22 shows the oxygen-17 spin-lattice relaxation time for Nafion containing 12 and 22 wt% $H_2{}^{17}O$. Compared with the ^2H T_1 pressure dependence, the ^{17}O T_1 pressure dependence is considerably larger in the range 1 bar to 0.9 kbar, and much weaker when the pressure is larger than 0.9 kbar, suggesting that hydrogen ionic and water molecular motions are not necessarily governed by the same process.

7.4 Conclusion

The nature of water in Nafion-117 has demonstrated significant departures from bulk water behavior. This conclusion is borne out in the present study by examination of low temperature properties, and by spectroscopic results which reflect the underlying anisotropy of the host polymer. The low T deuteron NMR lineshape suggest that the water molecules reside in glassy domains. The activation energy corresponding to deuteron spin-lattice relaxation in Nafion increases with increasing water content. Thus even fully saturated films do not exhibit behavior consistent with isotropically free water contained in voids. Despite the highly mobile state of the water molecules (at room T), residual orientation approximately in the plane of the film is evidenced by both ^2H and ^{17}O spectra. This anisotropy can be enhanced dramatically by modest stretching (less than 20%) of the film. The results of measurements on methanol containing films indicate rapid methanol molecular motion. Finally, activation volumes for deuteron motion have been extracted from high pressure ^2H T_1 measurements, which are observed to increase with decreasing water content. The pressure dependent of T_1 for oxygen-17 motion show a considerable difference to that of deuteron.

References

(1) R. A. Marino, T. Hirshfeld and S.M. Klainer, Fourier Transform NQR, in Fourier, Hadamard and Hilbert Transforms in Chemistry, A.G. Marshall, ed. (Plenum, N.Y., 1982).

(2) R. A. Marino, J. R. P. Jayakody and S. S. Kim, "Experimental Investigations of the Strong Off-Resonance Comb (SORC) Pulse Sequence in ^{14}N NQR", Z. Naturforsch. **47a**, 415-420 (1992).

(3) "Detection of Explosives and Narcotics by low power large sample Volume NQR", M. L. Buess, A. N. Garroway and J. B. Miller, U. S. Patent Application # 07/730,722, Field 16 July 1991.

(4) E. D. Ostroff and Waugh, Phys. Rev. Lett. **16**, 1097 (1966)

(5) J. S. Waugh and C. H. Wang, Phys. Rev. **162**, 209 (1967).

(6) P. Mansfield and D. Ware, Phys. Lett. **22**, 133 (1966).

(7) P. Mansfield and D. Ware, Phys. Rev. **168**, 318 (1968).

(8) W. K. Rhim, D. P. Barnum and D. D. Elleman, Phys. Rev. Lett. **37**, 1764 (1976)

(9) W. K. Rhim, D. P. Barnum and D. D. Elleman, J. Chem. Phys. **68**, 692 (1978).

(10) R. A. Marino and S. M. Klainer, J. Chem. Phys. **67**, 3388 (1977).

(11) T. Oja, R. A. Marino and P. J. Bray, Phys. Letters **26A**, 11 (1967).

(12) L. Guibé, Compt. Rend. **250**, 1635 (1960).

(13) S. Lee and S.Z. Tang, Phys. Rev. B31, 1308 and B32, 2761 (1985).

(14) S. Lee and A. Shetty, Phys. Rev. B35, 1 (1987).

(15) S. Lee, Phys. Rev. **B30**, 2353 (1984)

(16) Ian C. P. Smith, NMR of Newly Accessible Nuclei, Vol. 2, Ed. P. Laszlo, Academic Press, New York (1983), Ch.1.

(17) H. W. Spiess, Advance in Polymer Science, Vol. 66 Springer-Verlag, Berlin Heidelberg, (1985).

(18) L.W. Jelinski, in High-Resolution NMR Spectroscopy of Synthetic Polymers in Bulk, L. Komoroski, ed., VCH Publisher, New York (1986), Ch.10.

(19) H. J. C. Berendsen, J. Chem. Phys. **36,** 3297 (1962).

(20) H. J. C. Berendsen and C. Migchelsen, Ann. N. Y. Acad. Sci., **125**, 365 (1965).

(21) G.E. Chapman and K. A. Mclauchlan. Proc. Roy. Soc. **B.173**, 223, (1969).

(22) T. C. Wong and T. T. Ang, J. Phys. Chem. **89**, 4047 (1985)

(23) S. Krishnamaurthy, D. Mcintyre, E. R. Santee, Jr., and C. W. Wilson, J. Polym. Sci. Polym. Phys. **11,** 427 (1973)

(24) S. Z. Li, Y. S. Pak, K. Adamic and S. G. Greenbaum, B. S. Lim, G. Xu and A. S. Nowick, J. Electrochem. Soc. **139,** 662 (1992)

(25) R. L. Vold, J. S. Waugh, M. P. Klein, and D. E. Phelps, J. Chem. Phys., **48,** 3831 (1968)

(26) S.J. Sondheimer, N.J. Bunce, C.A. Fyfe, J. Macromol. Sci.-Rev. in Macromol. Chem. and Phys. C26, 353 (1986).

(27) T. A. Zawodzinski, Jr., M. Neeman, L. O. Sillerud, and S. Gottesfeld, J. Phys. Chem. **95,** 6040 (1991)

(28) M. Falk, Can. J. Chem. **58,** 1495 (1980)

(29) N. G. Boyle, V. J. McBrierty, D. C. Douglass, Macromolecules **16,** 75 (1983)

(30) K. Uosaki, K. Okazaki, H. Kita, J. Electroanal. Chem. 298, 163 (1990).

(31) R.S. Chen, J.R.P. Jayakody, S.G. Greenbaum, X. Gu, Y.S. Pak, M.G. McLin and J.J. Fontanella, J. Electrochem. Soc., submitted.

(32) M. W. Verbrugge, ibid. **136,** 417 (1989)

(33) W. J. Wrasidlo, J. Macromol. Sci., Phys., **B, 3,** 559 (1972)

(34) C. P. Slichter, Principles of Magnetic Resonance, III Edition, Springer-Verlag (New York, 1990).

(35) E.R. Andrew and R.G. Eades, Discuss. Faraday Soc. 34, 38(1962); E.R. Andrew, Prog. NMR Spec. 8, 1-39 (1971).

(36) R. T. Boere and R. G. Kidd Annual Reports on NMR Spectroscopy, Ed. G. A. Webb Vol 13, Academic Press, New York (1988)

(37) N. Bloembegen, E. M. Purcel and R. V. Pound "Relaxation Effect in NMR Absorption," Phys. Rev. **73,** 679-912 (1948)

(38) A. Abragam, The Principles of Nuclear Magnetism, Clarendon Press, Oxford (1961), Ch.VIII.

(39) E. Fukushima and S.B.W. Roeder, Experimental Pulse NMR, A Nuts and Bolts Approach, Addison-Wesly Publishing Company, Inc. (1981).

(40) C. P. Slichter and W. C. Holton, Phys. Rev. **122,** 1701 (1961).

(41) J. C. Pratt, P. Raghunathan and C. A. McDowell, J. Chem. Phys. **61,** 1016 (1974).

(42) J. C. Pratt, P. Raghunathan and C. A. McDowell, J. Mag. Res. **20,** 313 (1975).

(43) S. Alexander and A. Tzalmona, Phys. Rev. **138,** A845 (1965).

(44) F. N. H. Robinson, Rev. Sci. Instrum., **34,** 1260 (1963)

(45) S. J. Gravina's Thesis, Brown University, 1989

(46) J. F. Verwieck and C. D. Cornwell, Rev. Sci. Instr., **32,** 1383 (1961)

(47) Private communication, A. N. Garroway and M. L. Buess, Naval Research Laboratory, Washington, July 1992

(48) E. Lippmaa, M. Alla, and T. Tuherm, in Magnetic Resonance and Related Phenomena: Proceeding of the XIXth Congress Ampere, Heidelberg, September 1976, pp. 113-118.

(49) J. Herzfeld and A.E. Berger, J. Chem. Phys. 73(12), 15 Dec. 1980

(50) F. J. Owens, J. Macromol. Sci. -Phys., **B23**, 527 (1984)

(51) R.C.T. Slade, J. Barker, J.H. Strange, Solid State Ionics 35, 11 (1989).

(52) T.A. Zawodzinski, Jr., M. Neeman, L.O. Sillerud, S. Gottesfeld, J. Phys. Chem. 95, 6040 (1991).

(53) T.F. Fuller, J. Newman, J. Electrochem. Soc. 139, 136C (Abstr. #1).

(54) J.C. Hindman, A.J. Zielen, A. Svirmickas, M. Wood, J. Phys. Chem. 74, 621

(55) K. Matsumura, K. Hayamizu, T. Nakane, H. Yanagishita, O. Yamamoto, J. Polym. Sci.: Part B: Polym. Phys. 26, 2215 (1988).

(56) A. Vega, presented at the Bat-Sheva Workshop on New Developments and Applications in ESR and NMR Spectroscopy, Isral, 1990 (unpublished).

(57) A. Baram, Z. Luz and S. Alexander, J. Chem. Phys. 58, 4558 (1973).